Title
STRANGE-PARTICLE PRODUCTION BY n+p AT 3.7 GeV/c

Authors
Butler, W.R.
Coyne, D.G.
Goldhaber, G.
et al.

Publication Date
1972-11-01

Submitted to
Physical Review D

LBL-1373
Preprint

STRANGE-PARTICLE PRODUCTION BY $\pi^+ p$ AT 3.7 GeV/c

W.R. Butler, D.G. Coyne, G. Goldhaber,
J. MacNaughton, and G.H. Trilling

November 6, 1972

Prepared for the U.S. Atomic Energy
Commission under Contract W-7405-ENG-48

LBL-1373

DISCLAIMER

LBL-1373

STRANGE-PARTICLE PRODUCTION BY $\pi^+ p$ AT 3.7 GeV/c*

W. R. Butler,† D. G. Coyne,†† G. Goldhaber,‡

J. MacNaughton,‡‡ and G. H. Trilling

Department of Physics and Lawrence Berkeley Laboratory
University of California, Berkeley, California 94720

November 6, 1972

ABSTRACT

The results of a study of strange-particle production in $\pi^+ p$ interactions at 3.7 GeV/c are presented. Cross sections for a large number of strange-particle final states are given; the overall strange-particle production cross section is about 1.3 mb. Comparison of cross-section results on two-body and quasi-two-body final states with corresponding $\pi^- p$ data shows no evidence for exotic exchanges. Comparison of the peripheral cross sections for $\pi^+ p \to K^+\Sigma^+$ and $\pi^+ p \to K^+\Sigma^+(1385)$ with those for the line-reversed reactions shows reasonable agreement for $K^+\Sigma^+$ and gross disagreement for $K^+\Sigma^+(1385)$. Simultaneous $K^{*+}(891)\Sigma^+(1385)$ production occurs; but, unlike its nonstrange counterpart, it is not dominated by pseudoscalar exchange. There is significant $\varphi(1019)$ production via the reaction $\pi^+ p \to \varphi\pi^+ p$, but none of it appears to be associated with $\Delta^{++}(1236)$. Cross sections for resonance production in various three- and four-body final states are presented.

I. INTRODUCTION

Although $\pi^{\pm}$-proton interactions leading to nonstrange final states have been systematically studied in the multi-GeV energy domain, there is far less complete information on the production of strange-particle final states, particularly for $\pi^{+}p$ interactions. This is a consequence of the fact that the cross sections for production of such states are smaller by more than an order of magnitude than those of final states of similar multiplicity without strange particles.

In this Paper we describe the results of a bubble chamber study of strange-particle production by positive pions of momentum about 3.7 GeV/c. The events to be discussed, with one major exception, all involve a topology with a strange-particle signature, either a kink in a charged track or a vee decay. The exception, included for completeness, is the final state $K^{+}K^{-}\pi^{+}p$ which, except in the rare instances in which a $K^{\pm}$ decays in flight, has a simple four-prong topology.

In Sec. II, we present experimental details with particular emphasis on the data-handling procedures. In Sec. III, we discuss the determination of cross sections for the various strange-particle final states. In Secs. IV and V, we present some of the more detailed features, including angular and mass distributions, of two-body, three-body (Sec. IV), four-body and five-body (Sec. V) final states. Finally in Sec. VI, we summarize our results and conclusions.

II. EXPERIMENTAL DETAILS

A. Exposure

The data described in this paper were obtained in a 180,000-picture exposure of the LBL 72-inch hydrogen bubble chamber to a separated beam of

positive pions produced in an external target. The beam transport system is described elsewhere.[1]

Runs were made at five closely-spaced momenta, namely 3.56, 3.67, 3.73, 3.82 and 4.00 GeV/c. Unfortunately the beam had a non-negligible proton contamination, particularly at the highest momentum. For this reason the 4-GeV/c film was not used in the analysis of the strange particles, and several rolls at the lower momenta were deleted if the contamination exceeded limits which will be described below. Because of the limited statistics and the rather small variation of any significant parameter over the momentum range studied, the data for the four momenta used were combined, and correspond to a mean momentum of 3.71 GeV/c.

B. Scanning and Measuring Procedures

The most common strange-particle topologies studied in this experiment are shown in Fig. 1. To these must be added the ordinary four-prong topology from which our $K^+K^-\pi^+p$ sample was drawn.

Approximately 40% of the film was scanned for all interactions within a given scanning fiducial volume, including "ordinary" topologies (the term "ordinary" here and in the following discussion is used to denote nonstrange-particle events). In the remainder of the film, ordinary two-prong events without stopping protons were omitted from the scan.

The first measurement of the events was performed on the LBL Flying-Spot Digitizer (FSD). Geometric reconstruction and kinematic analysis were done through the program SIOUX (combined TVGP and SQUAW).[2]

The beam momentum profile for each section of film was obtained by fitting the ordinary four-prong events to the four-constraint hypotheses,

$$\pi^+p \rightarrow \pi^+\pi^-\pi^+p \qquad (1)$$

$$\pi^+ p \rightarrow K^+ K^- \pi^+ p \qquad (2)$$

$$pp \rightarrow \pi^+ \pi^- pp \quad . \qquad (3)$$

The mean value and root-mean-square (rms) width of the beam momentum spectrum were determined from the sample of events which fit reaction (1) unambiguously. The value of the width was typically ± 0.05 GeV/c. The average value and rms width of the beam momentum were then used as input to the fitting procedure through the usual beam-averaging procedure.

For the strange-particle events, the output from the SIOUX program was compared to each event at the scan table in order to make visual identification of tracks by ionization (track bubble density) and to correct mistakes made by the initial scanner. Interactions having only pi decays and/or electron pairs were removed from the strange-particle category. Except for about thirty percent which were remeasured on the FSD, failing strange-particle events were remeasured with on-line Franckenstein measuring projectors. A second measurement was performed on the Franckensteins for those events which failed again.

An accepted strange-particle event hypothesis was required to satisfy the following criteria:

1. The coordinates (x, y, z) of the interaction vertex must lie within a given fiducial volume.
2. The measured beam track momentum as well as the azimuthal and dip angles must lie within three standard deviations of the mean beam momentum vector. Before applying these criteria, the values of the momentum, azimuth, and dip are extrapolated to a standard location in the chamber to correct for energy loss and the curvature due to the magnetic field.

3. The geometric reconstruction is adequate in the sense that the point scatter on each track is consistent with the setting error plus multiple scattering, and that the tracks come together at the vertex within the errors.
4. The hypothesis is consistent with the track bubble densities as seen on the scan table.
5. If the hypothesis is a constrained fit, then the confidence level is greater than 0.01. If the hypothesis is not constrained at the primary vertex, then the missing mass is consistent with the presence of two or more missing neutrals and the missing momentum has a magnitude significantly different from zero.

When two or more hypotheses are acceptable, we accept only the one corresponding to the highest constraint class. For the most important case, namely the Λ-Σ^{o} ambiguity, a more detailed justification of this procedure is given further on. If several hypotheses of the same constraint class are acceptable, all are recorded and the event is tagged as ambiguous.

The scanning efficiency for all event types was determined by a second scan of ten rolls. The rescan events were subjected to the same acceptance criteria as the first scan. After correction for very low-momentum-transfer elastic scatters, the average single-scan efficiency for finding any event is 98%. The scanning efficiencies pertinent to the strange-particle topologies are discussed in the next section.

III. CROSS SECTIONS

A. General Considerations

Cross sections for the production of various strange-particle final states were determined from the relation,

$$\sigma_i = \frac{N_i}{N_{tot}} \sigma_{tot} \quad , \qquad (4)$$

where σ_i is the cross section for channel i, σ_{tot} is the total $\pi^+ p$ cross section which is taken to be 28.1 mb,[3] N_i is the number of events in channel i and N_{tot} the total number of events. The next few sections discuss in some detail the inputs into formula (4).

B. Proton Contamination

Events which fit uniquely the reaction $pp \rightarrow \pi^+\pi^- pp$ were taken as a measure of the proton contamination. Events produced by protons were subtracted out statistically using the information from two rolls of pure proton film and scaling according to the number of unique $\pi^+\pi^- pp$ fits in the pion film. Furthermore rolls where the ratio of $pp \rightarrow \pi^+\pi^- pp$ fits to all unique four-prong, four-constraint fits exceeds 20% were deleted from the data sample.

Fortunately, the strange-particle production due to proton-proton interactions is small in the momentum region of our experiment. Therefore the major effect of the proton correction on the pion strange-particle production cross sections is through a correction of N_{tot} in formula (4).

C. Normalization

In principle, the determination of the factor σ_{tot}/N_{tot} in formula (4) involves the straightforward procedure of counting all events. Its implementation is complicated by the two different procedures used in scanning the film, as mentioned earlier. A detailed discussion is given elsewhere,[4] and it suffices here to give the results in Table I. The 98% scanning efficiency for ordinary events discussed above has been incorporated into N_{tot}, and appropriate correction has been made for the substantial loss of elastic scatters with very short recoil protons.

D. Strange-Particle Scanning Efficiency

Losses of strange-particle events due to scanning inefficiency arise from either the complete missing of an event or the failure to recognize a strange-particle signature in an otherwise detected event. In order to examine the scanning efficiency specific to strange particles, a special scan was conducted over ten rolls. Each of these rolls was rescanned by two different scanning technicians searching only for strange-particle event types. Comparison of the results of these scans with that of the original scan provided efficiency information. With the decay cuts to be discussed below, efficiencies varied from 93% for vee and $\Sigma^{\pm} \rightarrow n\pi^{\pm}$ decays unaccompanied by other decays to 98% for events with more than one decay. Since the efficiency for detecting $\Sigma^{\pm}$ decays dropped off somewhat in the region of the film where most two-prongs were not recorded, only that sample of film where all events were recorded was used in determining cross sections involving $\Sigma^{\pm}$ decays unaccompanied by vee decays.

E. Decay Corrections

1. Decay of Charged Hyperons

For cross-section determinations involving $\Sigma^{\pm}$ hyperons, only the $n\pi^{\pm}$ decay modes were used. To correct for inability to detect $\Sigma^{\pm}$ with very short decay times, we removed events in which the $\Sigma^{\pm}$ travels less than 5 mm before decaying, and weighted the remaining events appropriately. The loss of events due to long decay times is negligible.

To correct for the loss of events in which the projected decay angle is so small as to be difficult to detect, we consider the scatter plot of decay cosine in the sigma rest system versus decay azimuth about the sigma direction shown in Fig. 2. The azimuth angle is twice folded and is defined

such that 90° represents a geometrical situation with the decay plane perpendicular to the camera film plane. Although this plot should have uniform density, Fig. 2 shows a definite depletion of events for forward decays and for decays with azimuths near 90°. To correct for this depletion, we have eliminated events which are either in the region from 0.7 to 1.0 in decay cosine, or the region 80° to 90° in azimuth. The remaining events were appropriately weighted to take account of these cuts.

2. "Vees"

All accepted vee decays were required to be within a fiducial volume whose boundaries are substantially beyond those used for the interaction fiducial volume and to have a minimum decay path of 5 mm. An appropriate correction was made for corresponding event loss. A scatter plot of decay cosine versus decay azimuth did not reveal any appreciable loss of vee events due to small angles.

F. Λ vs Σ^{o}

We have investigated the validity of accepting the highest constraint class hypothesis by studying in some detail the reactions

$$\pi^{+}p \rightarrow K^{+}\pi^{+}\Lambda \qquad (5)$$

and

$$\pi^{+}p \rightarrow K^{+}\pi^{+}\Sigma^{o} \quad . \qquad (6)$$

We therefore initially accepted both fits if both passed the criteria set forth above, even though (6) is a lower-constraint class than (5).

Each of the events ambiguous between hypotheses (5) and (6) is transformed to the Σ^{o} rest frame. For this set of ambiguous events, we then examine the distribution of the decay cosine of the photon from the Σ^{o} decay with respect to each of the three measured tracks at the primary

vertex--the beam, the outgoing pion and the kaon. These distributions (Figs. 3a,b,c) have extremely sharp peaks in the forward direction, whereas for pure Σ^o decay each should be uniform. Figure 3d shows a scatter plot of the decay cosine with respect to the outgoing pion versus the decay cosine with respect to the kaon, where events in the forward peak of the beam distribution (Fig. 3a) have been excluded. Almost all the events lie near the forward boundaries. We conclude therefore that all these events belong to hypothesis (5). Figure 3e shows the distribution of the decay cosine with respect to the beam for those events which fit (6) unambiguously. There is no appreciable loss of events in the forward direction suggesting that the separation of the two hypotheses is complete. The cross section for reaction (6) is determined from the events which fit it unambiguously; all of the ambiguous events are assigned to reaction (5).

The sharp peaks in Figs. 3a-c are qualitatively explained by the fact that the momentum uncertainties of the beam and outgoing charged particles are often large enough to hide a 70-MeV photon moving near the same direction as these particles. Coupling such a photon to the Λ can simulate a Σ^o decay and produce the observed ambiguity.

G. Other Ambiguities

For events which fit more than one hypothesis of the same constraint class, we express the number of events assigned to a particular hypothesis by an equation of the form,

$$N = U + fA \qquad (7)$$

where U is the number of unambiguous events for that hypothesis, A is the number of events ambiguous with that hypothesis, and f is the fraction of ambiguous events which actually contribute to the hypothesis. Sometimes f

can be determined from special topologies (for example, with vee decays) in which no ambiguities occur. If there is no experimental basis for determining f, it is assigned the value 1/2 for double ambiguities, 1/3 for triple ambiguities and 1/4 for quadruple ambiguities. The error then assigned to f is ± 0.25 for all three cases.

H. Results

Using the branching ratios, $[\Gamma(K_1 \rightarrow \pi^+\pi^-)]/[\Gamma(K_1 \rightarrow \text{all})] = 0.689$, $[\Gamma(\Lambda \rightarrow p\pi^-)]/[\Gamma(\Lambda \rightarrow \text{all})] = 0.642$ and $[\Gamma(\Sigma^+ \rightarrow n\pi^+)]/[\Gamma(\Sigma^+ \rightarrow \text{all})] = 0.484$,[5] plus all the corrections discussed earlier, we arrive at the cross sections summarized in Table II. The errors quoted are statistical, including the statistics of rescans and corrections. In some channels there may be some additional systematic errors arising from the uncertainties connected with the treatment of ambiguity problems. The total strange-particle production cross section is about 1.3 mb, of which roughly 30% is $K\bar{K}$ and 70% is YK.

Two comparisons involving these results are of particular interest. First of all, insofar as energy dependence is concerned, comparison with the results of an 8 GeV/c π^+p experiment[6] shows that (i) the three-body final state cross sections drop by about a factor of 3 between 3.7 and 8 GeV/c, (ii) the four-body cross sections remain flat in the same energy interval, (iii) the five-body cross sections rise by roughly a factor of 2 in this interval.

Secondly, we have compared our π^+p data with π^-p data at 3.9 GeV/c examining the relative cross sections for similar final states as shown in Table III.[7] The results are perhaps most remarkable for the closeness between corresponding π^+ and π^- cross sections for many of the final states.

IV. TWO- AND THREE-BODY FINAL STATES

A. $K^+\Sigma^+$

The reaction $\pi^+ p \rightarrow K^+\Sigma^+$ has been extensively studied in several counter-spark-chamber experiments with statistics far greater than the few hundred events in the present experiment.[8,9] We justify a discussion of our own data for this reaction by the strong control on systematic errors typical of a bubble chamber experiment.

The differential cross section based on a sample of 144 events with $\Sigma^+ \rightarrow n\pi^+$ decays, suitably weighted to take account of scanning inefficiencies and geometrical corrections is shown in Fig. 4a. The t distribution for forward angles and the u distribution for backward angles are shown in more detail in Figs. 4b and 4c. These data are in reasonable agreement with those of Bashian et al.,[9] and, insofar as shape is concerned, with those of Pruss et al. and Han et al.[8] However the magnitude of $d\sigma/dt$ in the low t region appears to be about 25% higher in our data than in the results of Pruss et al.

The striking features of Fig. 4 include: (i) a forward peak going from about 600 $\mu b/(GeV/c)^2$ in the forward direction to very low values at $-t > 2$ $(GeV/c)^2$, (ii) a region $2 \leq -t \leq 4$ $(GeV/c)^2$, where no events were detected and the average cross section is therefore significantly less than 1 $\mu b/(GeV/c)^2$ [one event in that t region would correspond to an average cross section of 0.4 $\mu b/(GeV/c)^2$], and (iii) a marked backward peak contributing about 10% of the total $K^+\Sigma^+$ cross section. We now consider both the forward and the backward angular regions in somewhat more detail.

1. The Forward Region

A fit to the angular region $-t \leq 0.4$ $(GeV/c)^2$ of the form,

$$\frac{d\sigma}{dt} = Ae^{Bt}$$

yields for the parameters

$$A = 0.64 \pm 0.15 \text{ mb}/(\text{GeV}/c)^2$$

$$B = 8.4 \pm 1.4 \ (\text{GeV}/c)^{-2} \ .$$

Near the forward direction, the $K^+\Sigma^+$ production is expected to be dominated by exchange of K_V and K_T, the strange members of the vector and tensor nonets. An immediate consequence is that the reaction $\pi^- p \to K^+\Sigma^-$ should be highly suppressed, and that by isospin invariance,

$$\frac{d\sigma}{dt}(\pi^+ p \to K^+\Sigma^+)\Big|_{t \text{ small}} = 2\frac{d\sigma}{dt}(\pi^- p \to K^o\Sigma^o)\Big|_{t \text{ small}} \ . \quad (8)$$

It is in fact already well established that the $K^+\Sigma^-$ final state is highly suppressed in the forward direction.[10] However deviations from (8) may depend linearly on any exotic exchange amplitude whereas the $K^+\Sigma^-$ rate itself depends quadratically on such amplitudes. Hence careful tests of relations such as (8) are worthwhile even if the forward cross section for the $K^+\Sigma^-$ state is known to be small. A further relationship involving near-forward cross sections follows from the Regge representation of the amplitudes for K_V and K_T exchange coupled with the notion of exchange degeneracy, namely the expected equality of the trajectory functions $\alpha(t)$ for K_V and K_T. This relation equates the cross sections near the forward direction for reactions related by $s \leftrightarrow u$ crossing:

$$\frac{d\sigma}{dt}(\pi^+ p \to K^+\Sigma^+)\Big|_{t \text{ small}} = \frac{d\sigma}{dt}(K^- p \to \pi^-\Sigma^+)\Big|_{t \text{ small}} \ . \quad (9)$$

To test relations (8) and (9), we have arbitrarily defined the forward region as the t-range $0.02 < -t < 0.60 \ (\text{GeV}/c)^2$, the lower limit corresponding

to a forward emitted K^+ at incident momentum 3.7 GeV/c. Cross sections for the various relevant reactions integrated over this t-range are given in Table IV. To permit direct comparisons, data from other experiments not precisely at 3.7 GeV/c have been scaled to that incident momentum using a $P^{-1.2}$ dependence.[11] To the extent that (8) and (9) are valid, all numbers in the fourth column of Table IV should be equal. Inspection of the Table leads to the following observations concerning the cross sections scaled to 3.7 GeV/c.

(a) Relation (8) seems reasonably satisfied, due account being taken of the disagreements between various experimental measurements of the same quantities.

(b) Both our $K^+\Sigma^+$ cross section and twice the $K^o\Sigma^o$ cross section of Dahl et al.[12] are very nearly equal to the cross section for $K^-p \to \pi^-\Sigma^+$ in this same t range. On the other hand the $K^o\Sigma^o$ result of Abramovich et al.[13] and the counter data of Pruss et al.[8] both suggest that the left side of relation (9) is, at this energy, somewhat lower than the right side. It should be pointed out that the chosen t range, when applied to the $\pi^-\Sigma^+$ final state, excludes, by virtue of the mass differences, the very forward end of the differential cross section. Evidently there is considerable uncertainty as to whether a comparison over just the same t range is the proper way of dealing with the differing kinematics of the exothermic and endothermic reactions.

Consequently it is difficult because of both experimental and theoretical uncertainties to draw any strong conclusion as to the validity of the exchange degeneracy relation (9) at the energy under study. There certainly is no evidence that (9) is significantly violated.

2. Backward Region

As is clear from Fig. 4, the $K^+\Sigma^+$ final state shows a significant backward peak. The cross section integrated over the backward hemisphere but receiving contributions exclusively for $-u < 1.5$ $(GeV/c)^2$ is 11±3 μb. Again comparison with K^oS^o and $K^+\Sigma^-$ data is of interest. At 4 GeV/c, the K^oS^o has no significant backward contribution, whereas the $K^+\Sigma^-$ has a cross section in the backward hemisphere of 5.3±1.1 μb.[12] At 3.15 GeV/c, the K^oS^o is still negligible and the $K^+\Sigma^-$ has a backward cross section of 15.8±1.3 μb.[12] Interpolating to 3.7 GeV/c the $K^+\Sigma^-$ cross section is 10.3±2 μb in excellent agreement with our $K^+\Sigma^+$ value of 11±3 μb. These results are strongly suggestive of u-channel isoscalar hyperon exchange as the dominant mechanism for the backward peak. Indeed Barger,[17] and more recently Kayser and Hayot[18] and Eisner et al.[19] have had success in accounting for other backward scattering data in an SU(3) symmetric way in terms of exchange-degenerate Λ_α and Λ_γ exchanges. It can easily be shown that in the context of such a model with a d/(f+d) coupling ratio of 1/2, SU(3) symmetry predicts

$$\frac{d\sigma}{du}(\pi^+ p \to K^+\Sigma^+)\Big|_{u\ small} = \frac{d\sigma}{du}(K^- p \to K^+\Xi^-)\Big|_{u\ small} \qquad (10)$$

The $K^+\Xi^-$ cross section (which is essentially all in the backward direction) at 3.9 GeV/c is reported by Eisner et al.[19] to be 17.8±3 μb. This is compatible with our measured value of 11±3 μb for $K^+\Sigma^+$. Since the appropriate d/(f+d) ratio may be slightly different from the value of 1/2 and in view of the statistical limitations of our data, these results should only be interpreted as showing that the size of the observed backward peak in $K^+\Sigma^+$ is of the expected order of magnitude.

B. $K^+\pi^+\Lambda$

The Dalitz plot for 247 events of the type $\pi^+p \to K^+\pi^+\Lambda$ is shown in Fig. 5. The significant features are a sizable $\Sigma^+(1385)$ signal and an absence of events in the region of the Dalitz plot adjacent to this $\Sigma^+(1385)$ band. These features are easily seen in Fig. 6 which shows the $\Lambda\pi^+$ projection of the Dalitz plot. There appears to be a pure $\Sigma^+(1385)$ resonance peak followed by a gap of about 150 MeV and then a fairly structureless population extending over the mass region from about 1600 to 2300 MeV. A fit to the Dalitz plot using a sum of phase space plus a relativistic P-wave Breit-Wigner gives a cross section for $\pi^+p \to K^+\Sigma^+(1385)$ of 29±5 μb, this process accounting for 26±4% of the $K^+\pi^+\Lambda$ final state. This cross section includes all decay modes of the $\Sigma^+(1385)$.

The differential cross section is shown in Fig. 7 as a function of t', where $t' = t - t_{min}$. The distribution shows a forward flattening-off or dip characteristic of dominance by helicity-flip amplitudes, a result already established at 5 GeV/c by Kalbaci et al.[20] and anticipated by analogy to the magnetic dipole (M1) ρ-exchange models for reactions such as $\pi^+p \to \pi^o\Delta^{++}$ and $K^+p \to K^o\Delta^{++}$.[21]

The decay distributions in the Gottfried-Jackson frame are shown in Figs. 8a and 8b. The curves shown are based on the predictions of the M1 model, which can be expressed in terms of the spin density-matrix elements

$$\rho_{3,3} = 0.375 \quad , \quad \text{Re}\ \rho_{3,-1} = 0.216 \quad , \quad \text{Re}\ \rho_{3,1} = 0 \quad .$$

The $\cos\alpha$ distribution appears to be more isotropic than the $1 + 3/2\ \sin^2\alpha$ implied by the model, and the measured density-matrix elements averaged over all $|t'| \leq 1\ (\text{GeV/c})^2$ are

$$\rho_{3,3} = 0.24\pm0.08 \quad , \quad \text{Re}\ \rho_{3,-1} = 0.19\pm0.08 \quad , \quad \text{Re}\ \rho_{3,1} = 0.07\pm0.06 \quad .$$

Presumably the dominant t-channel exchanges in $K^+\Sigma^+(1385)$ production are again those of K_V and K_T. By arguments identical to those used in justifying relations (8) and (9), one can obtain the analogous expressions,

$$\frac{d\sigma}{dt}(\pi^+p \to K^+\Sigma^+(1385))\Big|_{t\ \text{small}} = 2\,\frac{d\sigma}{dt}(\pi^-p \to K^0\Sigma^0(1385))\Big|_{t\ \text{small}} \qquad (11)$$

$$\frac{d\sigma}{dt}(\pi^+p \to K^+\Sigma^+(1385))\Big|_{t\ \text{small}} = \frac{d\sigma}{dt}(K^-p \to \pi^-\Sigma^+(1385))\Big|_{t\ \text{small}} . \qquad (12)$$

For the purposes of testing (11) and (12), we have integrated $d\sigma/dt$ from $-t = 0.04\ (\text{GeV/c})^2$, corresponding to the forward direction in the $K^+\Sigma^+(1385)$ final state at our momentum, to $-t = 0.64\ (\text{GeV/c})^2$. The results are shown in Table V, in which the validity of relations (11) and (12) would imply the equality of all the numbers in the fourth column. While relation (11) is satisfied within the sizable statistical uncertainties, the exchange degeneracy prediction (12) is violated by about a factor of two. This violation appears, at least at our momentum, to be much more marked than whatever violation of relation (9) might seem implied by the data. It is interesting to note that a similar situation exists with respect to analogous reactions involving ρ and A_2 exchange. Thus the line-reversed reactions $K^+n \to K^0p$ and $K^-p \to \overline{K^0}n$ do seem to satisfy a relation similar to (9)[24] whereas the reactions $K^+p \to K^0\Delta^{++}(1236)$ and $K^-n \to \overline{K^0}\Delta^-(1236)$ show a gross violation of a relation similar to (12).[11]

We conclude this discussion of the $K^+\Sigma^+(1385)$ final state by considering briefly the t-channel SU(3) relation

$$\frac{d\sigma}{dt}(\pi^+p \to K^+\Sigma^+(1385))\Big|_{t\ \text{small}} = \frac{1}{3}\,\frac{d\sigma}{dt}(K^-n \to \overline{K^0}\Delta^-(1236))\Big|_{t\ \text{small}} \qquad (13)$$

Although the data for the right side of (13) are somewhat sparse, an interpo-

lated value for the total $K^- n \to \overline{K^0}\Delta^-$ cross section at our momentum amounts to about 300 μb.[25] One third of that figure is 100 μb, a factor of about three larger than our $\pi^+ p \to K^+\Sigma^+(1385)$ cross section of 28 μb. Although (13) applies only to the forward t region, the dominance of the peripheral contribution implies that it is also applicable to the integrated cross section. It has been noted elsewhere that this factor of three discrepancy can be understood in terms of barrier effects connected with mass differences between members of SU(3) multiplets.[26]

C. $K^+\pi^+\Sigma^0$

The Dalitz plot for the reaction $\pi^+ p \to K^+\pi^+\Sigma^0$ is shown in Fig. 9, and the $\Sigma^0\pi^+$ mass spectrum in Fig. 10. The other mass projections show no significant structure.

Although the statistics are somewhat weak, Fig. 10 suggests some structure at $\Sigma^0\pi^+$ mass values of 1660 MeV and 1950 MeV. The Particle Data Tables[5] show Σ states at 1670 MeV (probably consisting of several resonances) and at 1915 MeV which may correspond to the $\Sigma^0\pi^+$ enhancements in Fig. 10. It is also worth noting that although the $\Lambda\pi^+$ mass region above 1550 MeV in Fig. 6 does not have obvious structure, the marked dip for $M(\Lambda\pi)$ near 1500 MeV suggests low background; hence the substantial population for $M(\Lambda\pi)$ around 1650-1700 MeV may be resonant. This interpretation is in good agreement with the 8-GeV/c $\pi^+ p \to K^+\pi^+\Lambda$ data of Aderholz et al.[6] which shows a marked $\Lambda\pi^+$ peak at 1698 MeV. It therefore appears likely that the state responsible for the 1670-MeV $\Sigma^0\pi^+$ enhancement also has a strong $\Lambda\pi$ decay mode.

D. $K^+\overline{K^0}p$

The Dalitz plot for the reaction $\pi^+ p \to K^+\overline{K^0}p$ is shown in Fig. 11, and the $K^+\overline{K^0}$ mass spectrum in Fig. 12. The only clearly discernible structure

is the A_2^+ meson with perhaps a hint of a bump at 1560 MeV. The branching ratio estimated from a comparison of Fig. 12 with our data on $\rho\pi$ and $\eta\pi$ modes of the A_2 is

$$\frac{\Gamma(A_2 \rightarrow K\bar{K})}{\Gamma(A_2 \rightarrow \text{all})} = 0.04 \pm 0.02$$

in good agreement with the world average value of 0.058 ± 0.008.[5]

E. $K^o\pi^+\Sigma^+$ and $K^+\pi^o\Sigma^+$

Of these final states, the only one which poses no ambiguity problem is the $K^o\pi^+\Sigma^+$ state with a visible $K_1^o \rightarrow \pi^+\pi^-$ decay. The Dalitz plot for this final state is shown in Fig. 13, and the $K^o\pi^+$ mass projection is given in Fig. 14. It is clear that the $K^*(891)\Sigma^+$ channel dominates very strongly. A fit to the Dalitz plot of Fig. 13 gives a cross section for $\pi^+p \rightarrow K^{*+}(891)\Sigma^+$, duly corrected to include all K^* decay modes, of 93 ± 19 μb.

To enhance the statistics on the production angular distribution of $K^*(891)\Sigma^+$, we include events ambiguous between $K^o\pi^+\Sigma^+$ and $K^+\pi^o\Sigma^+$ for which the $K\pi$ mass (whose value is approximately independent of how the ambiguity is resolved) lies in the K^* mass range, 840-940 MeV. The resulting t' distribution, shown in Fig. 15, has the following features:

(i) A peripheral part which dips in the forward direction and has a maximum near -0.3 $(\text{GeV}/c)^2$.

(ii) A marked backward contribution which rises to about 10% of the peripheral maximum.

The peripheral part of the distribution can be compared with that for $\pi^-p \rightarrow K^{*o}(891)\Sigma^o$. For $|t'| < 1$ $(\text{GeV}/c)^2$, our $K^{*+}\Sigma^+$ cross section is 60 ± 14 μb, whereas the data of Abramovich at 3.9 GeV/c give a $K^{*o}\Sigma^o$ cross section in the same t' range of 27 ± 5 μb.[27] The ratio of these is in satisfactory agreement

with the value of 2 expected in the absence of exotic exchanges.

For the study of the K^* decay, we confine ourselves to $K^o\pi^+\Sigma^+$ events with visible K^o_S decays. The distributions of Gottfried-Jackson angle α and Treiman-Yang angle φ are shown in Fig. 16. The corresponding density-matrix elements for $|t'| < 1$ (GeV/c)^2 are,

$$\rho_{00} = -0.02\pm0.09 \quad , \quad \rho_{1,-1} = 0.49\pm0.09 \quad , \quad \text{Re } \rho_{10} = 0.03\pm0.05 \ .$$

The almost total absence of natural parity exchange is evident and in good agreement with the results of Abramovich et al.[27] and Crennell et al.[22] for the $K^{*o}\Sigma^o$ final state. This absence can be readily understood in terms of the known very small $p\bar{\Sigma}K$ coupling. Indeed the smallness of this coupling has already manifested itself earlier in this Paper in connection with the absence of u-channel Σ_α exchange in the backward $K\Sigma$ production.

V. FOUR-BODY AND FIVE-BODY FINAL STATES

A. $K\pi\pi\Sigma$

Figures 17, 18, 19 show $\Sigma\pi$, $K\pi$ and $\pi\pi$ mass spectra from the $K^+\pi^+\pi^-\Sigma^+$, $K^+\pi^+\pi^+\Sigma^-$ and $K^o\pi^+\pi^o\Sigma^+$ final states. The major structures produced are $\Lambda(1405)$, $\Lambda(1520)$, $K^*(891)$, and $\rho(765)$. Cross sections for these are given in Table VI. It is worth noting that the production of these resonances accounts for almost the totality of the cross sections for all the $K\pi\pi\Sigma$ states studied.

As is clear from Table III, the cross section for $K^+\pi^+\pi^-\Sigma^+$ is substantially larger than that for the corresponding state made by π^-p, namely $K^+\pi^-\pi^-\Sigma^+$. The strong ρ^o production which accounts for almost half of the $K^+\pi^+\pi^-\Sigma^+$ cross section may be the major reason for the $\pi^+\pi^-$ asymmetry. It is also possible that Q^+ production via the reaction $\pi^+p \to Q^+\Sigma^+ \to (K\pi\pi)^+\Sigma^+$ may help account for part of the asymmetry. Indeed Crennell et al.[22,28] have reported evidence of structure in the $K\pi\pi$ mass spectrum produced in the reaction

$\pi^- p \rightarrow (K\pi\pi)^0 \Lambda$ at 4.5 and 6 GeV/c. Figure 20 shows our $(K\pi\pi)^+$ mass spectra from the combination of $K^+\pi^+\pi^-\Sigma^+$ and $K^0\pi^+\pi^0\Sigma^+$ final states. The effect of K^* selection is shown in the shaded histogram.

No structure is evident from Fig. 20, although, because of the relatively low energy of this experiment, the Q which extends from about 1100 to 1500 MeV would, if present, occupy almost the whole extent of the $K\pi\pi$ mass spectrum. We can therefore only give a rough upper limit to Q production in the $(K\pi\pi)^+\Sigma^+$ final states. If we assign all events for which the appropriate $K\pi$ combination is in the K^* range and for which $M(K\pi\pi)$ falls in the mass interval 1100 to 1500 MeV to the Q, we obtain for the sequence,

$$\pi^+ p \rightarrow Q^+\Sigma^+ \rightarrow (K^*\pi)^+\Sigma^+ \rightarrow K^+\pi^+\pi^-\Sigma^+$$

a cross section upper limit of 35±6 μb, and for the sequence

$$\pi^+ p \rightarrow Q^+\Sigma^+ \rightarrow (K^*\pi)^+\Sigma^+ \rightarrow K^0\pi^+\pi^0\Sigma^+$$

a cross section upper limit of 33±7 μb. It is worth noting that isospin 1/2 for the Q predicts equal values for these two cross sections just as obtained. Thus an upper limit to $Q^+\Sigma^+$ with Q^+ decaying via $K^*\pi$ to the $K^+\pi^+\pi^-$ and $K^0\pi^+\pi^0$ final states is given by a cross section of 68 μb.

It is interesting to compare this experimental upper limit to what might be expected in terms of real $Q^+\Sigma^+$ production. Brandenburg et al.[29] have shown the existence of a crossover in the differential cross sections for the $K^0 p \rightarrow Q^0 p$ and $\overline{K^0} p \rightarrow \overline{Q^0} p$ reactions. From this one can anticipate a finite Q production in charge exchange and hypercharge exchange processes. From the results of Brandenburg et al., plus the assumption that the couplings of $\bar{K}Q$ to the vector and tensor nonets are the same as those for $\bar{K}K$, we can estimate the expected cross section (see Appendix A for details) to be compared with the above 68 μb, namely 48 μb. Thus our upper limit is completely

consistent with the expectations and suggestive of the idea that most of the $(K^*\pi)^+$ observed between 1100 and 1500 MeV may indeed be Q^+ production.

B. $K\pi\pi\Lambda$

Figures 21, 22 and 23 show $\Lambda\pi$, $K\pi$ and $\pi\pi$ mass spectra from the $K^o\pi^+\pi^+\Lambda$ and $K^+\pi^o\pi^+\Lambda$ final states based entirely on events for which the Λ decays by its $p\pi^-$ mode. Figure 24 shows a $M(\Lambda\pi^+)$ vs $M(K^o\pi^+)$ triangle plot for the $K^o\pi^+\pi^+\Lambda$ state with each event plotted twice. It is clear that production of $\Sigma^+(1385)$, $\Sigma^o(1385)$, $K^{*+}(891)$ dominate the $K\pi\pi\Lambda$ final state, with a significant amount of $K^{*+}(891)\Sigma^+(1385)$ simultaneous production also being present. Cross sections for these channels are given in Table VII.

We have attempted a study of the $K^{*+}(891)\Sigma^+(1385)$ final state by selecting events for which $1.33 \leq M(\Lambda\pi^+) \leq 1.44$ GeV and $0.83 \leq M(K^o\pi^+ \text{ or } K^+\pi^o) \leq 0.95$ GeV. We estimate that the sample of 82 events so obtained contains about 70% actual $K^{*+}(891)\Sigma^+(1385)$ events, the remainder being principally single resonance production. With a 30% background, it is clear that some caution must be exercised in the interpretation of the results. Figure 25 shows the t' distribution for the 82 events selected in the manner just defined. The data are clearly quite peripheral with about 2/3 of the events having $|t'| \leq 0.3$ $(\text{GeV}/c)^2$. Density matrix elements for the $\Sigma^+(1385)$ and $K^*(891)$ decays are given in Table VIII, with two choices of t' cuts. The spin orientations of both $\Sigma^+(1385)$ and $K^{*+}(891)$ appear to be essentially random. Whereas double resonance production without strangeness exchange is strongly dominated by pion exchange, pseudoscalar exchange in the $K^{*+}(891)\Sigma^+(1385)$ process appears to be limited to roughly no more than 30% of the cross section.

C. $K\bar{K}\pi^+p$

1. General Features of $K^+K^-\pi^+p$ and $K^0\bar{K}^0\pi^+p$

Figure 26a shows a triangle plot for the final state $K^+K^-\pi^+p$. Figures 27, 28, 29, 30 show $p\pi^+$, K^+K^-, $K^-\pi^+$ and pK^- mass projections. Figure 31 shows a mass projection of the K^+K^- system recoiling against the $\Delta(1236)$. The main features of the data are the following

(i) There is substantial production of $\Delta^{++}(1236)$, $\overline{K^{*0}}(891)$, $\Lambda(1520)$, and $\varphi(1019)$.

(ii) In association with Δ^{++}, there is some K^+K^- structure in the mass region 1200-1350 MeV plus a broad enhancement near threshold although there seems to be essentially no φ production. The structure around 1200-1350 MeV presumably represents a superposition of f and A_2^0 decays.

Figures 26b and 26c show triangle plots for the final state $K^0\bar{K}^0\pi^+p$ with single-vee and double-vee events respectively. Figures 32, 33, 34, 35 show $p\pi^+$, $K^0\bar{K}^0$, $K^0\pi^+$ and pK^0 mass projections for (a) $K_S^0K_S^0\pi^+p$ (2 vee decays seen), (b) $K_S^0K^0\pi^+p$ (one vee decay seen), and (c) $K_S^0K_L^0\pi^+p$ (by calculation from two-vee and one-vee events). Again production of $\Delta^{++}(1236)$, $K^{*+}(891)$, and $\varphi(1019)$ is clearly in evidence. Cross sections for resonance production in both $K^+K^-\pi^+p$ and $K^0\bar{K}^0\pi^+p$ are given in Table IX and account for a large fraction of the overall cross section.

2. $\varphi(1019)\pi^+p$

Figures 28 and 33 show clear evidence for production of φ mesons. Figure 36 shows a $\varphi\pi^+p$ Dalitz plot, using both $K^+K^-\pi^+p$ and $K^0\bar{K}^0\pi^+p$ final states with a mass cut $1.009 < M(K\bar{K}) < 1.029$ GeV. There is no structure, and, in particular, a 90% confidence upper limit to $\varphi\Delta(1236)$ production of 2 μb can be set. Using the value (0.70 ± 0.08) mb for the $\pi^+p \to \omega\Delta^{++}$ cross section at this energy,[30] we obtain an upper limit to the cross-section ratio,

$$R^2 = \frac{\sigma(\pi^+ p \to \varphi\Delta^{++})}{\sigma(\pi^+ p \to \omega\Delta^{++})} < \frac{1}{350} \quad . \qquad (14)$$

In the framework of the quark model, the smallness of R^2 can be interpreted in terms of the quark content of the φ and ω mesons; namely they are almost entirely $\lambda\bar{\lambda}$ and $n\bar{n} + p\bar{p}$ respectively. Alexander et al.[31] have related R to the ω-φ mixing angle θ_1 by,

$$R = \left|\frac{\langle\pi^+ p|\varphi\Delta^{++}\rangle}{\langle\pi^+ p|\omega\Delta^{++}\rangle}\right| = \left|\frac{\cos\theta_1 - \sqrt{2}\sin\theta_1}{\sin\theta_1 + \sqrt{2}\cos\theta_1}\right| = \tan(\theta_o - \theta_1) \ , \qquad (15)$$

where $\theta_o = \tan^{-1}(1/\sqrt{2}) = 35.3^o$. This relation gives a model-dependent determination of the mixing angle θ_1, but is independent of the masses of mesons belonging to the vector nonet. From our upper limit on R, we find that $|\theta_o - \theta_1| < 3.1^o$, and hence that, to 90% confidence level, $32.2^o < \theta_1 < 38.4^o$. This result is in good agreement with the values based on the Gell-Mann-Okubo mass formula, namely $39.5^o \pm 1.1^o$ for the quadratic form and $36.4^o \pm 1.1^o$ for the linear form. It is also compatible with the squared coupling constant ratio $g^2_{\varphi\rho\pi}/g^2_{\omega\rho\pi} \approx 1/600$ determined collectively from the experimental ω and φ widths, the $\varphi \to \rho\pi$ branching fraction, and the ratio between the phase spaces available for $\varphi \to \rho\pi$ and $\omega \to \rho\pi$.[32]

It is worth pointing out that φ production in the $\varphi\pi^+ p$ final state has a flat angular distribution; and, in particular, shows no peripheral peaking. This feature, already observed in the reaction $\pi^- p \to \varphi n$ (Ref. 7) seems to be characteristic of φ production by incident pions.

3. $\underline{K\bar{K}\Delta^{++}(1236)}$

As shown by Table IX Δ^{++} production represents a significant part of the $K\bar{K}\pi^+ p$ final state. The distribution of t' between incident proton and final Δ^{++} is shown in Fig. 37, and indicates strongly peripheral behavior. The

distributions of Gottfried-Jackson and Yang-Treiman angles for the Δ^{++} in the low t' region ($|t'| < 0.3$ (GeV/c)^2) are shown in Fig. 38 and are very suggestive of dominance by pion exchange. The corresponding decay distributions for the K^+K^- system are shown in Fig. 39. To the extent that pion exchange dominates these correspond roughly to the inelastic process $\pi^+\pi^- \to K^+K^-$. Unfortunately the present statistics are too limited to warrant a more detailed study of this process.

D. $K^+\pi^+\pi^-\pi^0\Sigma^+$

The cross sections for the five-body final states are sufficiently small that it is unprofitable with the present data sample to attempt detailed study. We confine ourselves to examining the $\pi^+\pi^-\pi^0$ mass spectrum which is shown in Fig. 40. There is clear and substantial ω production, the cross section for the $K^+\omega\Sigma^+$ final state (including only the $\pi^+\pi^-\pi^0$ ω decay mode) being 8±3 μb. This is to be compared with the known significant ω production in the reaction $\pi^-p \to K^0\pi^+\pi^-\pi^0\Lambda$ at 3 to 4 GeV/c.[7]

VI. SUMMARY

We have made a fairly detailed study of strange particle production in π^+p collisions at 3.7 GeV/c. The major results can be summarized as follows:

(1) The overall strange particle production cross section is about 1.3 mb, of which roughly 30% is $K\bar{K}$ plus anything and 70% is YK plus anything.

(2) For three final states looked at in some detail, $K^+\Sigma^+$, $K^{*+}(891)\Sigma^+$ and $K^+\Sigma^+(1385)$, comparison with cross sections for the corresponding $K^0\Sigma^0$ states produced by π^-p collisions shows results consistent with the absence of exotic meson exchanges near the forward direction.

(3) Comparison of $\pi^+p \to K^+\Sigma^+$ with $K^-p \to \pi^-\Sigma^+$ shows no strong disagreement with the expectations from K_V, K_T exchange degeneracy. On the other hand,

comparison of $\pi^+ p \to K^+\Sigma^+(1385)$ with $K^- p \to \pi^-\Sigma^+(1385)$ shows gross violation of these expectations.

(4) Resonance production is significant in all multi-body final states. Resonance production for at least one outgoing particle pair accounts for most of the cross sections of the four-body final states.

(5) The only clear example of double resonance production seen was $K^{*+}(891)\Sigma^+(1385)$, but unlike its nonstrange counterparts, this process is not dominated by pseudoscalar exchange.

(6) There is a small but significant amount of φ production in the reaction $\pi^+ p \to \varphi\pi^+ p$. Within the statistical uncertainties, none of that φ production is associated with $\Delta^{++}(1236)$.

(7) The production and decay angular distributions of the $K^+\Sigma^+(1385)$ and $K^*(891)\Sigma^+$ final states have the following main features:

(a) The $K^+\Sigma^+(1385)$ production is qualitatively similar to such processes as $K^+ p \to K^o\Delta^{++}(1236)$ but appears to deviate more from the Stodolsky-Sakurai model predictions.

(b) The $K^*(891)\Sigma^+$ production seems to involve practically zero pseudoscalar exchange. The result, in agreement with $\pi^- p \to K^{*o}(891)\Sigma^o$ data, is presumably a consequence of the smallness of the ΣKN coupling.

(8) We are unable to obtain more than an upper limit to the cross section for Q^+ production via the process $\pi^+ p \to Q^+\Sigma^+ \to (K\pi\pi)^+\Sigma^+$. This upper limit lies close to the value which might be expected from the crossover seen in $K^o p \to Q^o p$ and $\overline{K^o} p \to \overline{Q^o} p$.

We want to express our appreciation to our scanning, measuring and programming staff, and to the FSD Operations Group under Howard White.

APPENDIX A

Estimate of Expected Cross Section for the Process $\pi^+ p \to Q^+ \Sigma^+$

We estimate Q^+ production to be expected in the reaction $\pi^+ p \to Q^+ \Sigma^+$ from the cross-over observed by Brandenburg et al. in their study of the reactions

$$K^o p \to Q^o p \to K^{*+} \pi^- p \to K_S^o \pi^+ \pi^- p \qquad (16a)$$

$$\overline{K^o} p \to \overline{Q^o} p \to K^{*-} \pi^+ p \to K_S^o \pi^- \pi^+ p \qquad (16b)$$

over a range of incident momenta whose average is about 7 GeV/c. Brandenburg et al. determined the forward differential cross sections for (16), defining the Q by the mass region $1.1 < M(K\pi\pi) < 1.5$ GeV and the K^* by the region $0.86 < M(K\pi) < 0.92$ GeV, with the following results,

$$\left.\frac{d\sigma}{dt'}(Q^o p)\right|_{t'=0} = 0.83 \text{ mb}/(\text{GeV}/c)^2$$

$$\left.\frac{d\sigma}{dt'}(\overline{Q^o} p)\right|_{t'=0} = 1.36 \text{ mb}/(\text{GeV}/c)^2 \ .$$

Isospin considerations lead to a correction factor of 9/2 to take account of the undetected $K^*\pi$ decay modes of Q^o.

If we assume that the t-channel exchanges relevant to Q production are the same as those relevant to K production in the corresponding reactions, and if we neglect the effects of mass differences between Q and K, we can write, for small t'

$$\frac{\frac{d\sigma}{dt'}(\pi^+ p \to Q^+ \Sigma^+)}{\frac{d\sigma}{dt'}(\pi^+ p \to K^+ \Sigma^+)} \approx \left\{ \frac{\frac{d\sigma}{dt'}(\overline{K^o} p \to \overline{Q^o} p) - \frac{d\sigma}{dt'}(K^o p \to Q^o p)}{\frac{d\sigma}{dt'}(\overline{K^o} p \to \overline{K^o} p) - \frac{d\sigma}{dt'}(K^o p \to K^o p)} \right\}^2 \frac{\frac{d\sigma}{dt'}(K^o p \to K^o p)}{\frac{d\sigma}{dt'}(K^o p \to Q^o p)} \cdot \qquad (17)$$

The squaring of the bracketed quantity on the right side of (17) reflects the fact that its dominant contribution is an interference between non-pomeron

and pomeron exchange and hence is linear in the non-pomeron amplitude.[29]

We substitute for $\frac{d\sigma}{dt}(\overline{K^o}p \to \overline{K^o}p)$ and $\frac{d\sigma}{dt}(K^o p \to K^o p)$ the optical points, taking for the total cross sections at 7 GeV/c, $\sigma_t(\overline{K^o}p) = \sigma_t(K^- n) = 21.0$ mb and $\sigma_t(K^o p) = \sigma_t(K^+ n) = 17.2$ mb.[33] Thus we find that the right side of (17) amounts to 0.41, from which $\sigma(\pi^+ p \to Q^+\Sigma^+ \to (K^*\pi)^+\Sigma^+) \approx 0.41\ \sigma(\pi^+ p \to K^+\Sigma^+)$ = 43 μb. Taking account of the fact that the channel $K^+\pi^o\pi^o\Sigma^+$ is not detected, and of the fact that the K^* mass interval in our analysis (0.84 - 0.94 GeV) is somewhat larger than that used in the work of Brandenburg et al. (0.86-0.92 GeV), we predict for our effective $\sigma(\pi^+ p \to Q^+\Sigma^+)$ the cross section of 48 μb given in Section V-A. It should be noted that in (17), we have evaluated the right side at the mean momentum of Brandenburg et al., namely 7 GeV/c, and the left side at our momentum of 3.7 GeV/c on the assumption that the ratios involved are essentially energy independent.

REFERENCES

* Work supported by the U. S. Atomic Energy Commission.

† Present address: Department of Physics, David Lipscomb College, Nashville, Tennessee 37203.

†† Present address: Department of Physics, Princeton University, Princeton, New Jersey 08540.

‡ On sabbatical leave from University of California, Berkeley; Guggenheim Fellow at CERN.

‡‡ Present address: Fysich Laboratorium, Toernooiveld, Nijmegen, The Netherlands.

1. W. Chinowsky et al., Phys. Rev. 165, 1466 (1968); David Gordon Brown, $\pi^+ p$ 4-Prong Interactions Between 3 and 4 GeV/c, UCRL-18254 (Ph.D. Thesis), 1968 (unpublished).

2. Alvarez Group Program Note P-117 (unpublished); Alvarez Group Program Note P-126 (unpublished).

3. A. Citron, W. Galbraith, T. F. Kycia, B. A. Leontic, R. H. Phillips, A. Rousset, and P. H. Sharp, Phys. Rev. 144, 1101 (1966).

4. William Ralph Butler, Strange Particle Production in $\pi^+ p$ Interactions Near 3.7 GeV/c, UCRL-19845 (Ph.D. Thesis), 1970 (unpublished).

5. Particle Data Group, Phys. Letters 39B, 1 (1972).

6. M. Aderholz et al., Nucl. Physics B11, 259 (1970).

7. O. I. Dahl, L. M. Hardy, R. I. Hess, J. Kirz and D. H. Miller, Phys. Rev. 163, 1377 (1967).

8. S. M. Pruss et al., Phys. Rev. Letters 23, 189 (1969); K. S. Han et al., Phys. Rev. Letters 24, 1353 (1970).

9. A. Bashian et al., Phys. Rev. D4, 2667 (1971).

10. C. W. Akerlof, P. K. Caldwell, C. T. Coffin, P. Kalbaci, D. I. Meyer, P. Schmueser and K. C. Stanfield, Phys. Rev. Letters 27, 539 (1971); A.

Bashian et al., Phys. Rev. D4, 2680 (1971).

11. K. W. Lai and J. Louie, Nucl. Physics B19, 205 (1970).

12. O. I. Dahl, L. M. Hardy, R. I. Hess, J. Kirz, D. H. Miller and J. A. Schwartz, Phys. Rev. 163, 1430 (1967).

13. M. Abramovich et al., Nucl. Physics B27, 477 (1971).

14. Birmingham-Glasgow-London (I.C.)-Oxford-Rutherford Collaboration, Phys. Rev. 152, 1148 (1966).

15. L. Moscoso et al., Nucl. Physics B36, 332 (1972).

16. J. S. Loos, U. E. Kruse and E. L. Goldwasser, Phys. Rev. 173, 1330 (1968).

17. V. Barger, Phys. Rev. 179, 1371 (1969).

18. B. Kayser and F. Hayot, SLAC-PUB-1003 (1972).

19. R. L. Eisner, R. D. Field, S. U. Chung and M. Aguilar-Benitez, BNL Report 16874 (1972).

20. P. Kalbaci, C. W. Akerlof, P. K. Caldwell, C. T. Coffin, D. I. Meyer, P. Schmueser and K. C. Stanfield, Phys. Rev. Letters 27, 74 (1971).

21. L. Stodolsky and J. J. Sakurai, Phys. Rev. Letters 11, 90 (1963).

22. D. J. Crennell, H. A. Gordon, K. W. Lai and J. M. Scarr, Phys. Rev. D6, 1221 (1972).

23. M. Aguilar-Benitez, S. U. Chung, R. L. Eisner and N. P. Samios, Phys. Rev. D6, 29 (1972).

24. D. Cline, J. Matos and D. D. Reeder, Phys. Rev. Letters 23, 1318 (1969); A. Firestone, G. Goldhaber, A. Hirata, D. Lissauer, and G. H. Trilling, Phys. Rev. Letters 25, 958 (1970).

25. D. D. Carmony et al., Purdue University Preprint COO-1428-66 (1970); G. Bakker et al., Nucl. Physics B16, 53 (1970).

26. G. H. Trilling, Nucl. Physics B40, 13 (1972).

27. M. Abramovich et al., quoted in Ref. 23 above.

28. D. J. Crennell, G. R. Kalbfleisch, K. W. Lai, J. M. Scarr, and T. G. Schumann, Phys. Rev. Letters 19, 44 (1967).

29. G. W. Brandenburg et al., Phys. Rev. Letters 28, 932 (1972).

30. Benjamin C. Shen, Resonance Production in Pion-Proton Interactions at 3.65 BeV/c and 3.7 BeV/c, UCRL-16170 (Ph.D. Thesis), 1965 (unpublished).

31. G. Alexander, H. Lipkin and F. Scheck, Phys. Rev. Letters 17, 412 (1966).

32. J. Yellin, Phys. Rev. 147, 1080 (1966).

33. W. Galbraith, E. W. Jenkins, T. F. Kycia, B. A. Leontic, R. H. Phillips, A. L. Read, and R. Rubinstein, Phys. Rev. 138, B913 (1965).

Table I. Microbarn equivalents for different sections of the film.

Total sample	(0.230±0.004) μb/event
Sample where all events were recorded	(0.542±0.009) μb/event
Sample where not all events were recorded*	(0.399±0.007) μb/event

*2-prongs without stopping protons were not recorded.

Table II. Cross sections.

Final state	Cross section (μb)	Final state	Cross section (μb)
$K^+\Sigma^+$	104±17	$K^o_S K^o_L \pi^+ p$	24±5
$K^+\pi^o\Sigma^+$	127±23	$K^o\bar{K}^o\pi^+ p$ (total)	66±7
$K^+\pi^+\Sigma^o$	44±5	$K^+\pi^+\pi^-\pi^o\Sigma^+$	25±9
$K^o\pi^+\Sigma^+$	99±17	$K^+\pi^+\pi^+\pi^-\Sigma^o$	3±1.2
$K^+\pi^+\Lambda$	99±7	$K^+\pi^+\pi^+\pi^o\Sigma^-$	5±3
$K^+\bar{K}^o p$	71±9	$K^o\pi^+\pi^+\pi^-\Sigma^+$	5±4
$K^+\pi^+\pi^-\Sigma^+$	110±15	$K^o\pi^+\pi^+\pi^+\Sigma^-$	4±2
$K^+\pi^+\pi^+\Sigma^-$	19±4	$K^+\pi^+\pi^+\pi^-\Lambda$	20±3
$K^o\pi^+\pi^o\Sigma^+$	62±13	$K^o\pi^+\pi^+\pi^o\Lambda$	26±6
$K^o\pi^+\pi^+\Sigma^o$	22±6	$K^+\bar{K}^o\pi^+\pi^- p$	14±3
$K^+\pi^+\pi^o\Lambda$	145±20	$K^o_S K^o_S \pi^+\pi^o p$	3±1.5
$K^o\pi^+\pi^+\Lambda$	61±9	$K^o_S K^o_S \pi^+\pi^+ n$	1.5±1
$K^+K^-\pi^+ p$	81±8	$K^o K^-\pi^+\pi^+ p$	18±4
$K^+\bar{K}^o\pi^o p$	57±8		
$K^+\bar{K}^o\pi^+ n$	42±8	$K^+K^+\Xi^o$	4±1.3
$K^o_S K^o_S \pi^+ p$	21±4	$K^+K^+\pi^+\Xi^-$	1±1

Table III. Comparison of π^+p and π^-p cross sections.

Final state	π^-p at 3.9 GeV/c	π^+p at 3.7 GeV/c
$K^+\pi^\pm\Sigma^o$	43±7	44±5
$K^o\pi^\pm\Sigma^+$	42±8	99±17
$K^+\pi^\pm\Lambda$	99±13	99±7
$K^\pm K^o p$	80±13	71±9
$K^+\pi^\pm\pi^-\Sigma^+$	24±6	110±15
$K^+\pi^\pm\pi^+\Sigma^-$	20±4	19±4
$K^o\pi^\pm\pi^o\Sigma^+$	34±9	62±13
$K^o\pi^\pm\pi^+\Sigma^o$	38±11	22±6
$K^+\pi^\pm\pi^o\Lambda$	103±13	145±20
$K^o\pi^\pm\pi^+\Lambda$	122±14	61±9
$K^+K^-\pi^\pm p$	63±20	81±8
$K^\pm K^o\pi^o p$	35±8	57±8
$K^\pm K^o\pi^+ n$	71±14	42±8
$K_S^oK_S^o\pi^\pm p$	12±4	21±4
$K_S^oK_L^o\pi^\pm p$	32±6	20±5
$K^o\overline{K^o}\pi^\pm p$	56±7	66±7

Table IV. Tests of relations (8) and (9).

Reaction	Momentum (GeV/c)	$\int_{-0.6}^{-0.02} \frac{d\sigma}{dt} dt$ (μb)	Corrected[a] $\int_{-0.6}^{-0.02} \frac{d\sigma}{dt} dt$ (μb)	Technique	Reference
$\pi^+ p \rightarrow K^+\Sigma^+$	3.7	72±12	72±12	Bub. Ch.	This expt.
$\pi^+ p \rightarrow K^+\Sigma^+$	4.0	51±3[b]	56±3	Counters	Ref. 8
$\pi^- p \rightarrow K^o\Sigma^o$	3.9	22.5±4.5	48±10	Bub. Ch.	Ref. 13
$\pi^- p \rightarrow K^o\Sigma^o$	4.0	33±5	72±12	Bub. Ch.	Ref. 12
$K^- p \rightarrow \pi^-\Sigma^+$	3.5	84±8	79±8	Bub. Ch.	Ref. 14
$K^- p \rightarrow \pi^-\Sigma^+$	3.95	70±4	75±5	Bub. Ch.	Ref. 15
$K^- p \rightarrow \pi^-\Sigma^+$	4.1	69±21	76±23	Bub. Ch.	Ref. 16

a. Correction consists of two parts: (i) conversion to 3.7 GeV/c incident momentum assuming $P^{-1.2}$ dependence of the cross section, (ii) multiplication of $K^o\Sigma^o$ final state cross sections by a factor of 2.

b. Extrapolated to $-t = 0.02$ $(GeV/c)^2$ since measurement goes down to only 0.05 $(GeV/c)^2$.

Table V. Tests of relations (11) and (12).

Reaction	Momentum (GeV/c)	$\int_{-0.64}^{-0.04} \frac{d\sigma}{dt} dt$ (μb)	Corrected[a] $\int_{-0.64}^{-0.04} \frac{d\sigma}{dt} dt$ (μb)	Technique	Reference
$\pi^+ p \rightarrow K^+\Sigma^+(1385)$	3.7	19±6	19±6	Bub. Ch.	This expt.
$\pi^- p \rightarrow K^o\Sigma^o(1385)$	4.5	10±2	26±5	Bub. Ch.	Ref. 22
$K^- p \rightarrow \pi^-\Sigma^+(1385)$	3.5	60±11	55±10	Bub. Ch.	Ref. 14
$K^- p \rightarrow \pi^-\Sigma^+(1385)$	3.9	49±6	54±7	Bub. Ch.	Ref. 23

a. Correction consists of two parts: (i) conversion to 3.7 GeV/c incident momentum assuming $P^{-1.5}$ dependence of the cross section, (ii) multiplication of $K^o\Sigma^o(1385)$ final cross section by a factor of 2.

Table VI. Cross sections for resonance production in $K\pi\pi\Sigma$ states.

Final state	Cross section (μb)
$K^+\pi^+\Lambda(1405)$, $\Lambda(1405) \rightarrow (\Sigma\pi)^o$	45±15
$K^+\pi^+\Lambda(1520)$, $\Lambda(1520) \rightarrow (\Sigma\pi)^o$	14±7
$K^{*+}(891)\pi^o\Sigma^+$	42±15
$K^{*o}(891)\pi^+\Sigma^+$	42±15
$K^+\rho^o(765)\Sigma^+$	49±14
$K^o\rho^+(765)\Sigma^+$	21±14

Table VII. Cross sections for resonance production in $K\pi\pi\Lambda$ states.

Final state	Cross section (μb)
$K^+\pi^o\Sigma^+(1385)$[a], $\Sigma^+(1385) \to \Lambda\pi^+$	42±9
$K^o\pi^+\Sigma^+(1385)$, $\Sigma^+(1385) \to \Lambda\pi^+$	35±7
$K^+\pi^+\Sigma^o(1385)$, $\Sigma^o(1385) \to \Lambda\pi^o$	12±7
$K^{*+}(891)\Lambda\pi^+$, $K^{*+}(891) \to (K\pi)^+$	51±12
$K^{*+}(891)\Sigma^+(1385)$, $\left\{ \begin{array}{l} K^{*+}(891) \to (K\pi)^+ \\ \Sigma^+(1385) \to \Lambda\pi^+ \end{array} \right\}$	31±12

a. This includes all $K^+\pi^o$ states, resonant and nonresonant. The same convention is followed for the other final states.

Table VIII. Density matrix elements for $K^{*+}(891)\Sigma^{+}(1385)$ final state.

	$\|t'\| < 0.3$ (GeV/c)^2	$\|t'\| < 1.0$ (GeV/c)^2
ρ_{00}	0.30±0.10	0.32±0.08
Re ρ_{10}	-0.07±0.06	-0.09±0.05
$\rho_{1,-1}$	0.08±0.08	0.08±0.06
ρ_{33}	0.17±0.08	0.20±0.06
Re ρ_{31}	-0.06±0.07	-0.12±0.07
Re $\rho_{3,-1}$	-0.06±0.07	-0.04±0.06

Table IX. Cross sections for resonance production in $K\bar{K}\pi^+p$ states.

		Cross section (μb)
$K^+K^-\Delta^{++}(1236)$		40±7
$K^+\overline{K^{*o}}(891)p$,	$K^{*o}(891) \rightarrow (K\pi)^o$	24±6
$K^+\pi^+\Lambda(1520)$,	$\Lambda(1520) \rightarrow (\bar{K}N)^o$	16±7
$\varphi(1019)\pi^+p$,	$\varphi(1019) \rightarrow$ all	10±3
$\varphi(1019)\Delta^{++}(1236)$,	$\varphi(1019) \rightarrow$ all	< 2
$K_S^oK_S^o\Delta^{++}(1236)$		11±5
$K_S^oK_L^o\Delta^{++}(1236)$		< 5
$K^{*+}(891)\overline{K^o}p$,	$K^{*+}(891) \rightarrow (K\pi)^+$	29±10

FIGURE CAPTIONS

Fig. 1. Most common strange-particle topologies studied.

Fig. 2. Scatter plot of azimuth versus cosine of polar angle for $\Sigma^+ \rightarrow n\pi^+$ decays.

Fig. 3. Distribution of decay cosine of photon in the Σ^o rest frame with respect to (a) incident π^+; (b) outgoing π^+; (c) outgoing K^+, for 176 events ambiguous between (5) and (6); (d) scatter plot of decay cosine with respect to the outgoing pion versus the decay cosine with respect to the kaon for events not in the forward peak of (a); (e) same distribution as in (a) for events which fit (6) unambiguously.

Fig. 4. (a) Differential cross section in the center of mass for $\pi^+ p \rightarrow K^+\Sigma^+$ based on 144 $\Sigma^+ \rightarrow n\pi^+$ decays; (b) t distribution near the forward direction; (c) u distribution near the backward direction. No events are observed in the angular range $0.3 > \cos\theta_{prod} > -0.3$.

Fig. 5. Dalitz plot for the $K^+\pi^+\Lambda$ final state.

Fig. 6. $\Lambda\pi^+$ mass spectrum from the $K^+\pi^+\Lambda$ final state.

Fig. 7. Differential cross section for the $K^+\Sigma^+(1385)$ final state.

Fig. 8. (a) Distribution of decay cosine of $\Sigma(1385)$ in Gottfried-Jackson frame; (b) distribution of decay azimuth.

Fig. 9. Dalitz plot for the $K^+\pi^+\Sigma^o$ final state.

Fig. 10. $\Sigma^o\pi^+$ mass spectrum from the $K^+\pi^+\Sigma^o$ final state.

Fig. 11. Dalitz plot for the $K^+\bar{K}^o p$ final state.

Fig. 12. $K^+\bar{K}^o$ mass spectrum from the $K^+\bar{K}^o p$ final state.

Fig. 13. Dalitz plot for the $K^o\pi^+\Sigma^+$ final state, including both decay modes of the Σ^+.

Fig. 14. $K^o\pi^+$ mass spectrum from $K^o\pi^+\Sigma^+$ final state.

Fig. 15. Differential cross section for the $K^{*+}(891)\Sigma^+$ final state.

Fig. 16. (a) Decay cosine and (b) azimuth in Gottfried-Jackson frame for $K^*(891)$ from the $K^{*+}\Sigma^+$ final state.

Fig. 17. $\Sigma\pi$ mass spectra from $K\pi\pi\Sigma$ final states: (a) $\Sigma^+\pi^o$ from $K^o\pi^+\pi^o\Sigma^+$, (b) $\Sigma^+\pi^-$ from $K^+\pi^+\pi^-\Sigma^+$, (c) $\Sigma^-\pi^+$ from $K^+\pi^+\pi^+\Sigma^-$.

Fig. 18. $K\pi$ mass spectra from $K\pi\pi\Sigma$ final states: (a) $K^o\pi^o$ from $K^o\pi^+\pi^o\Sigma^+$, (b) $K^o\pi^+$ from $K^o\pi^+\pi^o\Sigma^+$, (c) $K^+\pi^-$ from $K^+\pi^+\pi^-\Sigma^+$.

Fig. 19. $\pi\pi$ mass spectra from $K\pi\pi\Sigma$ final states: (a) $\pi^+\pi^-$ from $K^+\pi^+\pi^-\Sigma^+$, (b) $\pi^+\pi^o$ from $K^o\pi^+\pi^o\Sigma^+$.

Fig. 20. $(K\pi\pi)^+$ mass spectrum from $K^+\pi^+\pi^-\Sigma^+$ and $K^o\pi^+\pi^o\Sigma^+$ final states. Shaded portion has additional requirement that one $(K\pi)^+$ or $(K\pi)^o$ combination be in the K^* region.

Fig. 21. $\Lambda\pi$ mass spectra from $K\pi\pi\Lambda$ final states: (a) $\Lambda\pi^+$ from $K^o\pi^+\pi^+\Lambda$, (b) $\Lambda\pi^+$ from $K^+\pi^+\pi^o\Lambda$, (c) $\Lambda\pi^o$ from $K^+\pi^+\pi^o\Lambda$.

Fig. 22. $K\pi$ mass spectra from $K\pi\pi\Lambda$ final states: (a) $K^o\pi^+$ from $K^o\pi^+\pi^+\Lambda$, (b) $K^+\pi^o$ from $K^+\pi^+\pi^o\Lambda$.

Fig. 23. $\pi\pi$ mass spectra from $K\pi\pi\Lambda$ final states: (a) $\pi^+\pi^+$ from $K^o\pi^+\pi^+\Lambda$, (b) $\pi^+\pi^o$ from $K^+\pi^+\pi^o\Lambda$.

Fig. 24. Triangle plot for $K^o\pi^+\pi^+\Lambda$ system; each event is plotted twice.

Fig. 25. Differential cross section for $K^{*+}(891)\Sigma^+(1385)$ final state.

Fig. 26. Triangle plots for $K\bar{K}\pi^+p$ final states: (a) $K^+K^-\pi^+p$, (b) $K_S^oK^o(\text{unseen})\pi^+p$, (c) $K_S^oK_S^o\pi^+p$.

Fig. 27. $p\pi^+$ mass spectrum from $K^+K^-\pi^+p$ final state.

Fig. 28. K^+K^- mass spectrum from $K^+K^-\pi^+p$ final state. Inset shows spectrum in 4-MeV bins near the φ mass.

Fig. 29. $K^-\pi^+$ mass spectrum from $K^+K^-\pi^+p$ final state.

Fig. 30. pK^- mass spectrum from $K^+K^-\pi^+p$ final state.

Fig. 31. K^+K^- mass spectrum from $K^+K^-\Delta^{++}(1236)$ final state. Shaded region has additional requirement that $K^*(891)$ and $\Lambda(1520)$ events are removed.

Fig. 32. $p\pi^+$ mass spectrum from $K^0\bar{K}^0\pi^+p$ final state. (a) $K_S^0K_S^0\pi^+p$ events, (b) $K_S^0K^0$(unseen)π^+p events, (c) $K_S^0K_L^0\pi^+p$ events as deduced from (a) and (b).

Fig. 33. $K^0\bar{K}^0$ mass spectrum from $K^0\bar{K}^0\pi^+p$ final state. Categories (a), (b), (c) are the same as for Fig. 32.

Fig. 34. $K^0\pi^+$ mass spectrum from $K^0\bar{K}^0\pi^+p$ final state. Categories (a), (b), (c) are the same as for Fig. 32.

Fig. 35. pK^0 mass spectrum from $K^0\bar{K}^0\pi^+p$ final state. Categories (a), (b), (c) are the same as for Fig. 32.

Fig. 36. $\phi\pi^+p$ Dalitz plot taken from both $K^+K^-\pi^+p$ and $K^0\bar{K}^0\pi^+p$ final states.

Fig. 37. Differential cross section for Δ^{++} production in the final state $K^+K^-\Delta^{++}$.

Fig. 38. Distribution of (a) decay cosine and (b) decay azimuth in the Gottfried-Jackson frame for Δ^{++} from $K^+K^-\Delta^{++}$ final state with the cut $-t' < 0.3$ (GeV/c)^2.

Fig. 39. Distribution of (a) decay cosine and (b) decay azimuth in the Gottfried-Jackson frame for K^+K^- system from $K^+K^-\Delta^{++}$ final state with the cut $-t' < 0.3$ (GeV/c)^2.

Fig. 40. $\pi^+\pi^-\pi^0$ mass spectrum from final state $K^+\pi^+\pi^-\pi^0\Sigma^+$.

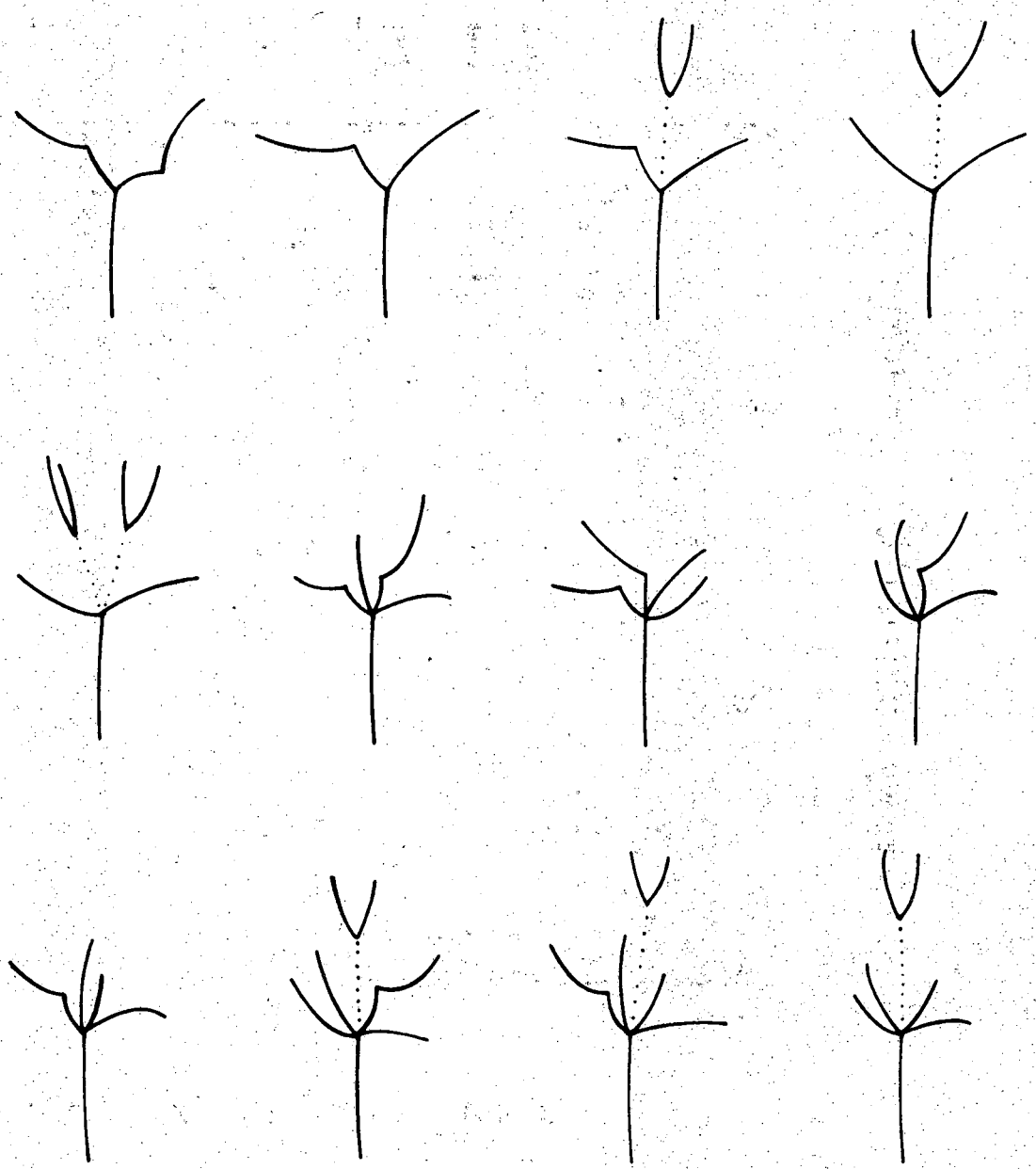

XBL 706-1117

Fig. 1

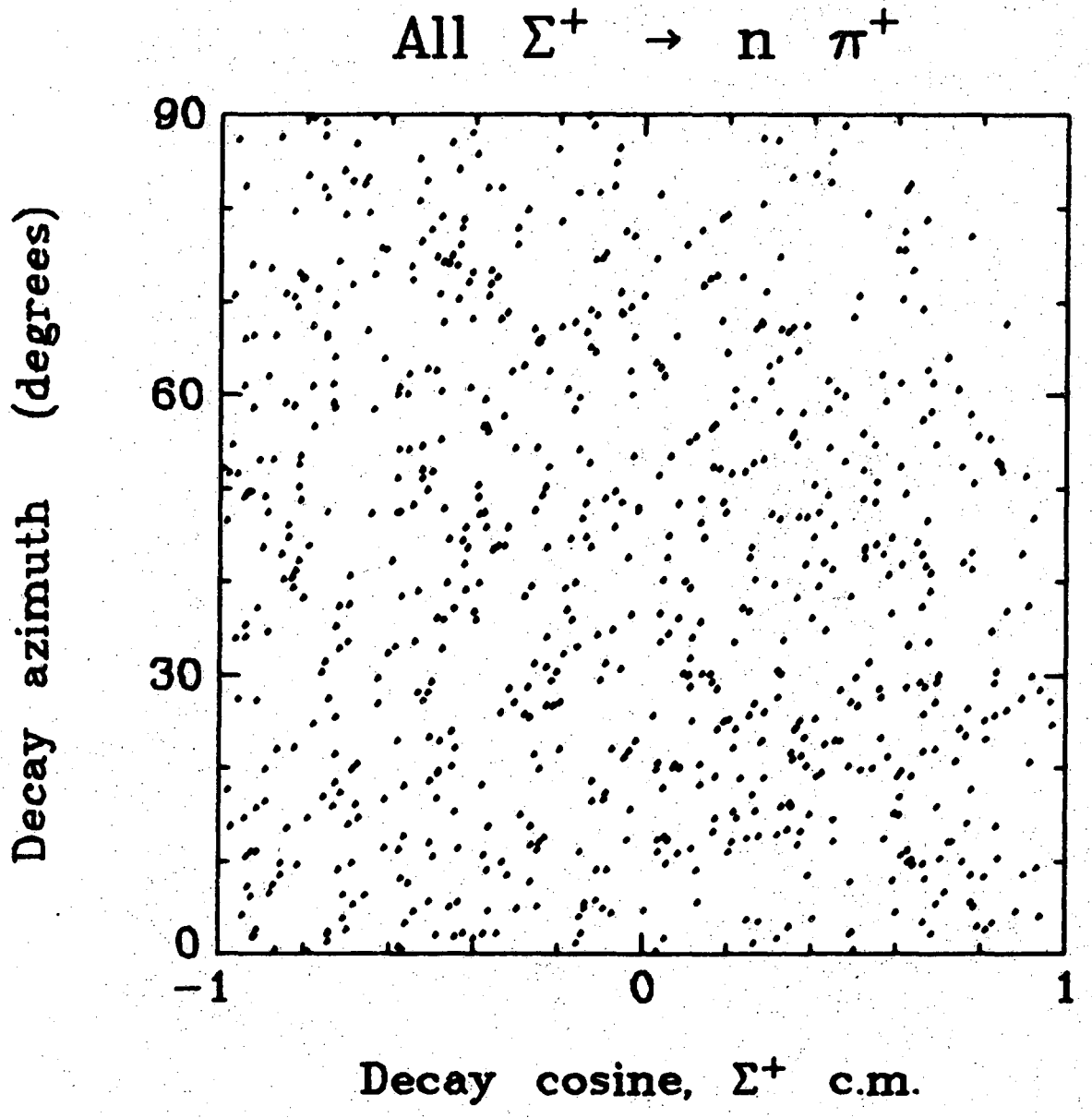

XBL 729-1843

Fig. 2

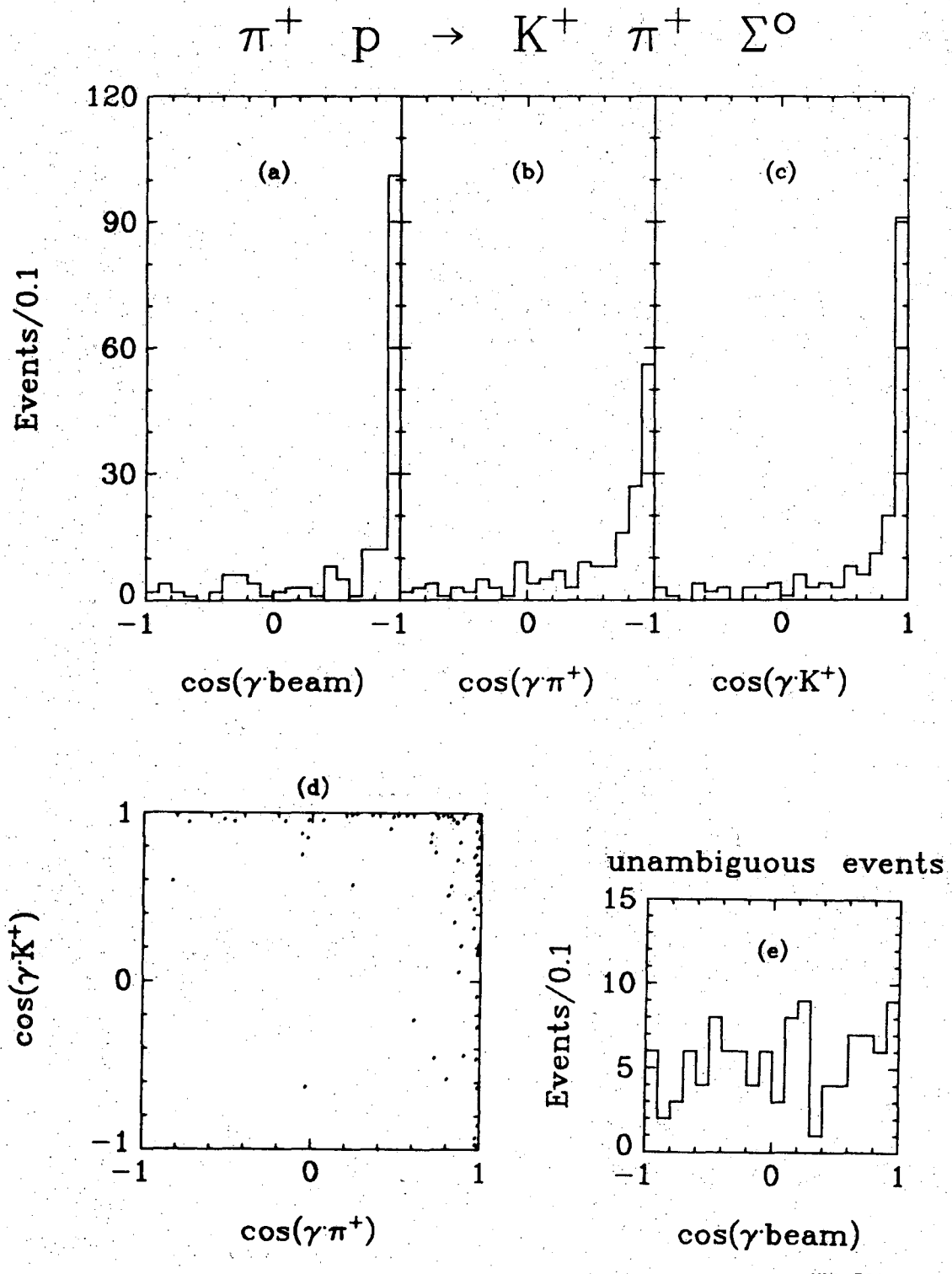
$\pi^+ \; p \rightarrow K^+ \; \pi^+ \; \Sigma^o$
(a)
(b)
(c)
Events/0.1
120
90
60
30
0
−1
0
1
cos(γ·beam)
cos(γ·π+)
cos(γ·K+)
(d)
cos(γ·K+)
cos(γ·π+)
unambiguous events
(e)
Events/0.1
15
10
5
0
cos(γ·beam)
XBL 729-1859

Fig. 3

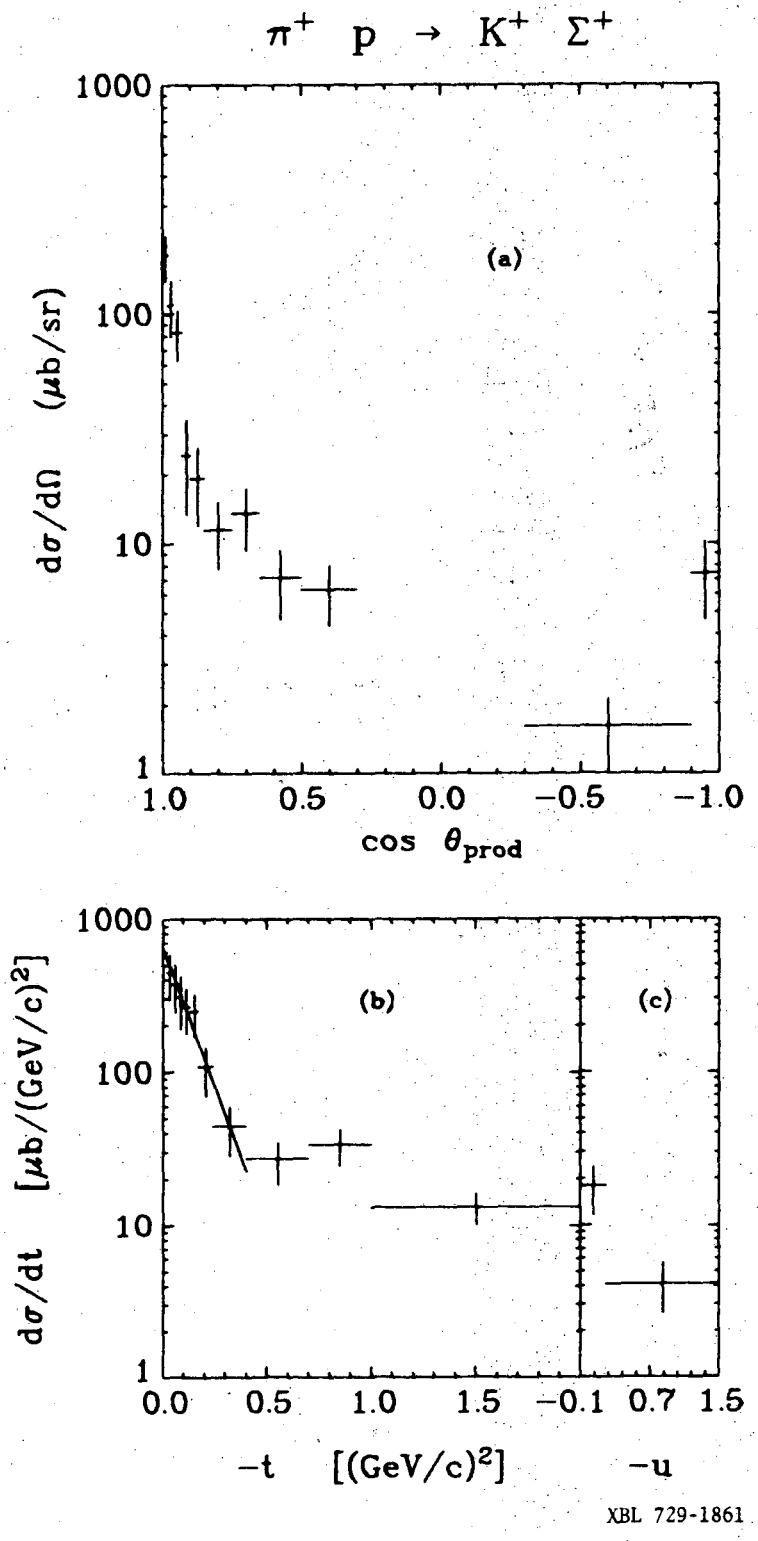
$\pi^+ \; p \rightarrow K^+ \; \Sigma^+$
1000
100
10
1
(a)
$d\sigma/d\Omega \quad (\mu b/sr)$
1.0
0.5
0.0
−0.5
−1.0
cos θ_{prod}
1000
100
10
1
(b)
(c)
$d\sigma/dt \quad [\mu b/(GeV/c)^2]$
0.0
0.5
1.0
1.5
−0.1
0.7
1.5
−t [(GeV/c)^2]
−u
XBL 729-1861

Fig. 4

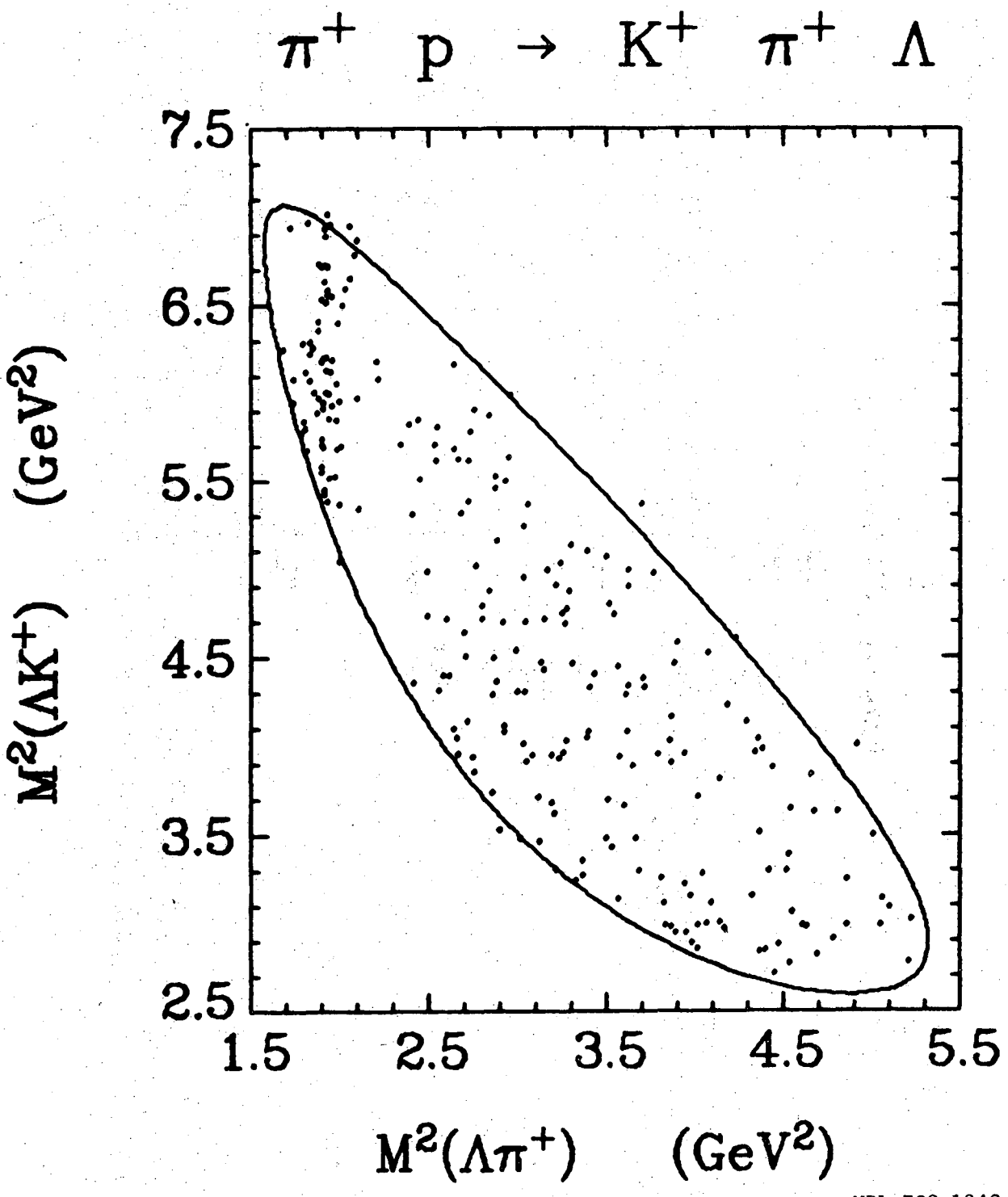

XBL 729-1842

Fig. 5

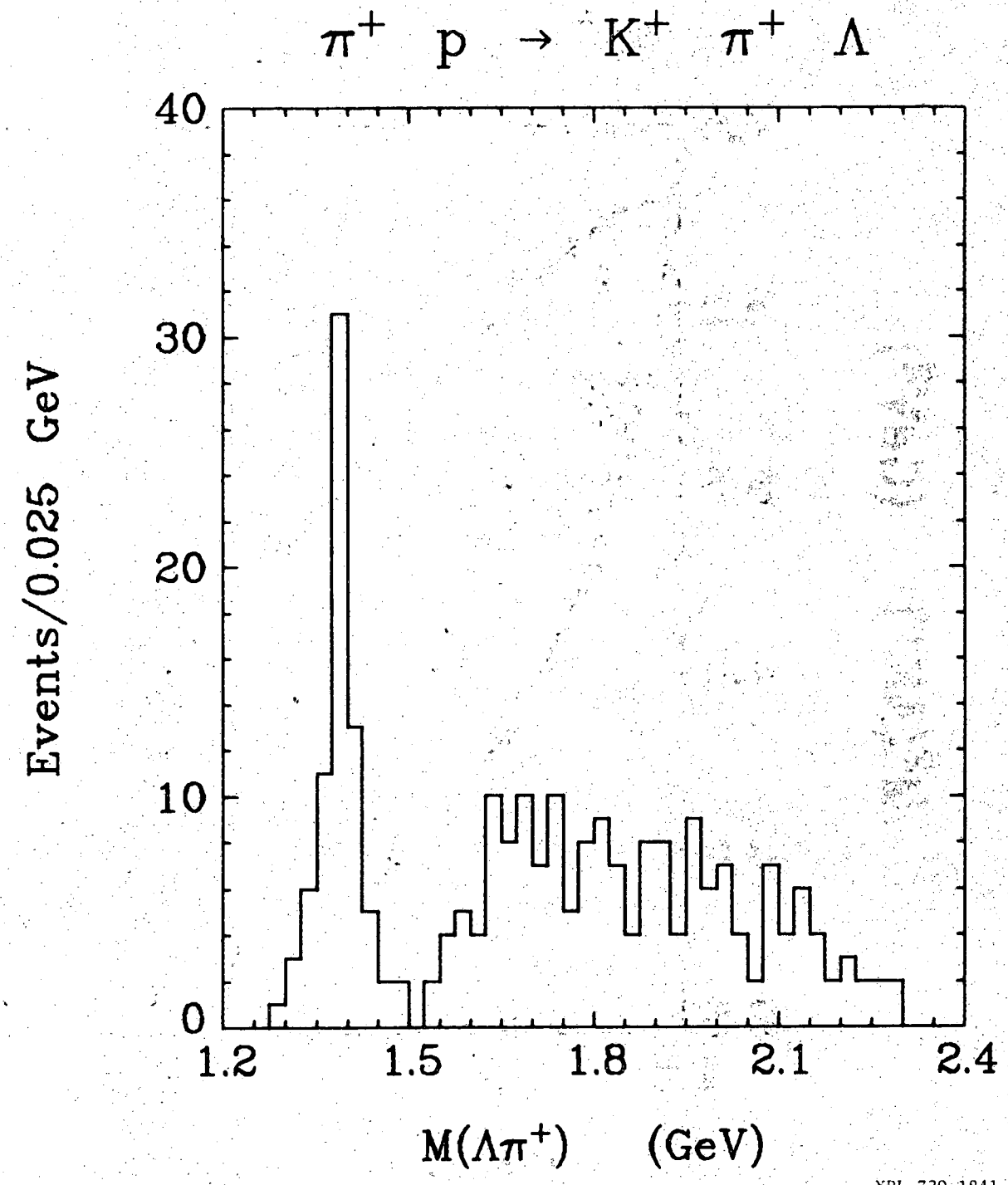
$\pi^+ \; p \rightarrow K^+ \; \pi^+ \; \Lambda$
Events/0.025 GeV
40
30
20
10
0
1.2
1.5
1.8
2.1
2.4
$M(\Lambda\pi^+)$ (GeV)
XBL 729-1841

Fig. 6

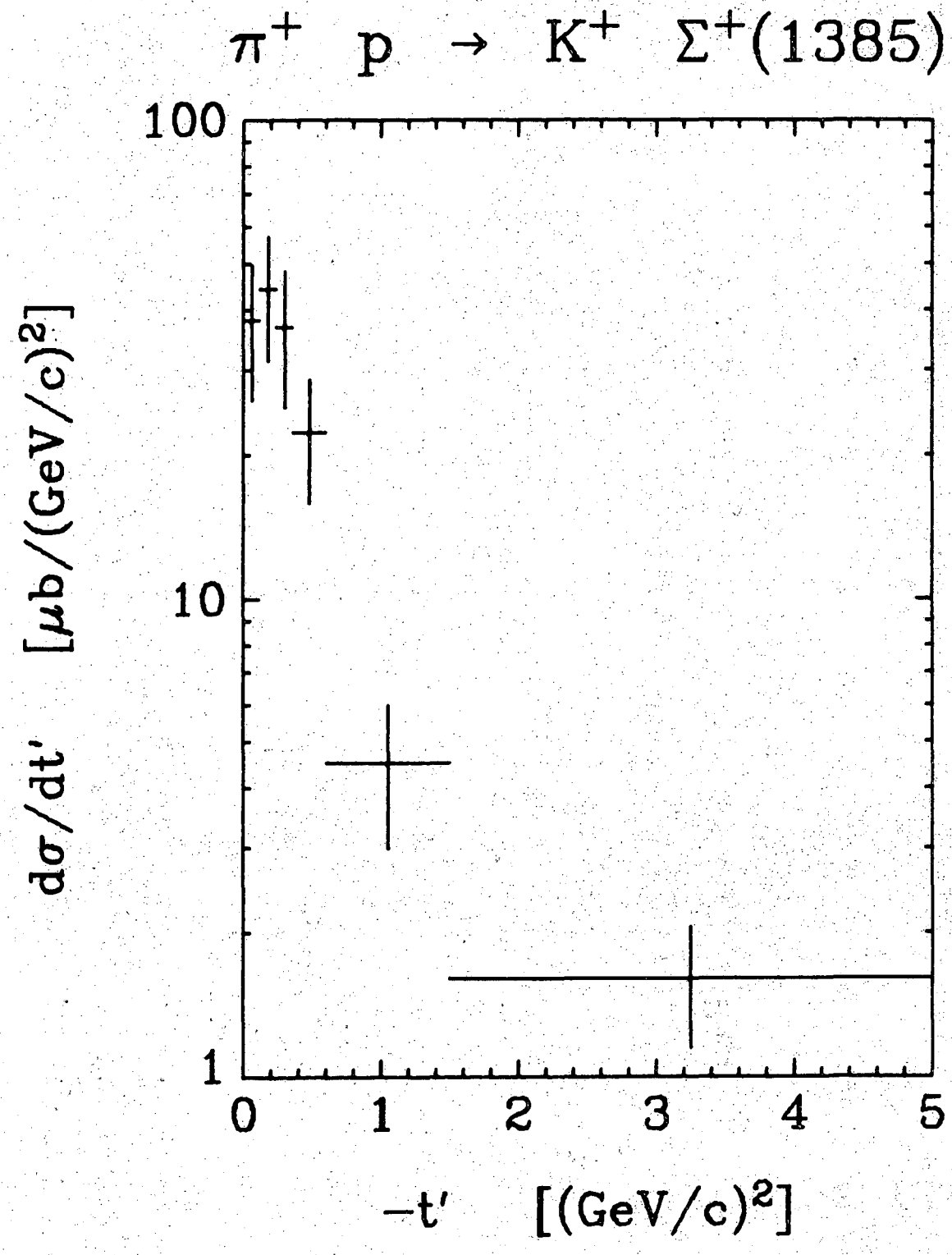
$\pi^+ \; p \rightarrow K^+ \; \Sigma^+(1385)$
100
10
1
0
1
2
3
4
5
$d\sigma/dt'$ [μb/(GeV/c)^2]
$-t'$ [(GeV/c)^2]
XBL 729-1840

Fig. 7

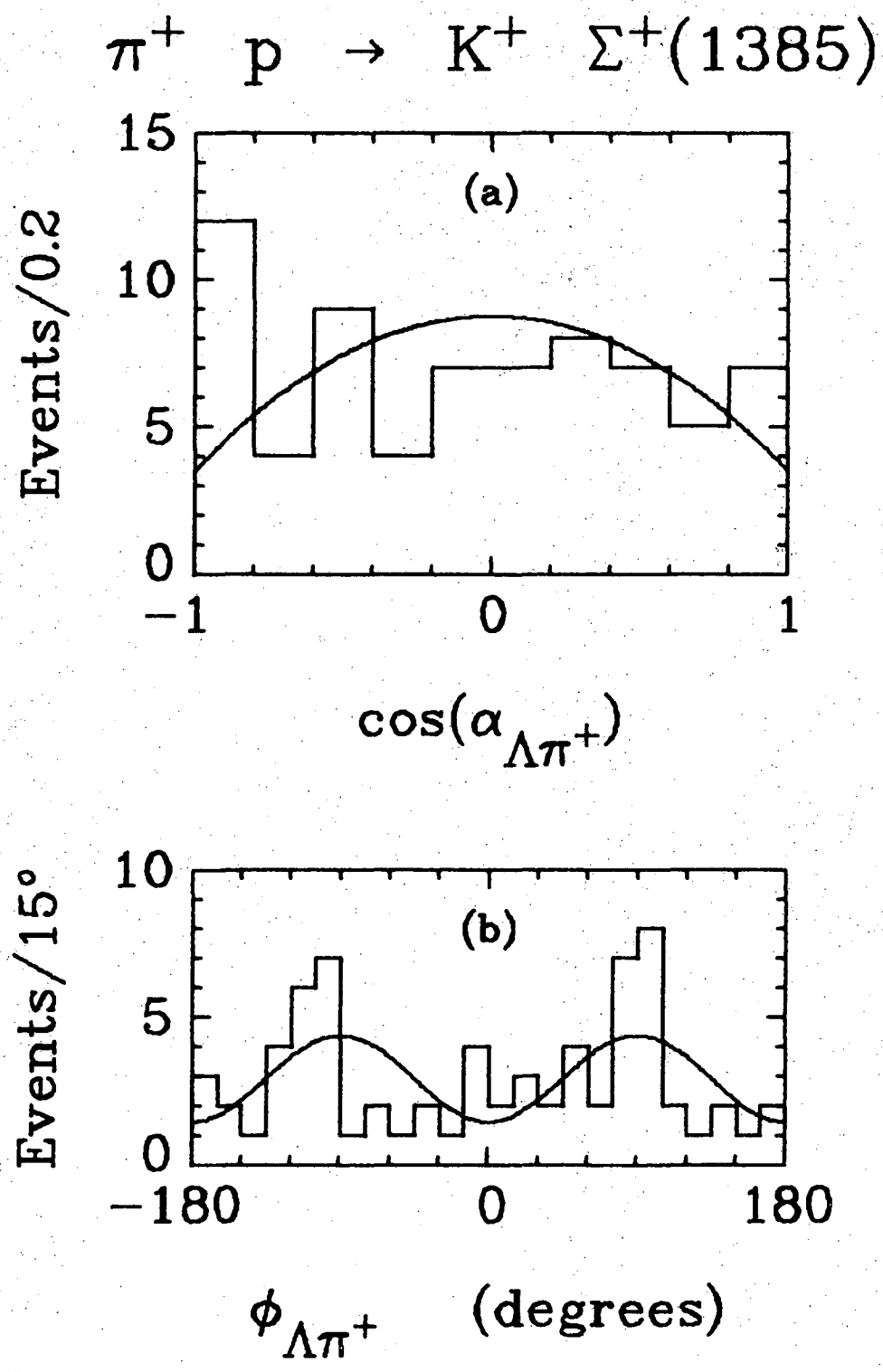

XBL 729-1839

Fig. 8

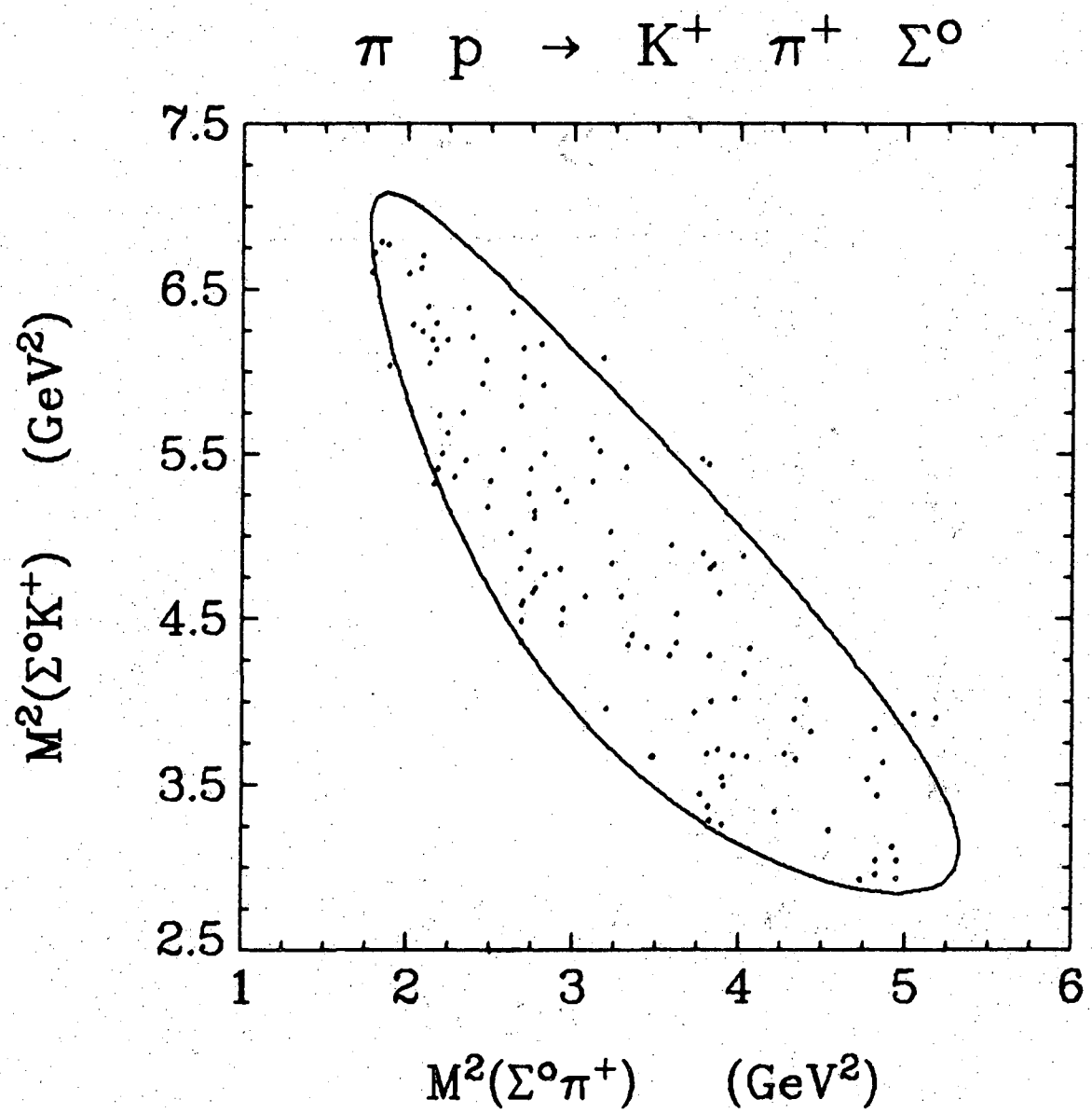

XBL 729-1838

Fig. 9

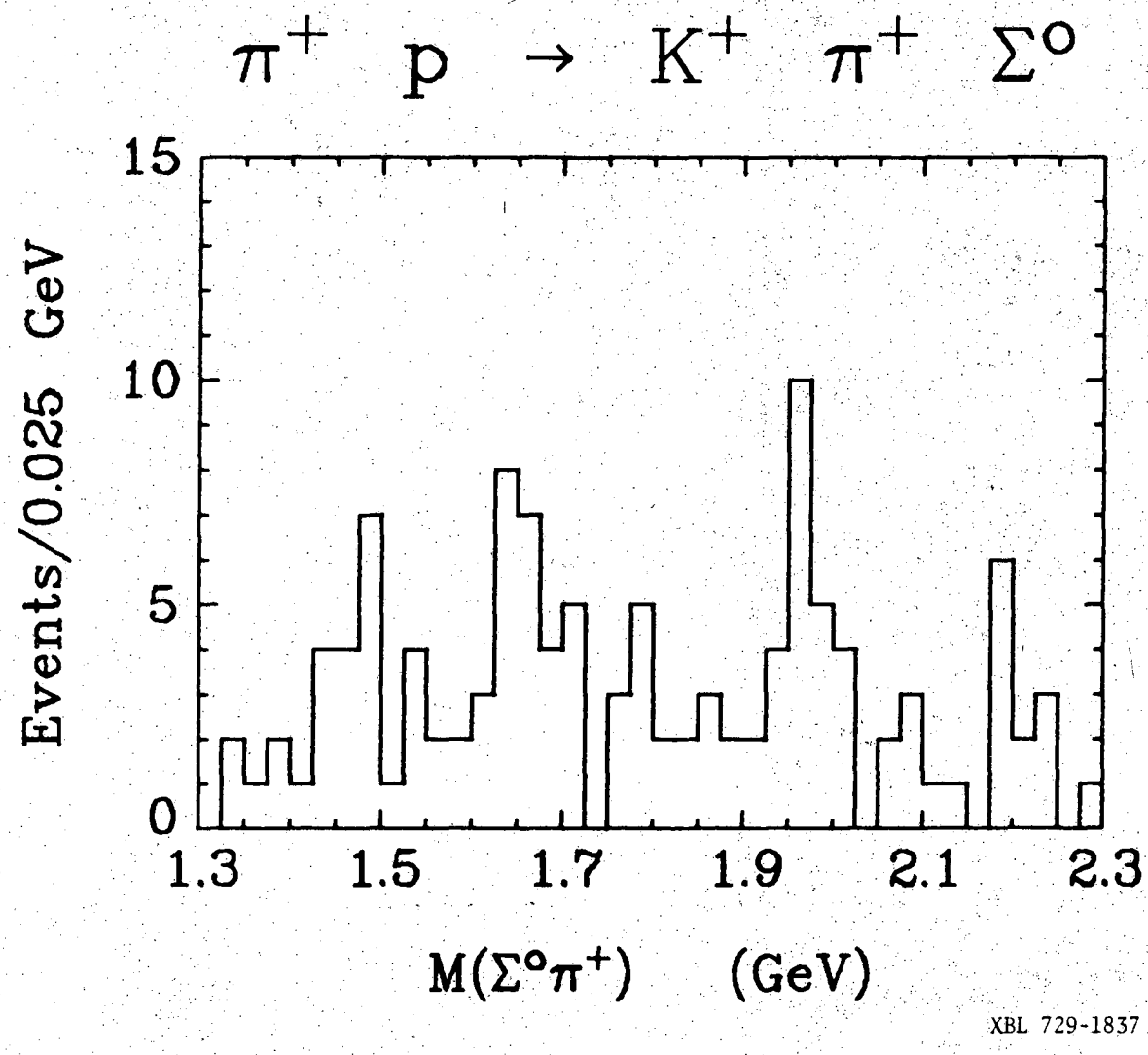
$\pi^+ \; p \rightarrow K^+ \; \pi^+ \; \Sigma^o$
Events/0.025 GeV
15
10
5
0
1.3
1.5
1.7
1.9
2.1
2.3
$M(\Sigma^o\pi^+)$ (GeV)
XBL 729-1837

Fig. 10

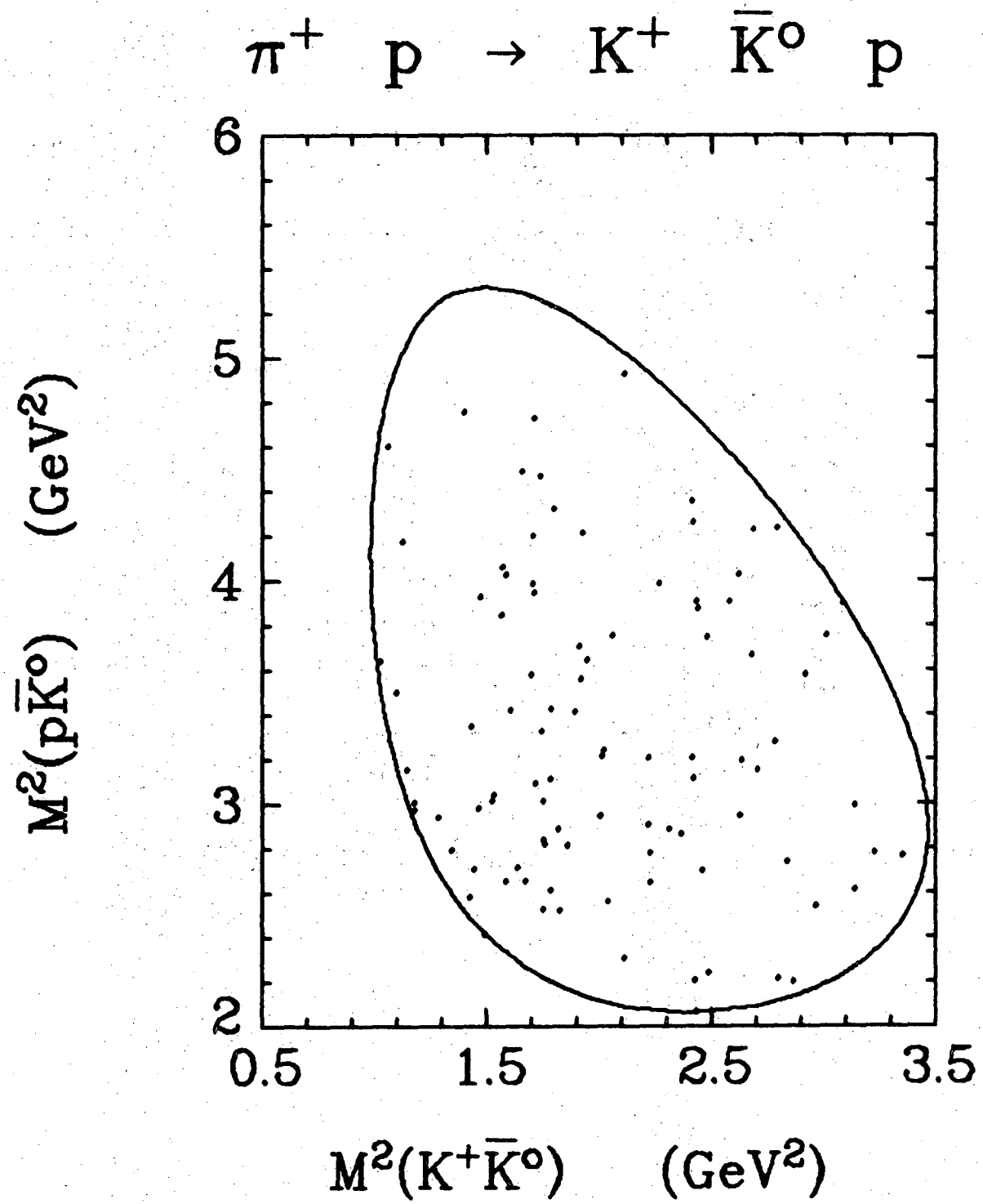

XBL 729-1836

Fig. 11

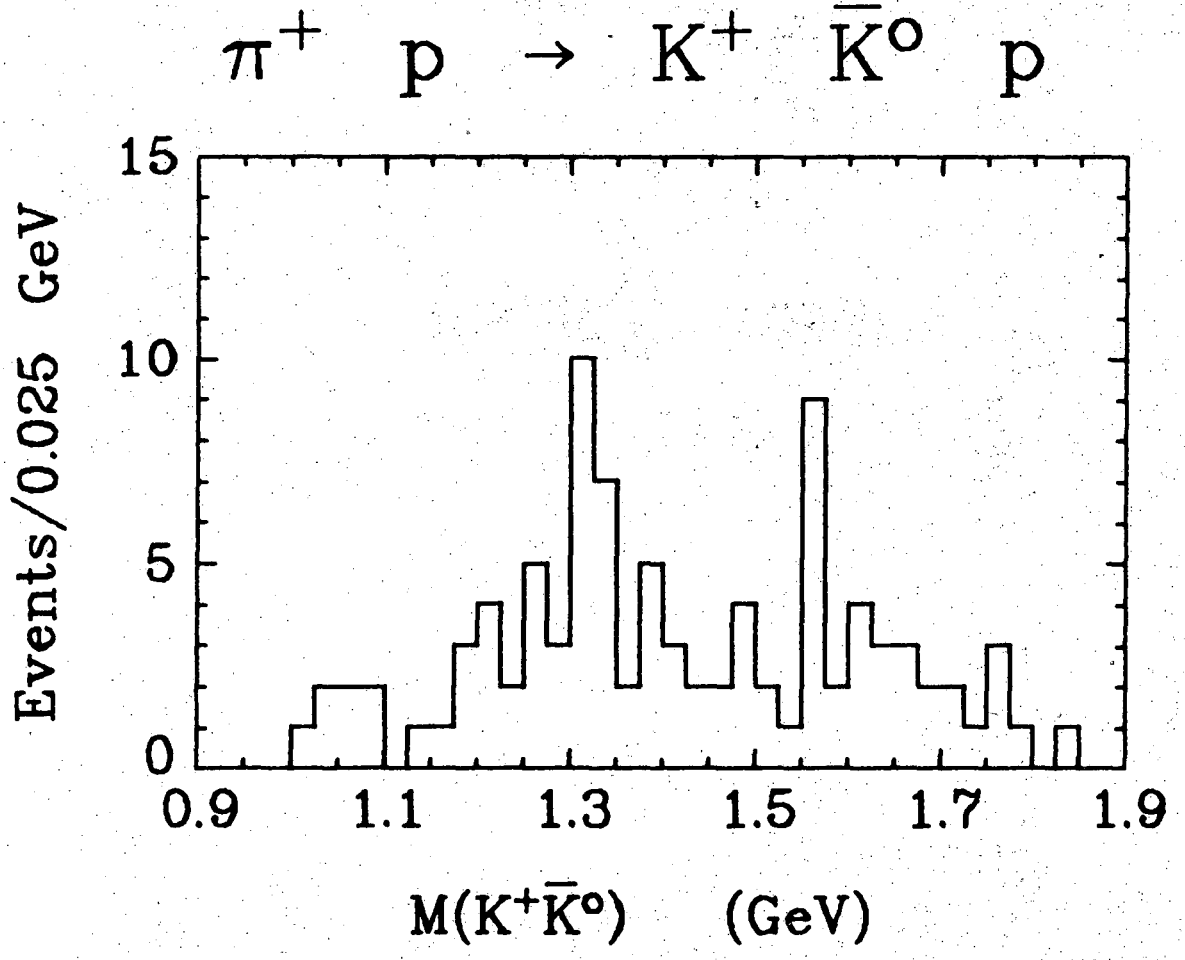

XBL 729-1835

Fig. 12

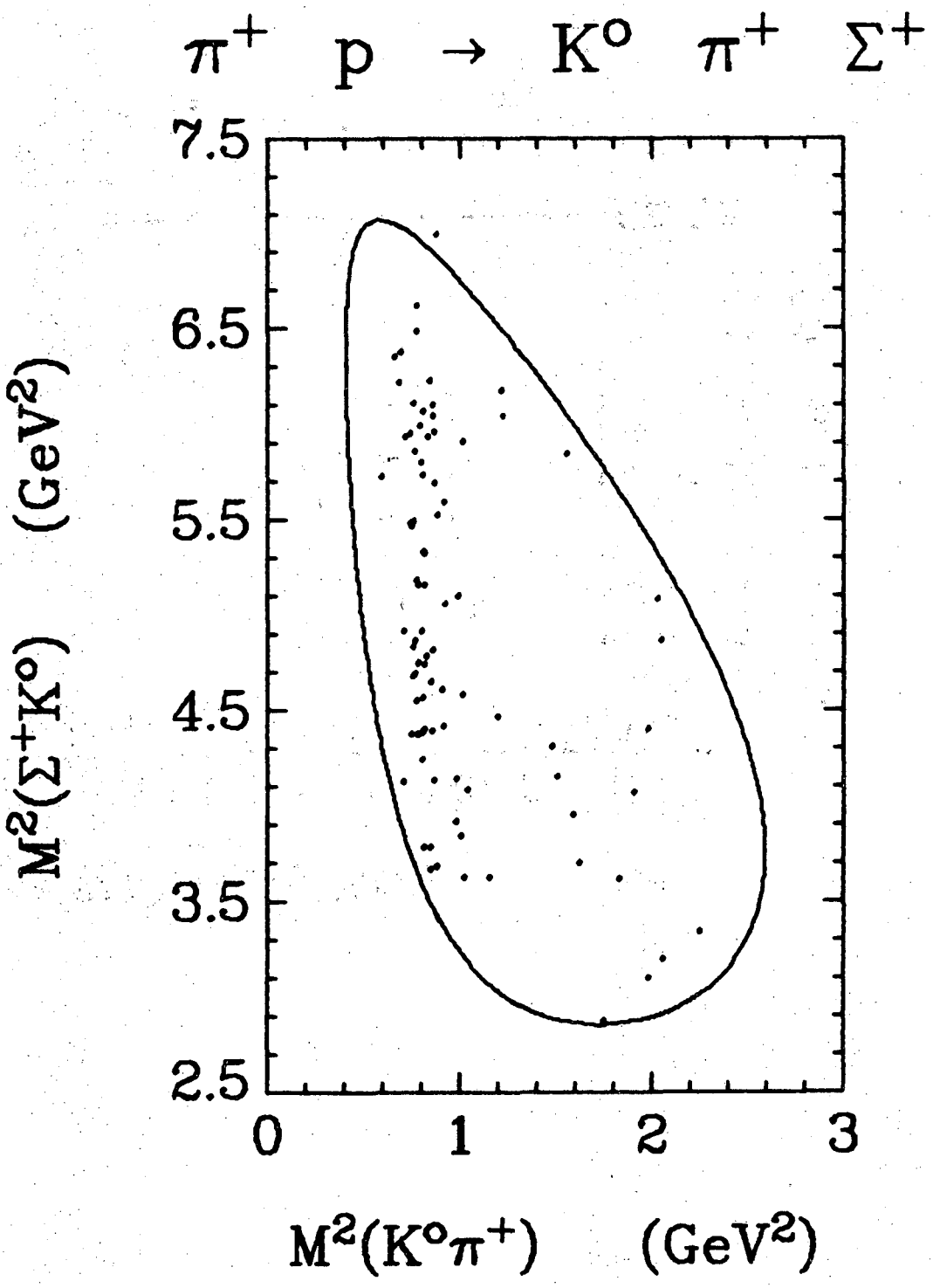

XBL 729-1834

Fig. 13

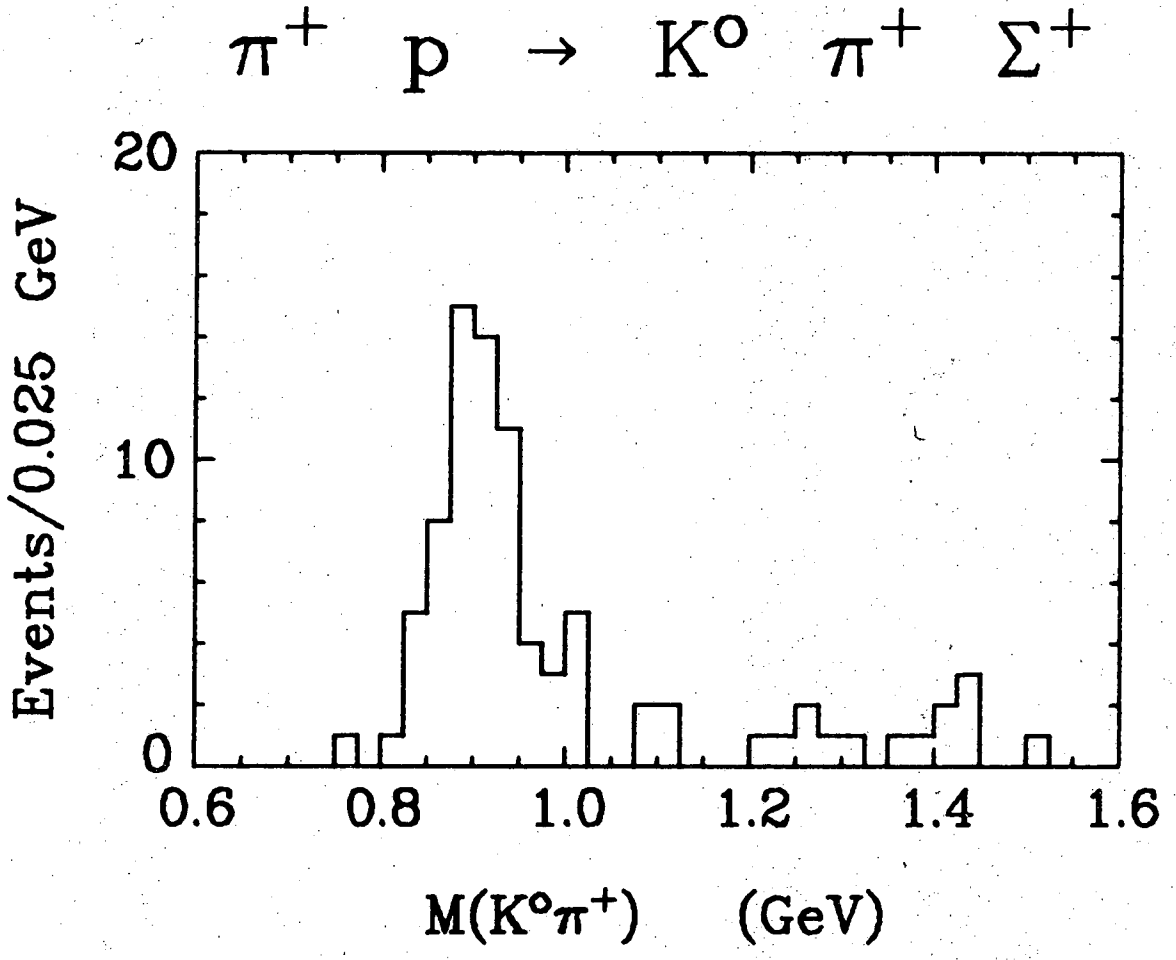

XBL 729-1833

Fig. 14

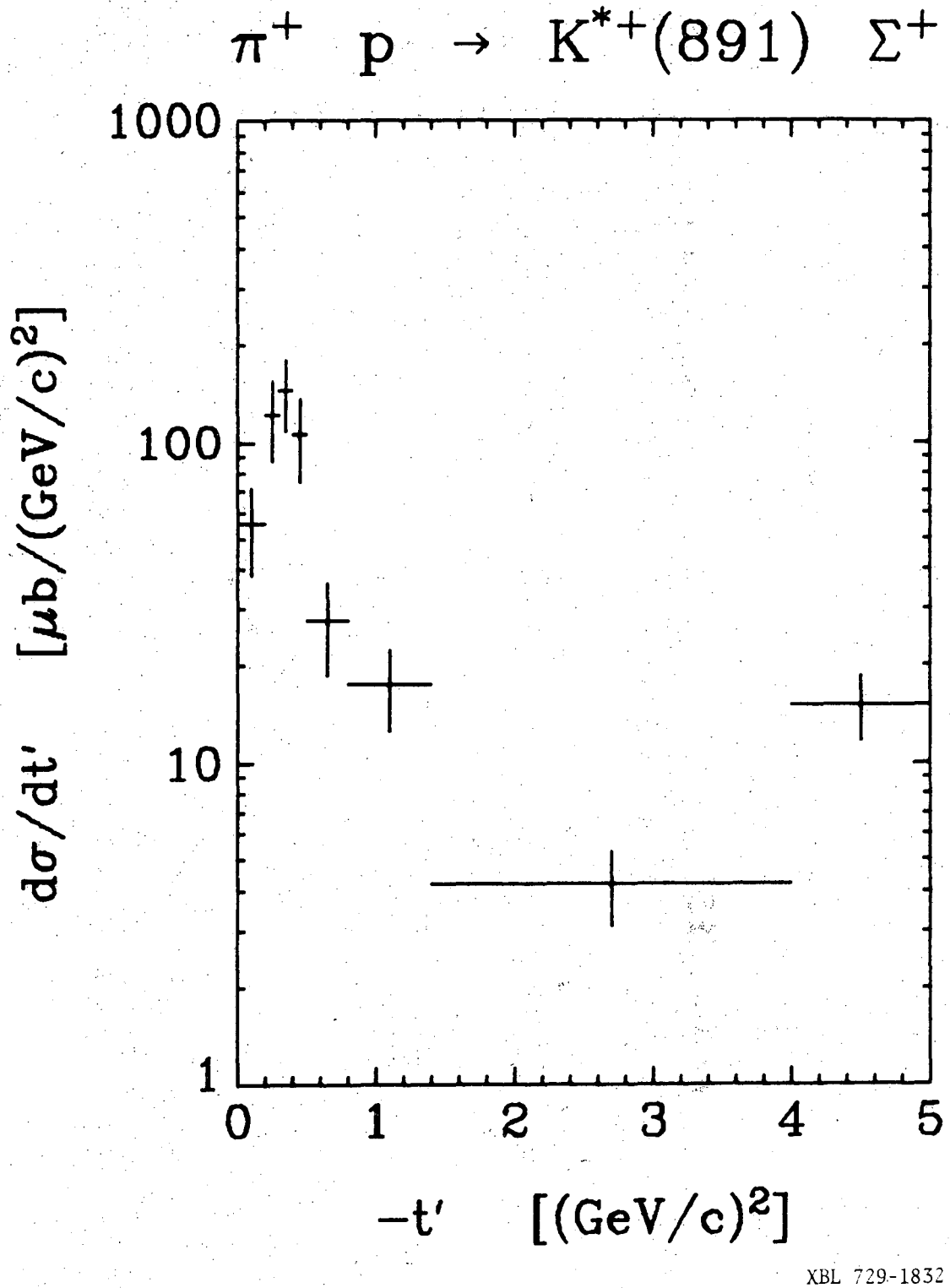

XBL 729-1832

Fig. 15

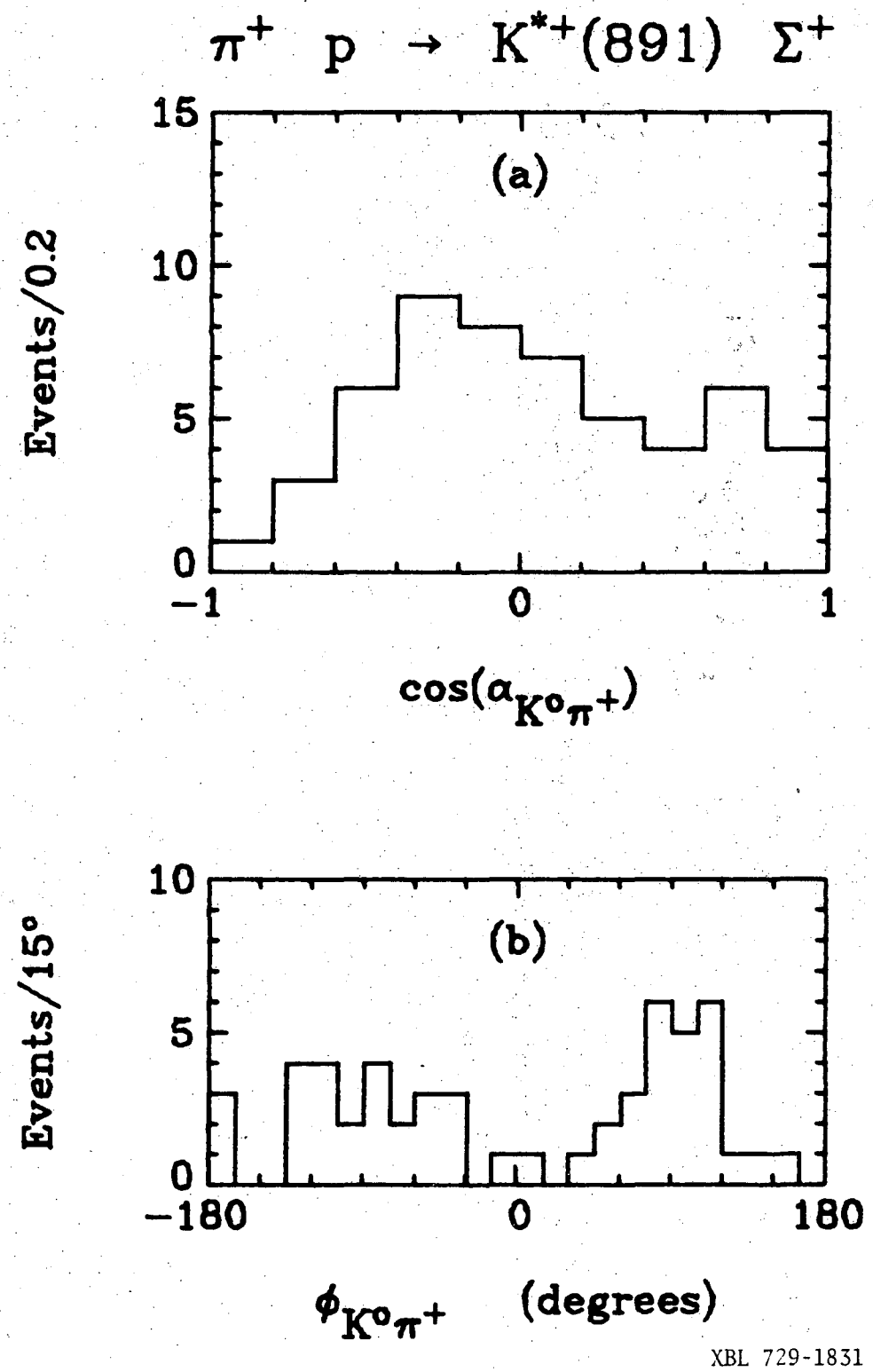

XBL 729-1831

Fig. 16

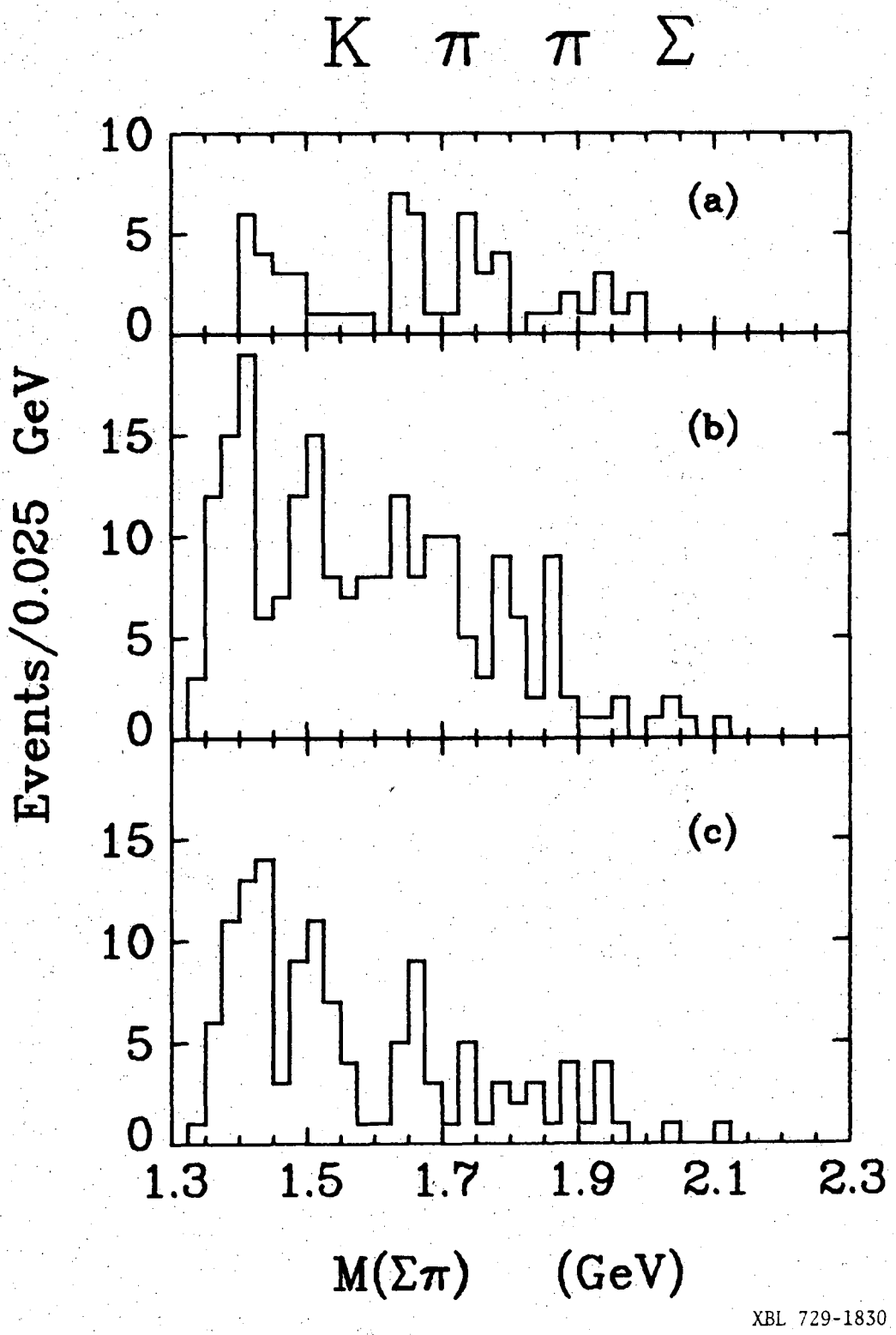
K π π Σ
10
5
0
(a)
15
10
5
0
(b)
15
10
5
0
(c)
Events/0.025 GeV
1.3
1.5
1.7
1.9
2.1
2.3
M(Σπ) (GeV)
XBL 729-1830

Fig. 17

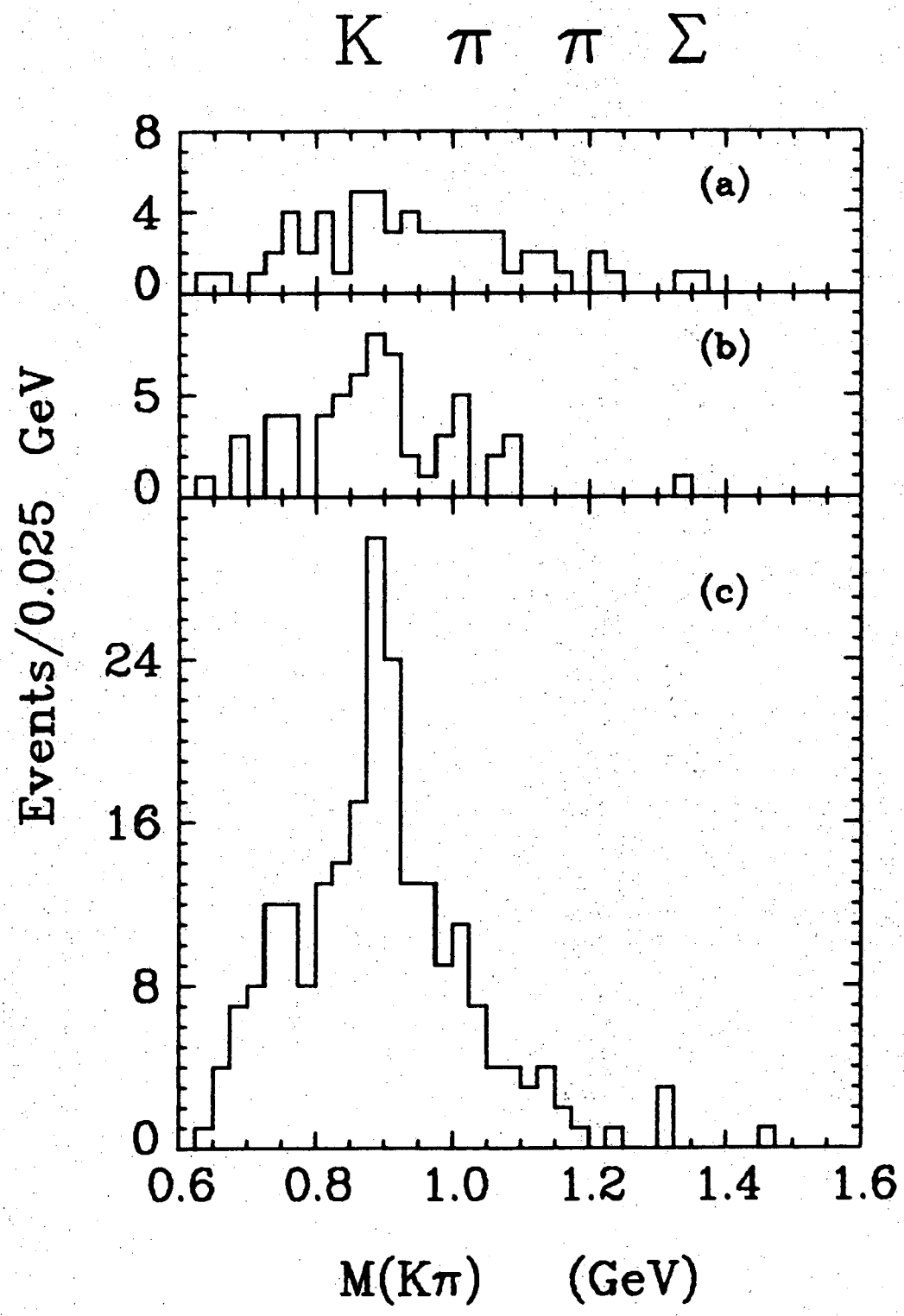
K π π Σ
(a)
(b)
(c)
8
4
0
5
0
24
16
8
0
Events/0.025 GeV
0.6
0.8
1.0
1.2
1.4
1.6
M(Kπ) (GeV)
XBL 729-1829

Fig. 18

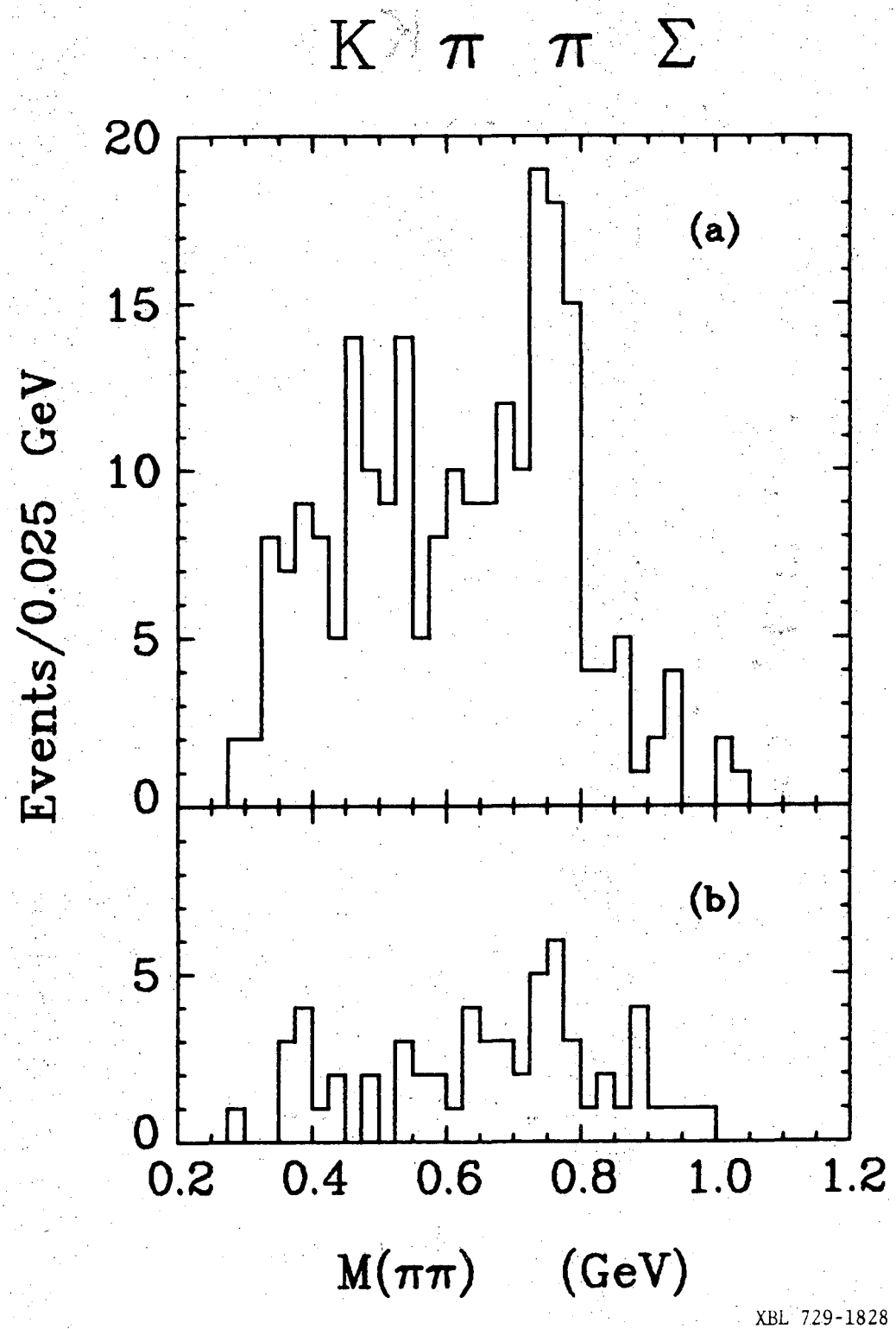
K π π Σ
20
15
10
5
0
(a)
(b)
5
0
Events/0.025 GeV
0.2
0.4
0.6
0.8
1.0
1.2
M(ππ) (GeV)
XBL 729-1828

Fig. 19

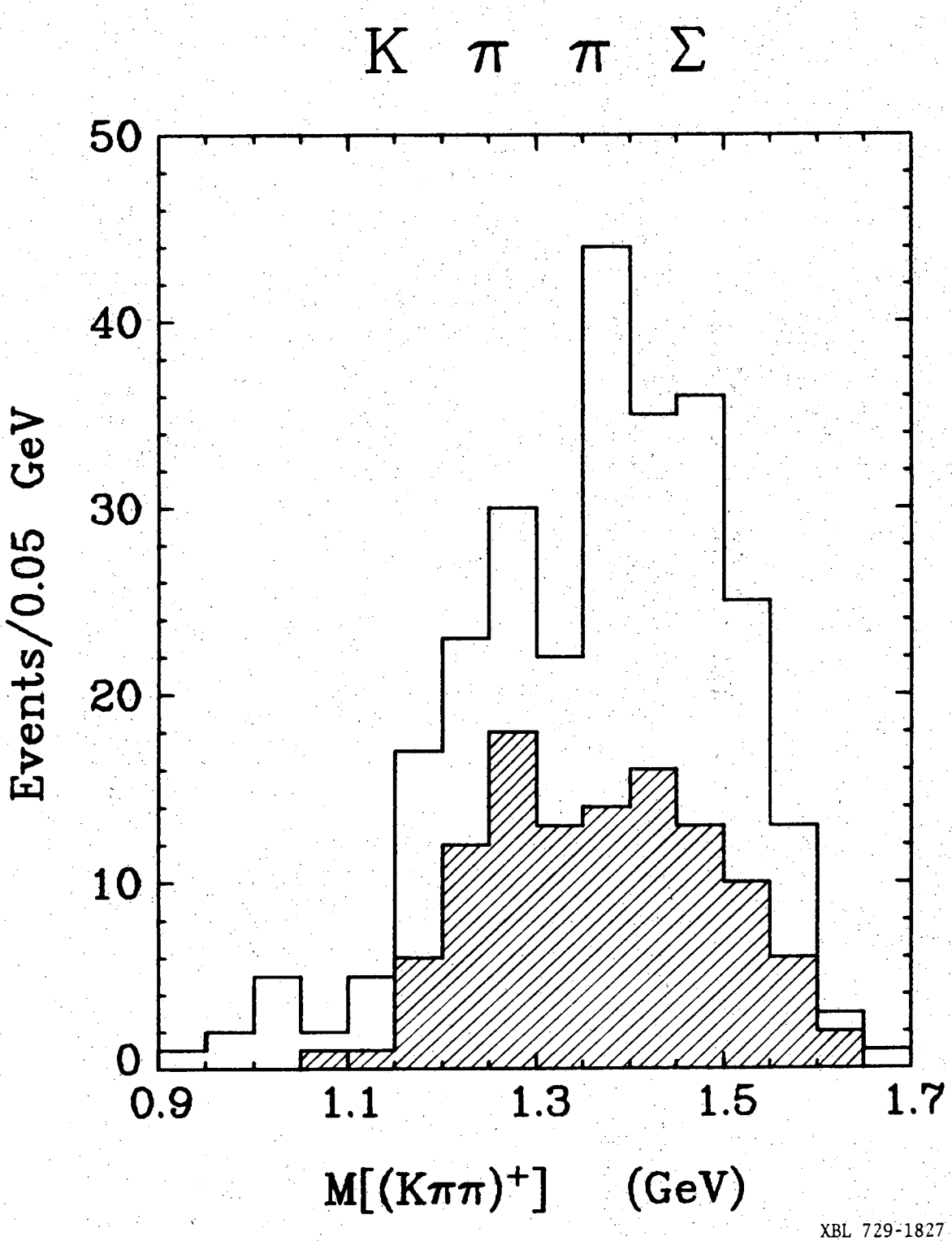
K π π Σ
50
40
30
20
10
0
Events/0.05 GeV
0.9
1.1
1.3
1.5
1.7
M[(Kππ)+] (GeV)
XBL 729-1827

Fig. 20

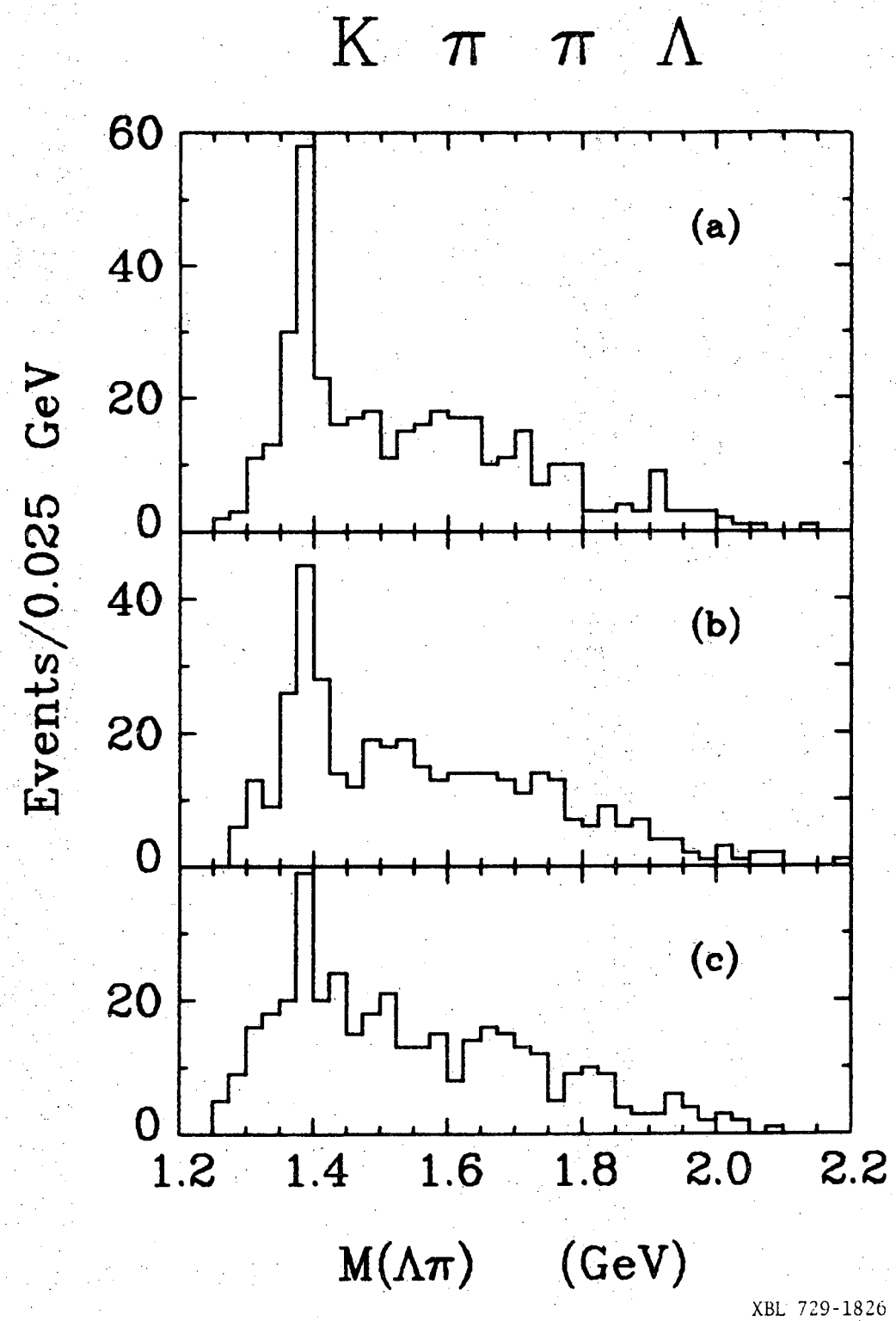
K π π Λ
60
40
20
0
(a)
40
20
0
(b)
20
0
(c)
Events/0.025 GeV
1.2
1.4
1.6
1.8
2.0
2.2
M(Λπ) (GeV)
XBL 729-1826

Fig. 21

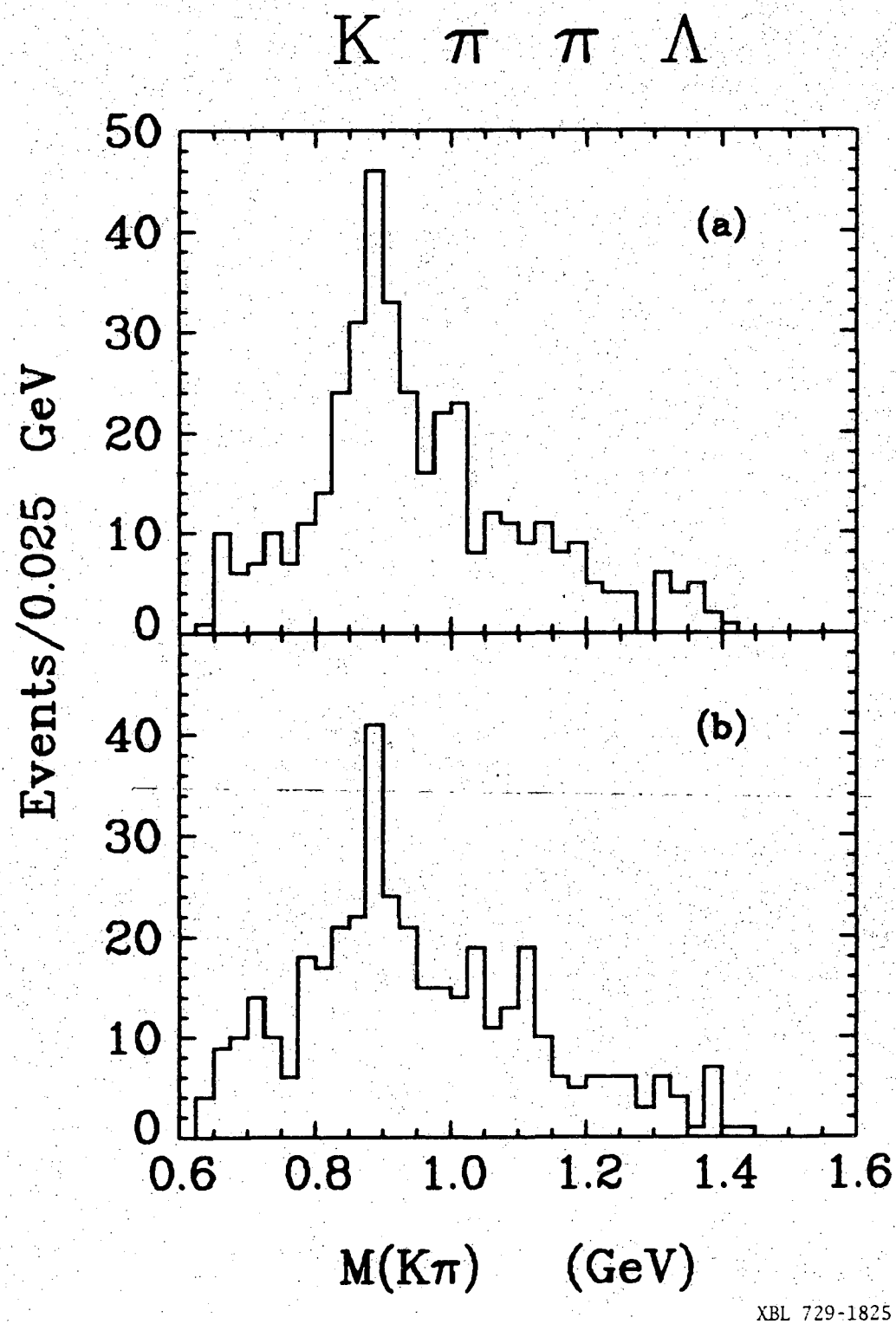
K π π Λ
(a)
(b)
Events/0.025 GeV
0
10
20
30
40
50
0.6
0.8
1.0
1.2
1.4
1.6
M(Kπ) (GeV)
XBL 729-1825

Fig. 22

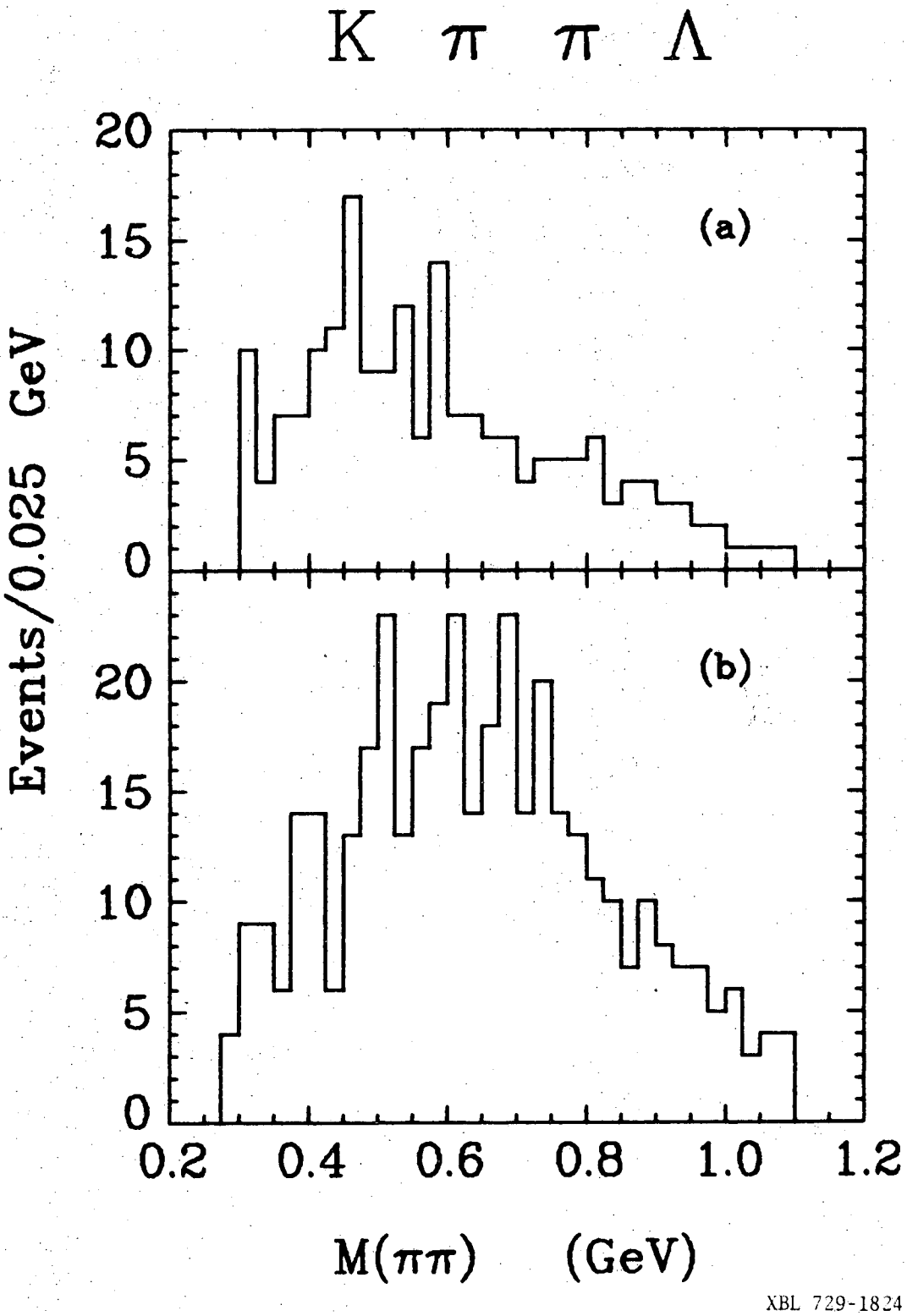
K π π Λ
(a)
(b)
Events/0.025 GeV
0
5
10
15
20
0.2
0.4
0.6
0.8
1.0
1.2
M(ππ) (GeV)
XBL 729-1824

Fig. 23

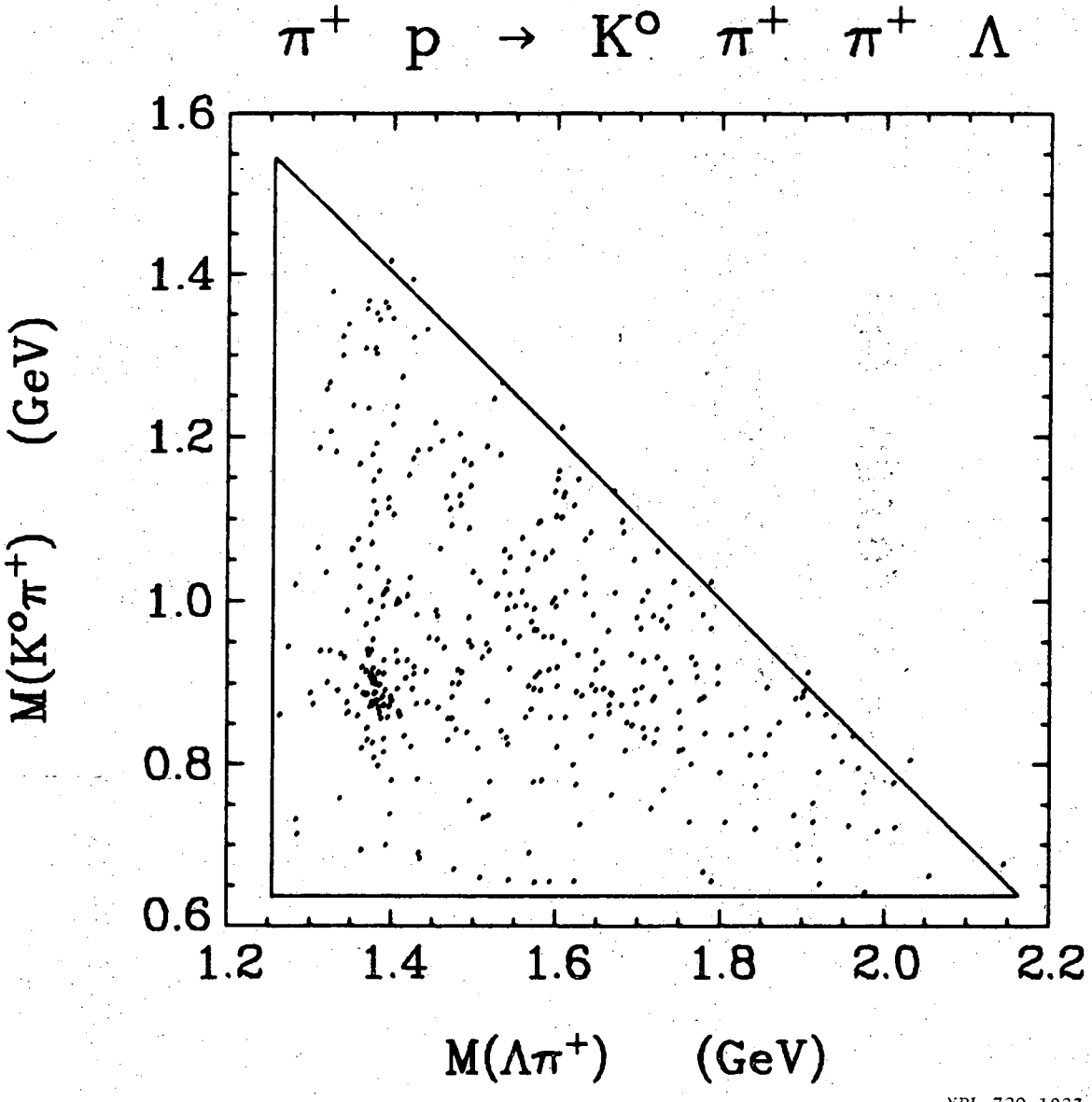
$\pi^+ \; p \rightarrow K^o \; \pi^+ \; \pi^+ \; \Lambda$
1.6
1.4
1.2
1.0
0.8
0.6
$M(K^o\pi^+)$ (GeV)
1.2
1.4
1.6
1.8
2.0
2.2
$M(\Lambda\pi^+)$ (GeV)
XBL 729-1823

Fig. 24

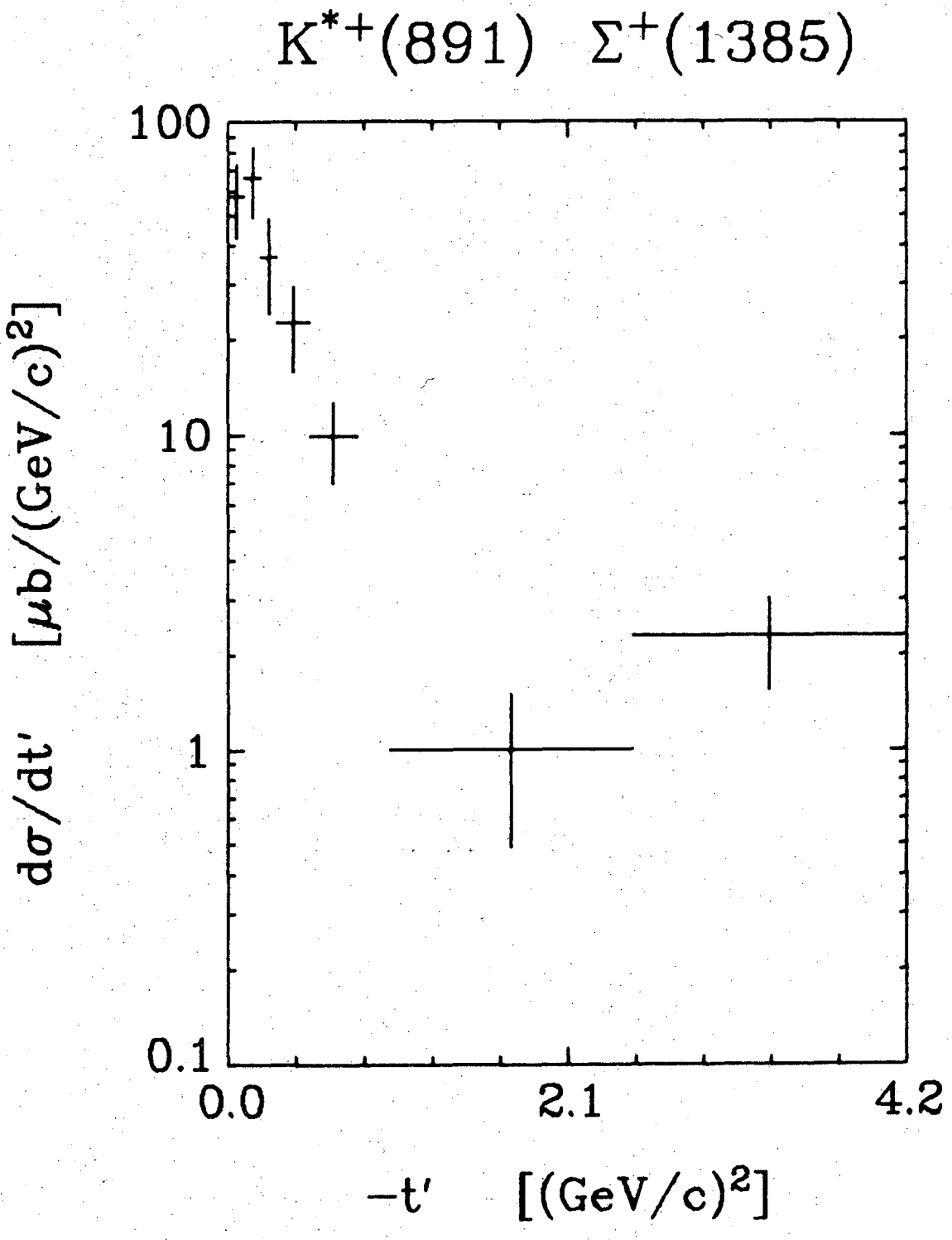
K*+(891) Σ+(1385)
100
10
1
0.1
0.0
2.1
4.2
dσ/dt' [μb/(GeV/c)²]
−t' [(GeV/c)²]
XBL 729-1844

Fig. 25

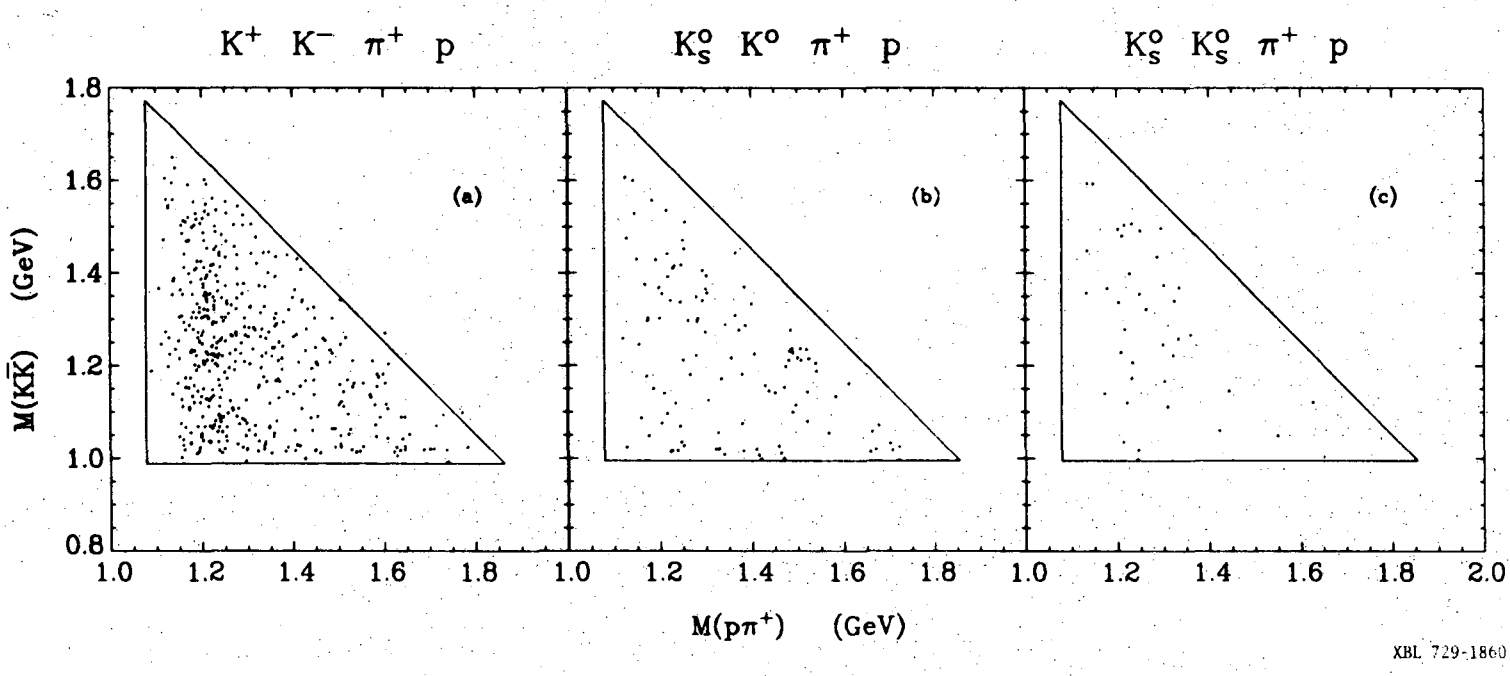
$K^+ K^- \pi^+ p$
$K^o_s K^o \pi^+ p$
$K^o_s K^o_s \pi^+ p$
(a)
(b)
(c)
$M(K\bar{K})$ (GeV)
$M(p\pi^+)$ (GeV)
1.8
1.6
1.4
1.2
1.0
0.8
1.0
1.2
1.4
1.6
1.8
2.0
XBL 729-1860

Fig. 26

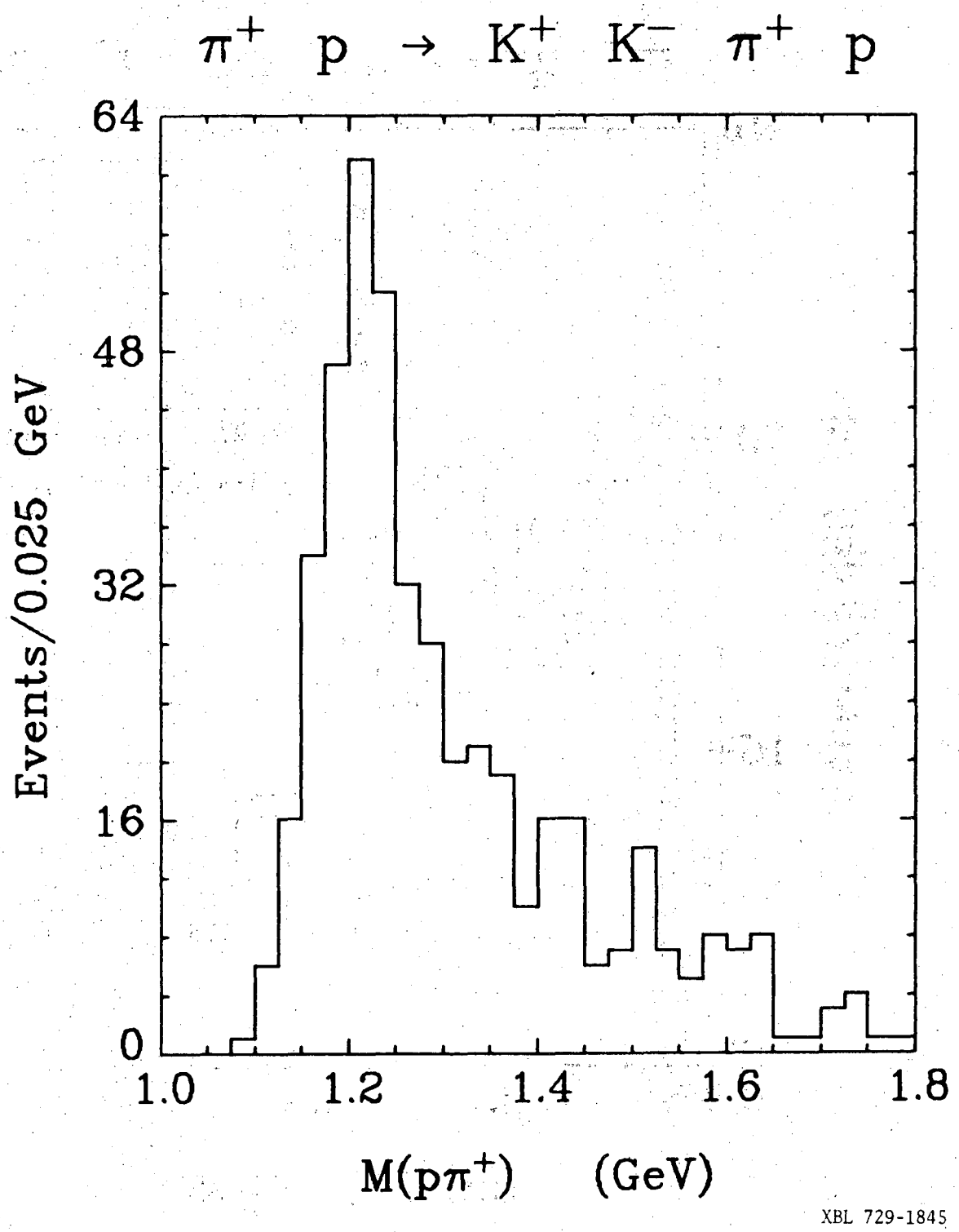
$\pi^+ \; p \rightarrow K^+ \; K^- \; \pi^+ \; p$
64
48
32
16
0
Events/0.025 GeV
1.0
1.2
1.4
1.6
1.8
M(pπ^+) (GeV)
XBL 729-1845

Fig. 27

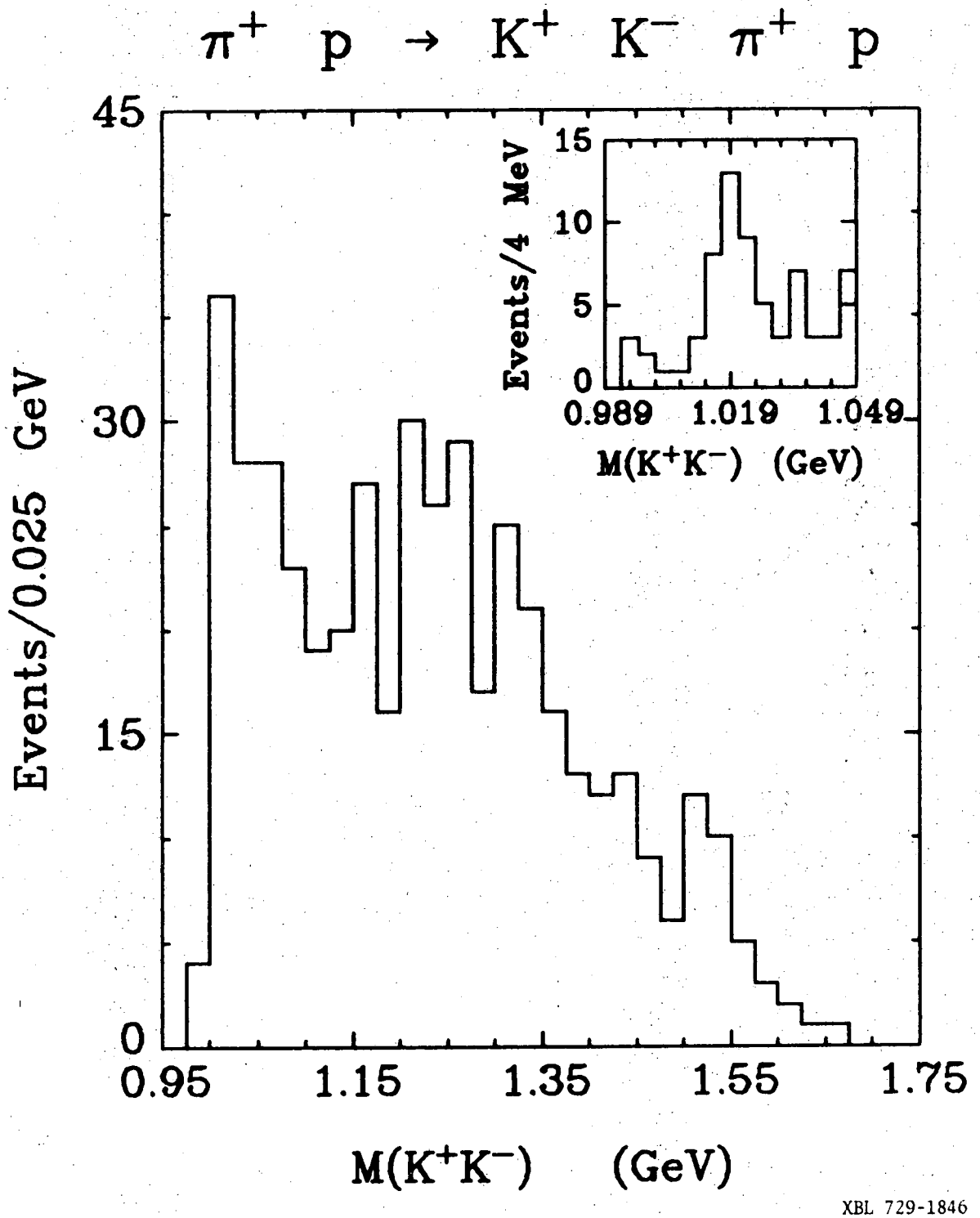
$\pi^+ \; p \rightarrow K^+ \; K^- \; \pi^+ \; p$
Events/0.025 GeV
45
30
15
0
0.95
1.15
1.35
1.55
1.75
M(K⁺K⁻) (GeV)
Events/4 MeV
15
10
5
0
0.989
1.019
1.049
M(K⁺K⁻) (GeV)
XBL 729-1846

Fig. 28

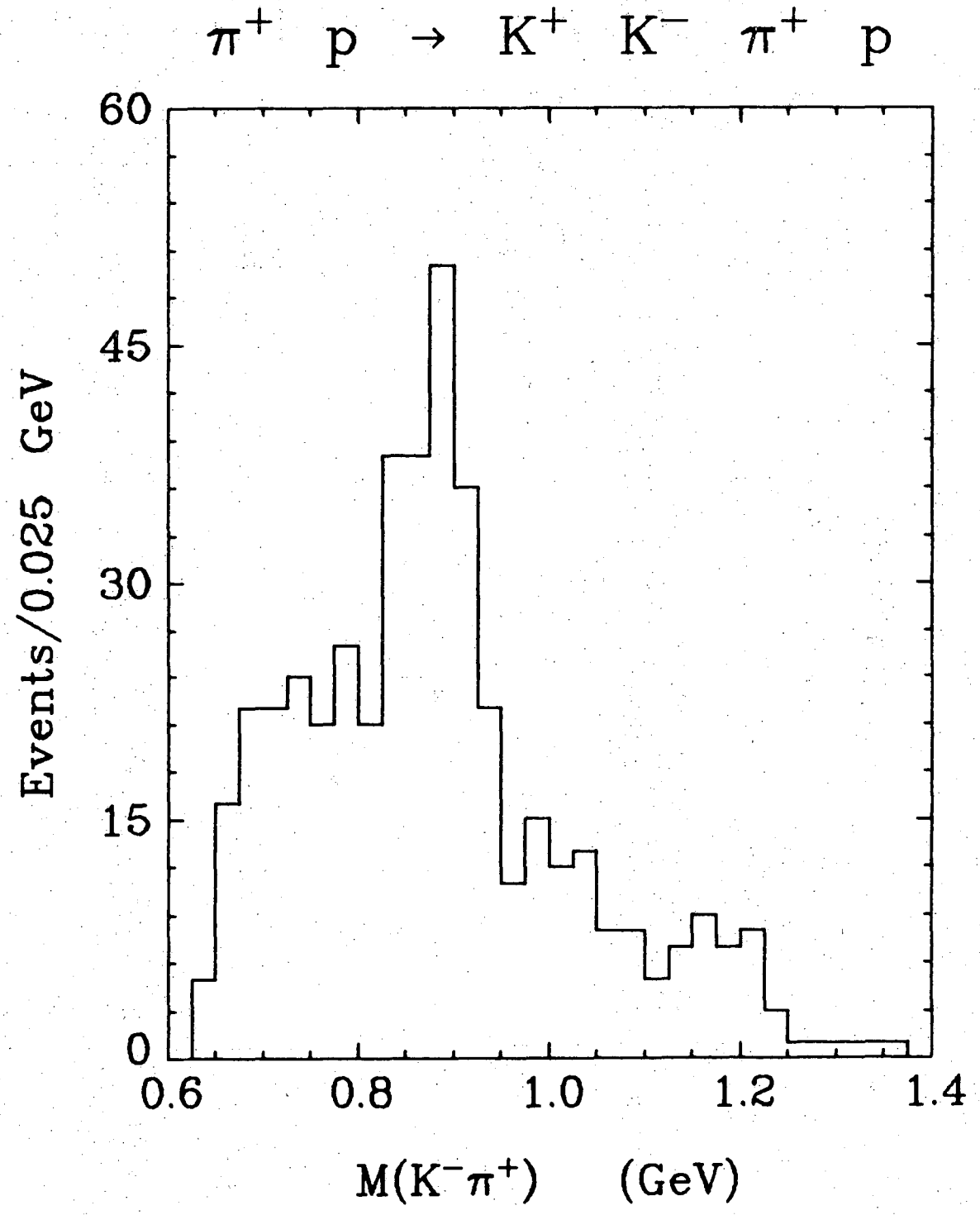

XBL 729-1847

Fig. 29

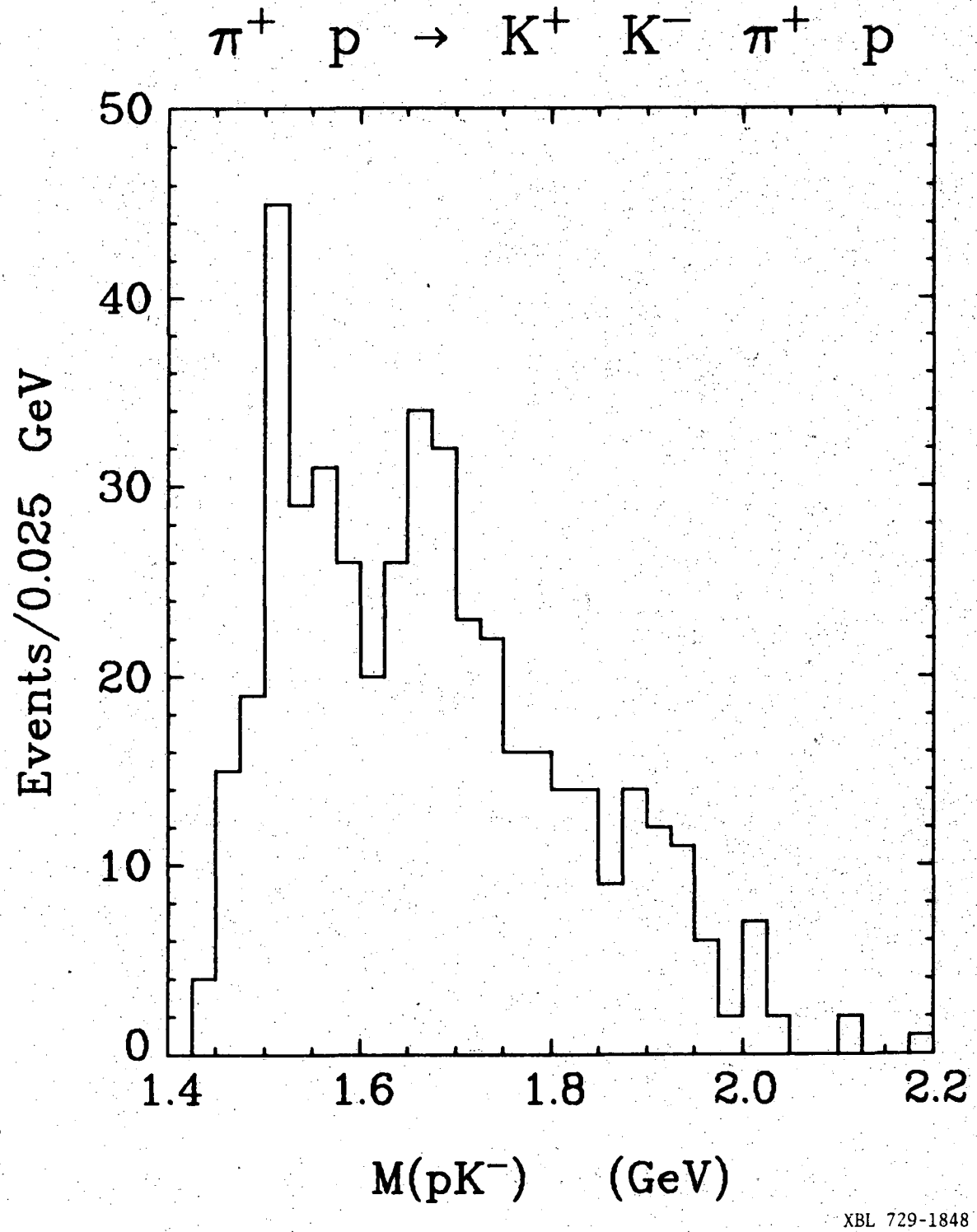
$\pi^+ \; p \rightarrow K^+ \; K^- \; \pi^+ \; p$
Events/0.025 GeV
0
10
20
30
40
50
1.4
1.6
1.8
2.0
2.2
M(pK⁻) (GeV)
XBL 729-1848

Fig. 30

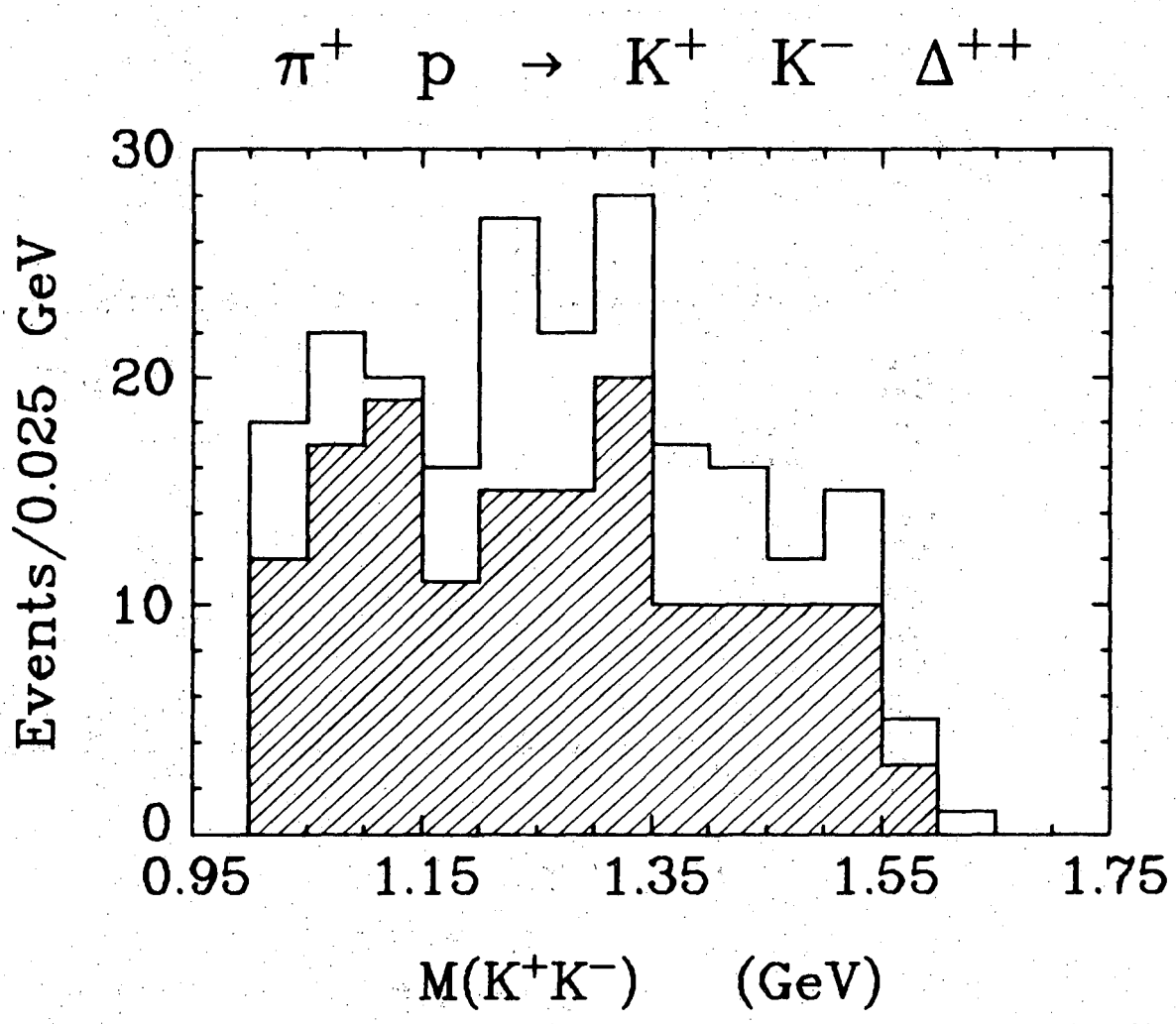

XBL 729-1849

Fig. 31

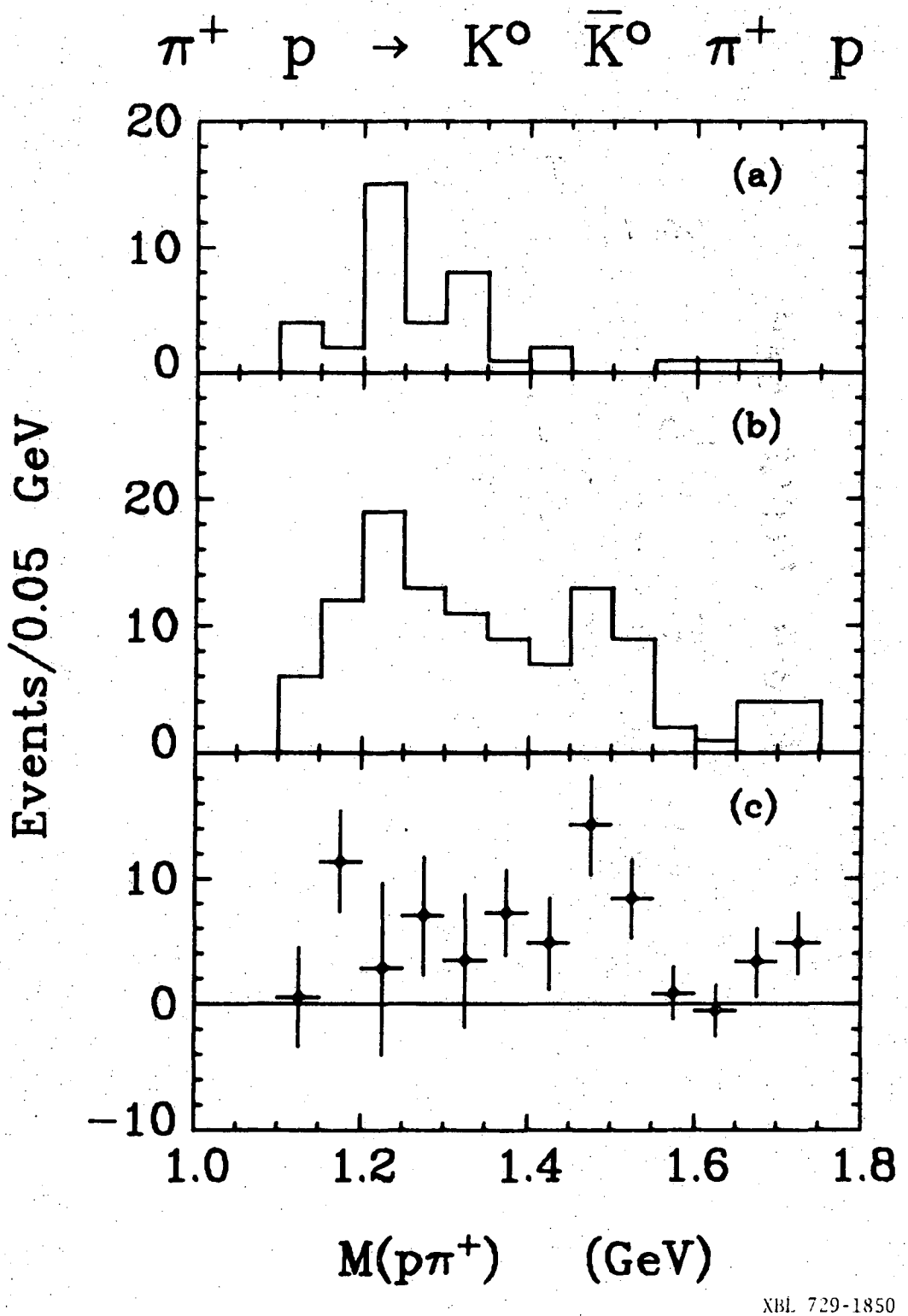
$\pi^+ \; p \rightarrow K^o \; \bar{K}^o \; \pi^+ \; p$
(a)
(b)
(c)
20
10
0
20
10
0
10
0
−10
Events/0.05 GeV
1.0
1.2
1.4
1.6
1.8
M(pπ+) (GeV)
XBL 729-1850

Fig. 32

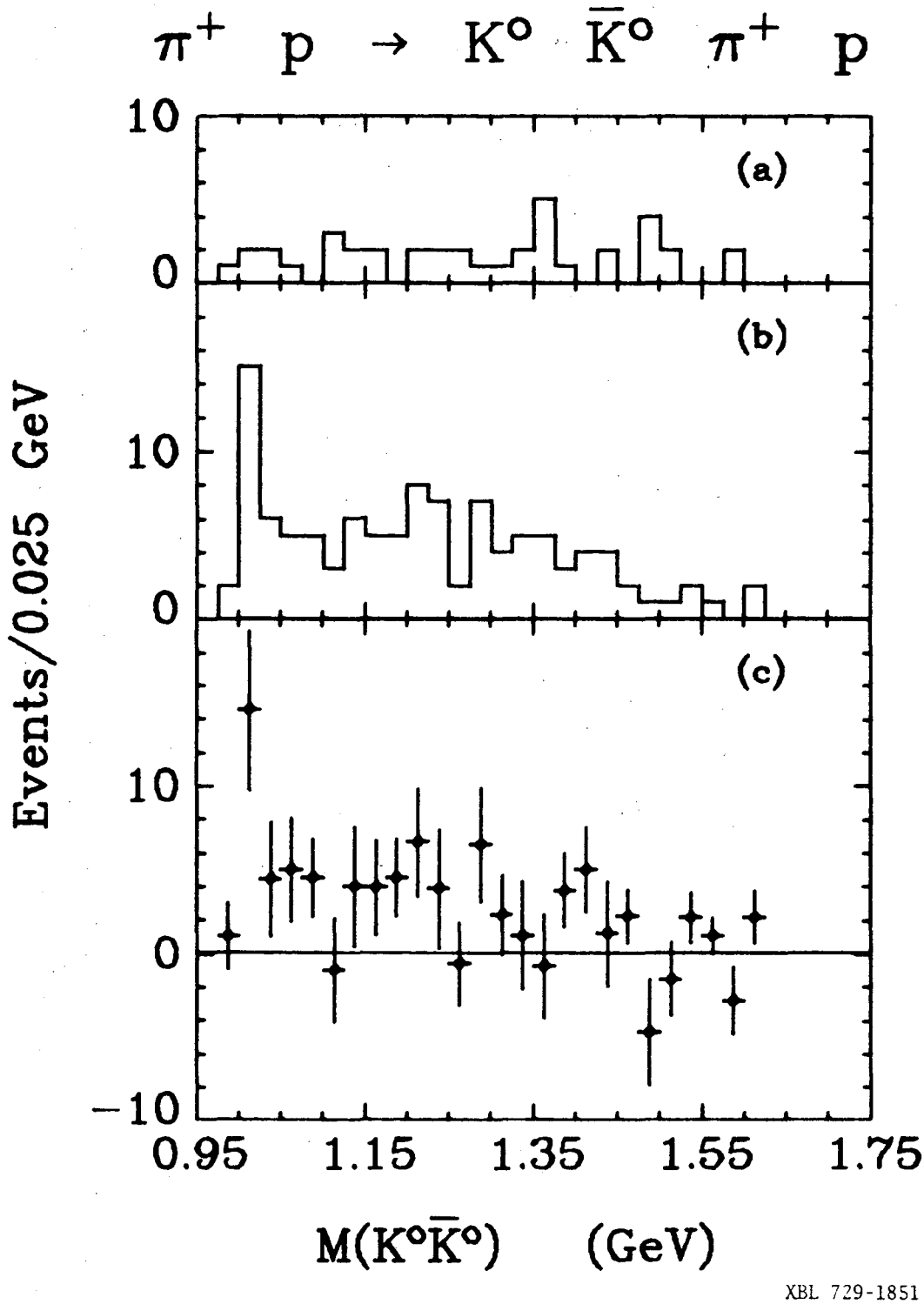

XBL 729-1851

Fig. 33

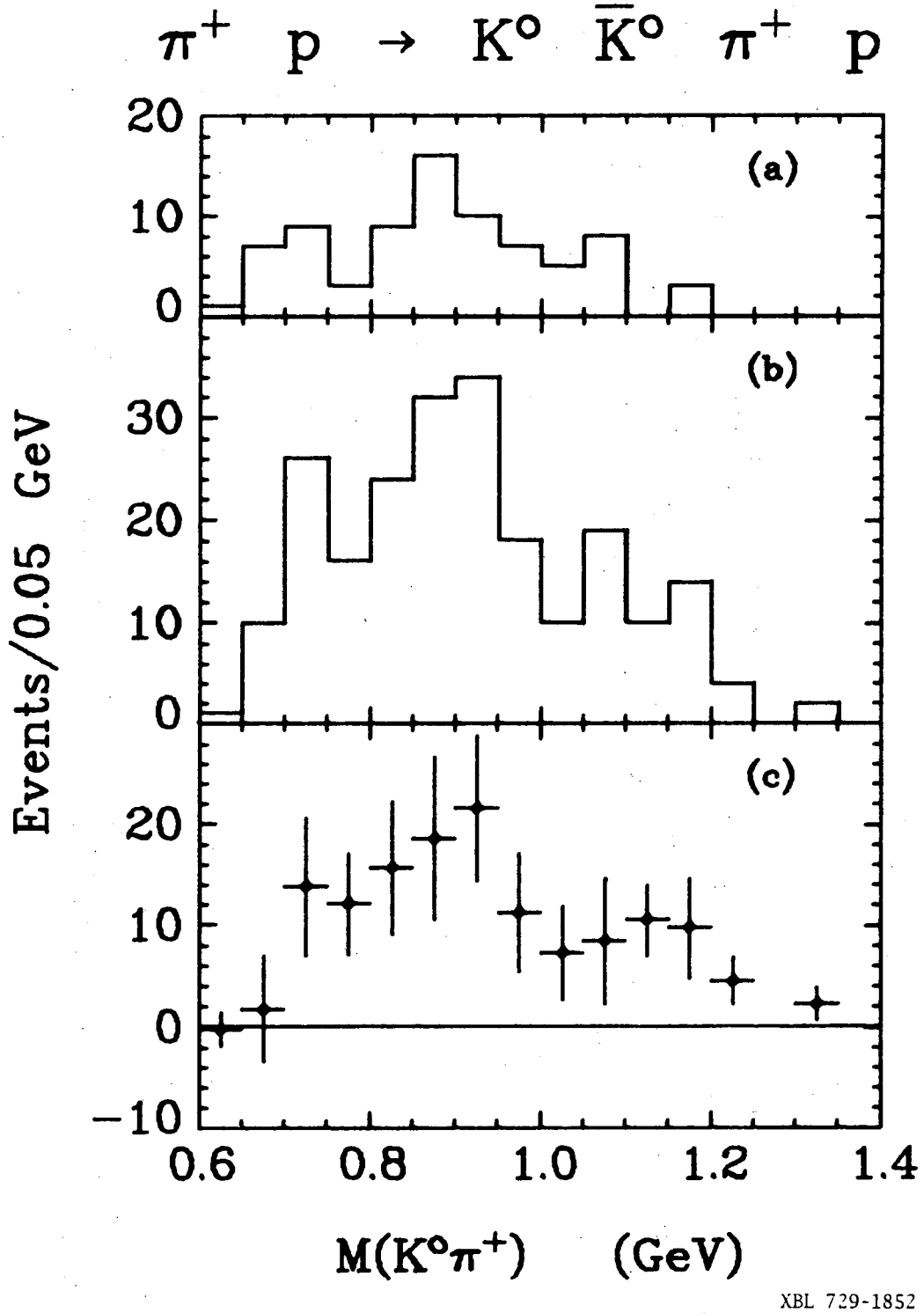
$\pi^+ p \rightarrow K^o \bar{K}^o \pi^+ p$
(a)
(b)
(c)
Events/0.05 GeV
20
10
0
30
20
10
0
20
10
0
−10
0.6
0.8
1.0
1.2
1.4
$M(K^o\pi^+)$ (GeV)
XBL 729-1852

Fig. 34

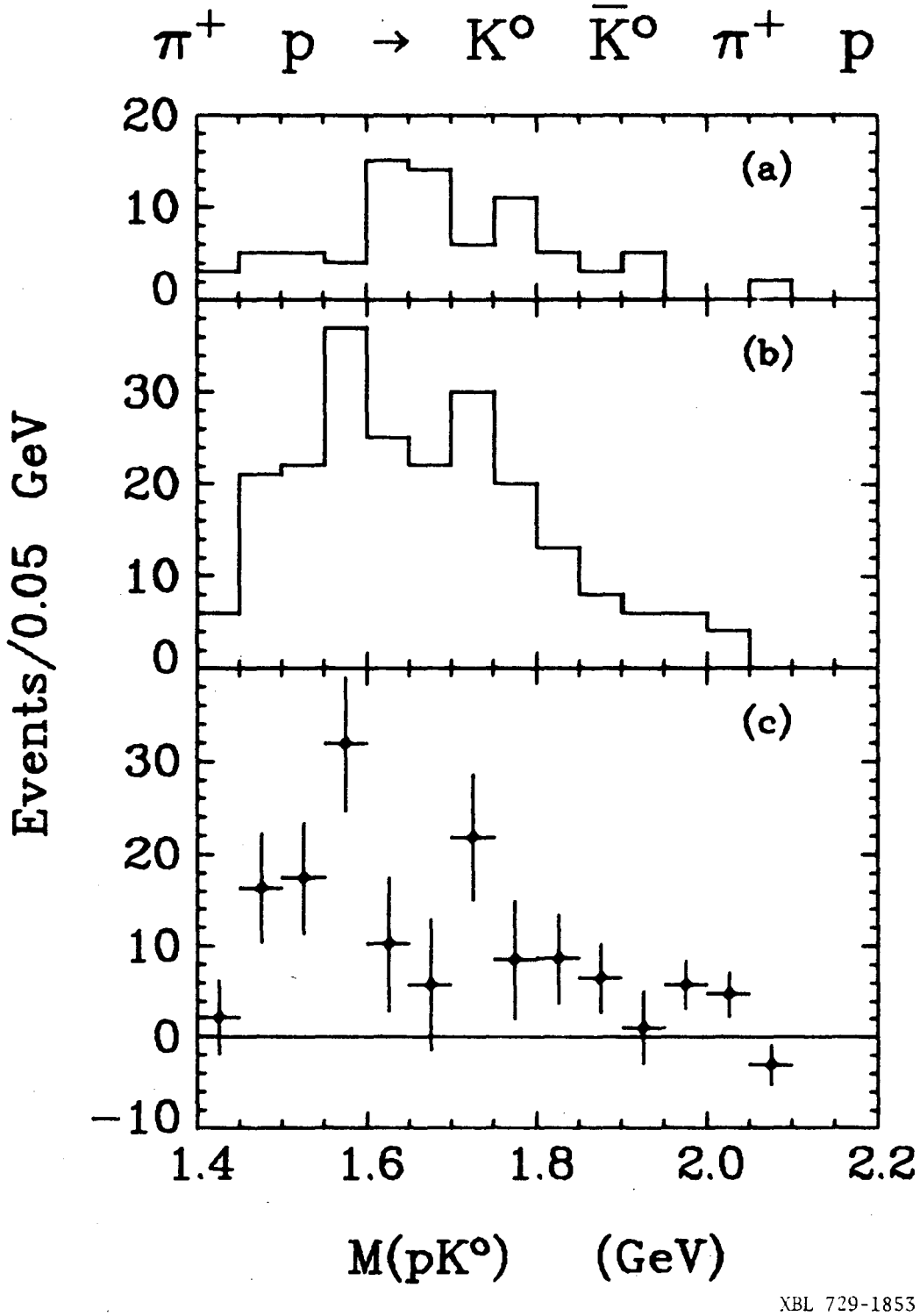
$\pi^+ p \rightarrow K^\circ \bar{K}^\circ \pi^+ p$
(a)
(b)
(c)
Events/0.05 GeV
M(pK°) (GeV)
1.4
1.6
1.8
2.0
2.2
20
10
0
30
20
10
0
30
20
10
0
−10
XBL 729-1853

Fig. 35

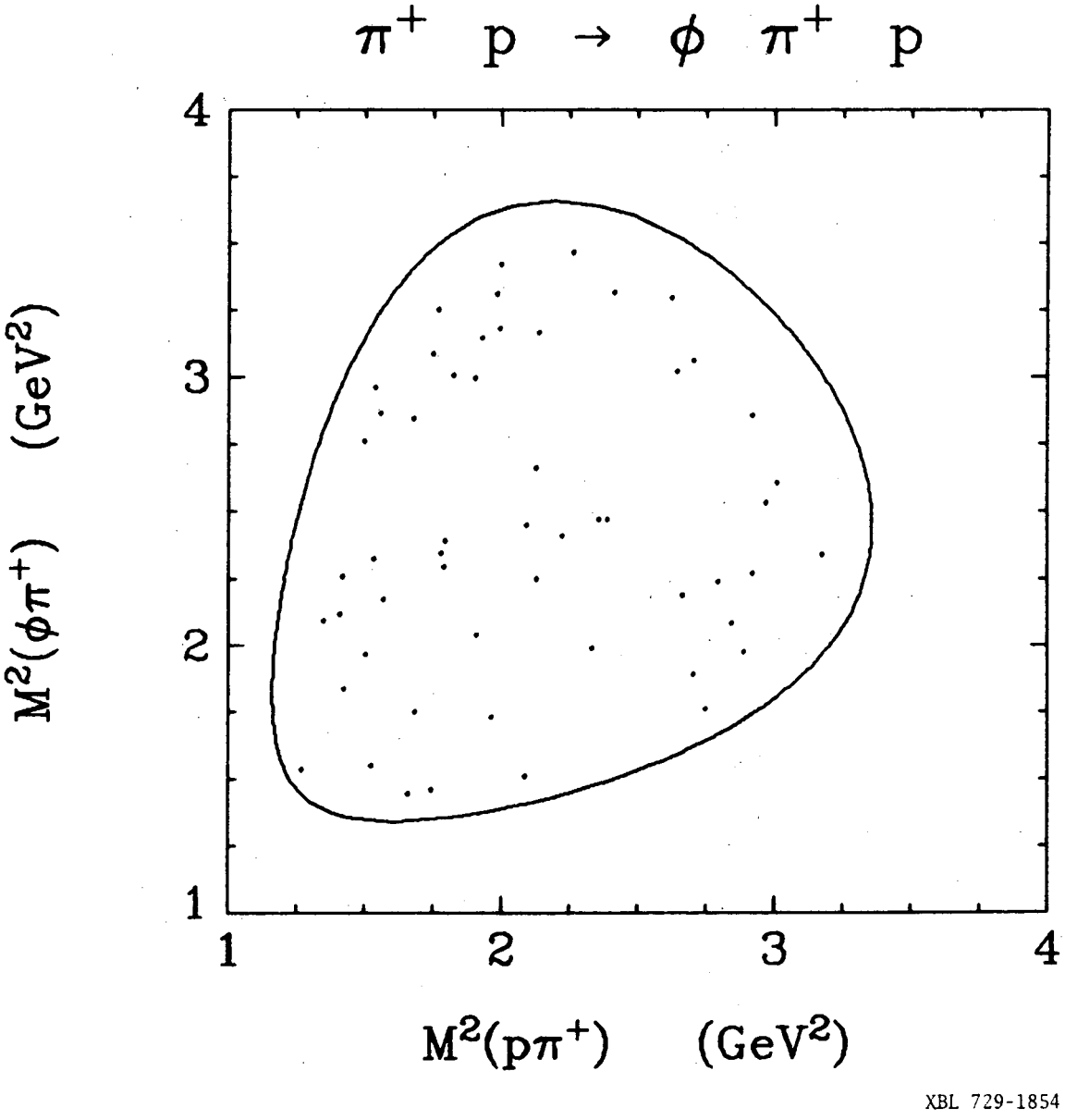
$\pi^+ \; p \rightarrow \phi \; \pi^+ \; p$
$M^2(\phi\pi^+)$ (GeV^2)
$M^2(p\pi^+)$ (GeV^2)
1
2
3
4
XBL 729-1854

Fig. 36

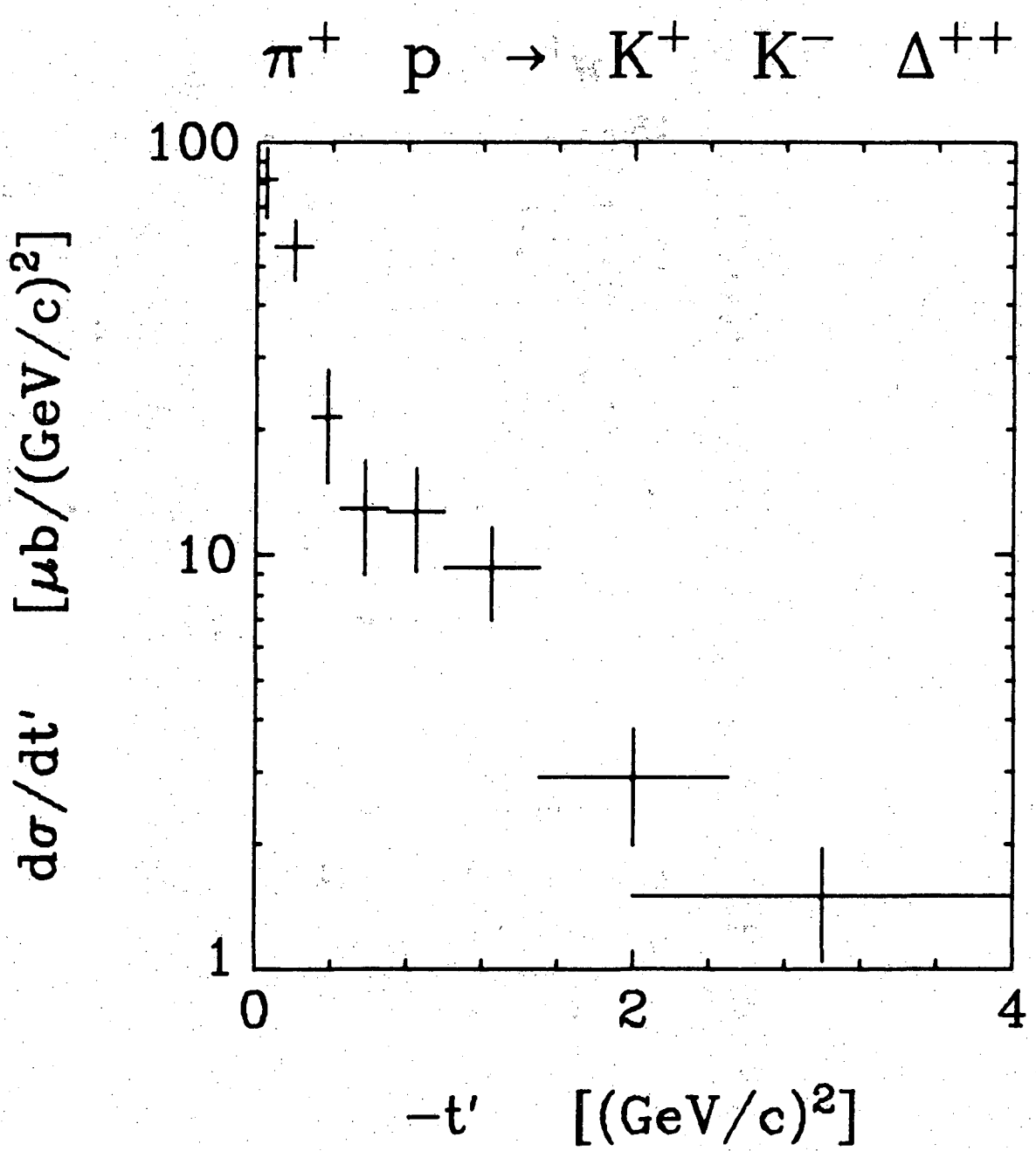

XBL 729-1855

Fig. 37

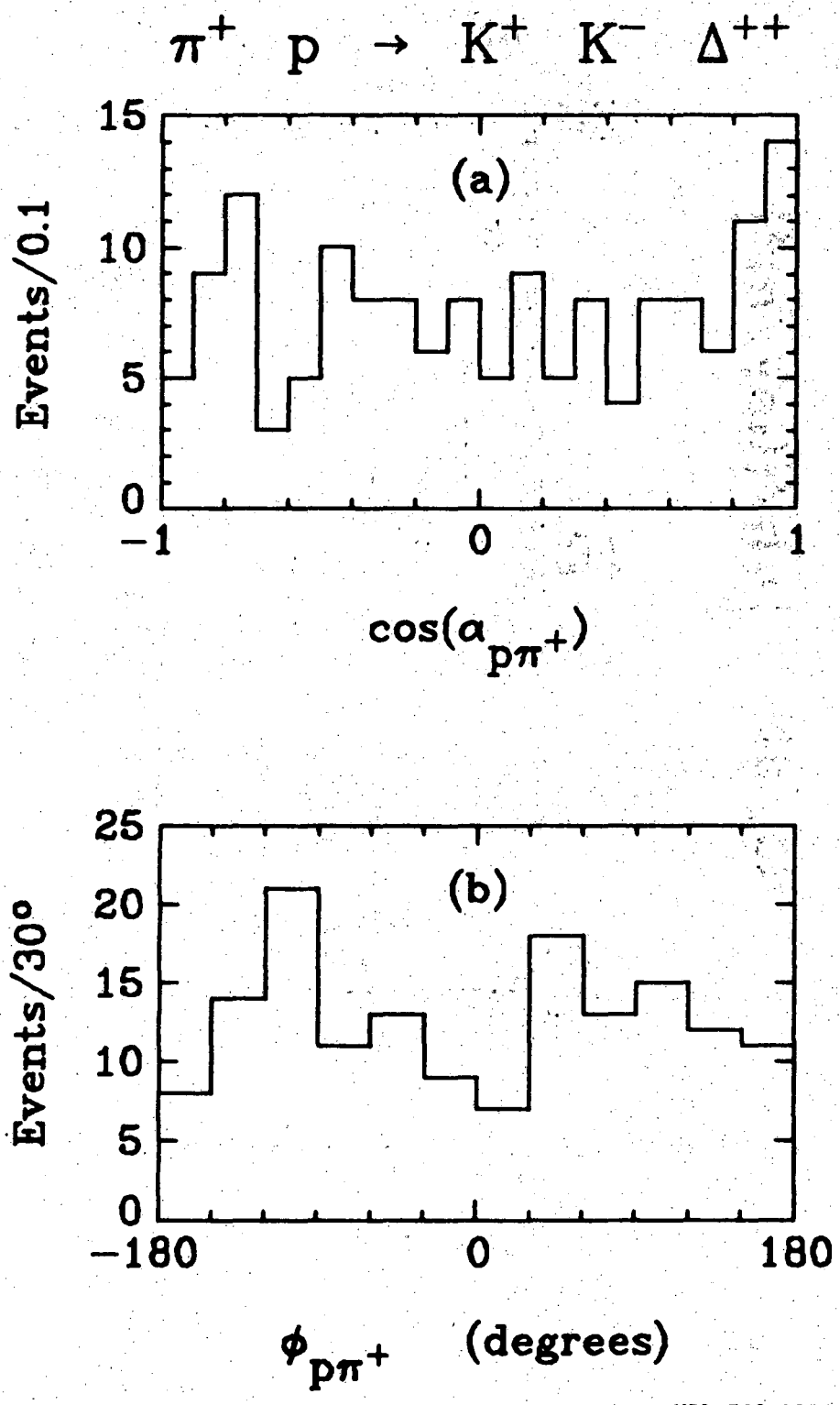

XBL 729-1856

Fig. 38

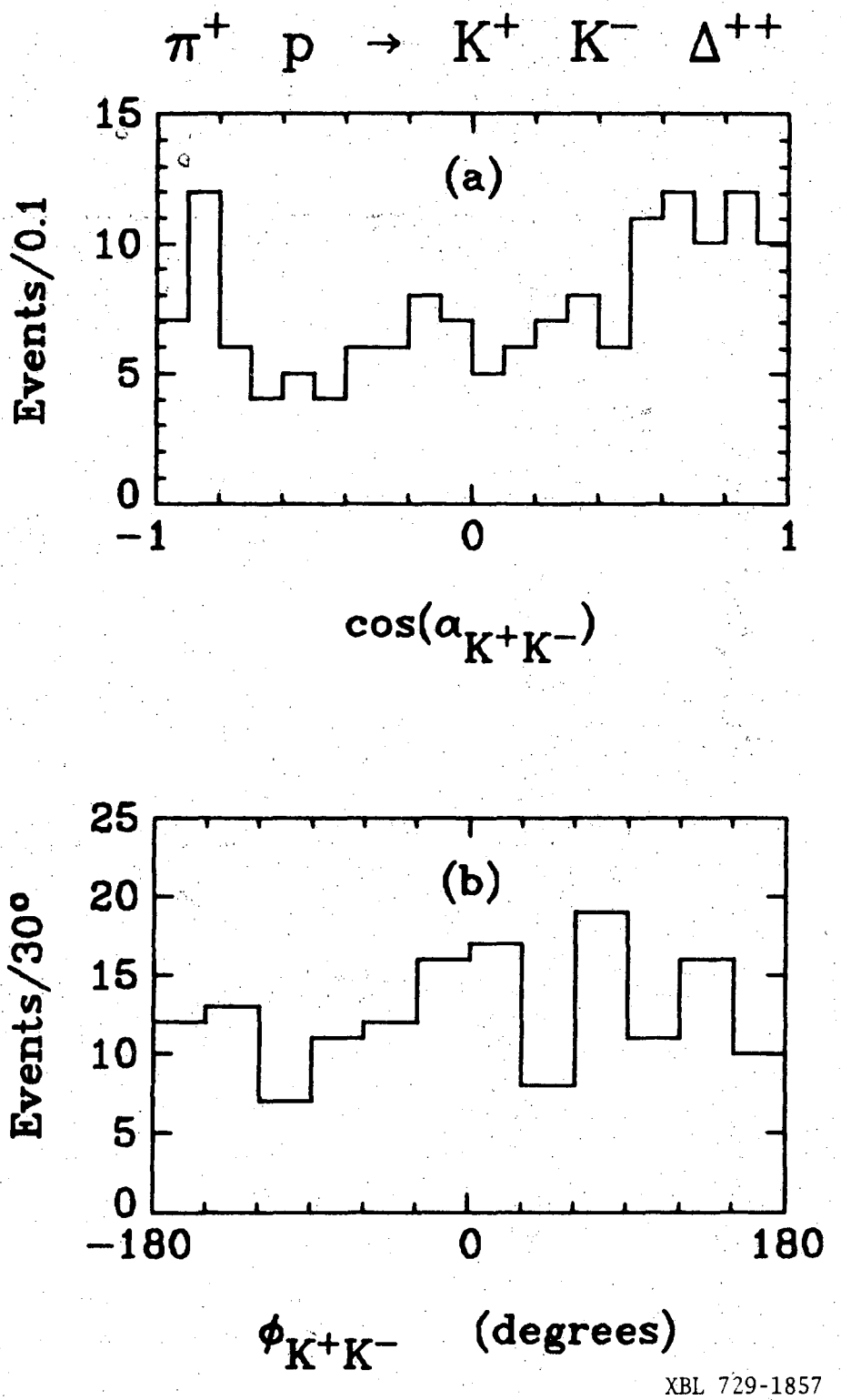

XBL 729-1857

Fig. 39

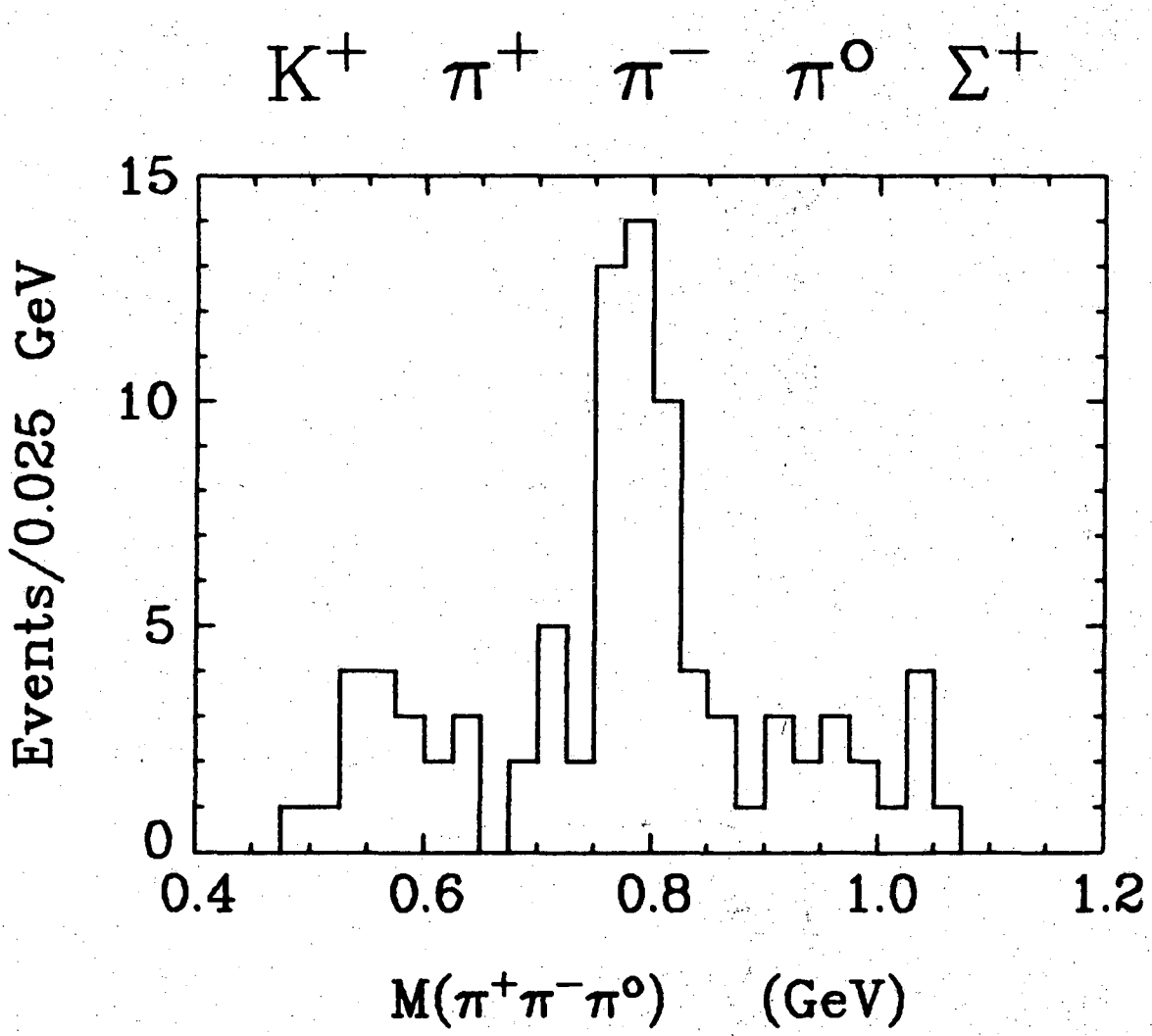
$K^+ \pi^+ \pi^- \pi^o \Sigma^+$
Events/0.025 GeV
15
10
5
0
0.4
0.6
0.8
1.0
1.2
$M(\pi^+\pi^-\pi^o)$ (GeV)
XBL 729-1858

Fig. 40

TECHNICAL INFORMATION DIVISION
LAWRENCE BERKELEY LABORATORY
UNIVERSITY OF CALIFORNIA
BERKELEY, CALIFORNIA 94720